PB86-109485

Isotopic Study of the Inhalation Toxicology of Oxidants

Indiana Univ. at Bloomington

Prepared for

Health Effects Research Lab.
Research Triangle Park, NC

Jun 85

U.S. Department of Commerce
National Technical Information Service
NTIS

TECHNICAL REPORT DATA

(Please read Instructions on the reverse before completing)

1. REPORT NO. EPA/600/1-85/013	2.	3. RECIPIENT'S ACCESSION NO. PB86 109485/AS
4. TITLE AND SUBTITLE AN ISOTOPIC STUDY OF THE INHALATION TOXICOLOGY OF OXIDANTS		5. REPORT DATE June 1985
		6. PERFORMING ORGANIZATION CODE
7. AUTHOR(S) Dr. John M. Hayes, Dr. Jeffrey Santrock		8. PERFORMING ORGANIZATION REPORT NO.
9. PERFORMING ORGANIZATION NAME AND ADDRESS Department of Chemistry Indiana University Bloomington, IN 47405		10. PROGRAM ELEMENT NO. C9GA1A
		11. CONTRACT/GRANT NO. CR807322 and CR811261
12. SPONSORING AGENCY NAME AND ADDRESS Office of Research & Development Health Effects Research Laboratory USEPA Research Triangle Park, NC 27711		13. TYPE OF REPORT AND PERIOD COVERED
		14. SPONSORING AGENCY CODE EPA-600/11

15. SUPPLEMENTARY NOTES

16. ABSTRACT

The purpose of these studies was to develop novel methods to investigate the biological fate of inhaled ozone and other oxygen-containing pollutants in animal and human tissues using the heavy isotope of oxygen, oxygen-18 (^{18}O). Methods were developed which facilitated the conversion of tissue oxygen to CO_2 and the subsequent trapping of the CO_2 so that it could be subjected to isotope-ratio mass spectrometry. The ratios of the various masses of evolved CO_2 were used to calculate the ^{18}O content of the original tissues, thus enabling the detection of isotopic enrichments as small as 0.4%. The above procedures were performed by modification of a commercially available elemental analyzer to include effluent columns and trapping devices, development of oxygen isotopic standards, and by derivation of mathematical models for correction of blank and memory effects originating during sample pyrolysis. These techniques were applied with success to the determination of the biological fate of inhaled ozone, and to the measurement of tissue oxidation induced by a model peroxidation initiator, carbon tetrachloride.

17. KEY WORDS AND DOCUMENT ANALYSIS

a. DESCRIPTORS	b. IDENTIFIERS/OPEN ENDED TERMS	c. COSATI Field/Group

18. DISTRIBUTION STATEMENT Release to Public	19. SECURITY CLASS *(This Report)* Unclassified	21. NO. OF PAGES 201
	20. SECURITY CLASS *(This page)* Unclassified	22. PRICE

EPA Form 2220-1 (Rev. 4-77) PREVIOUS EDITION IS OBSOLETE

PB86-109485

EPA/600/1-85/013
June 1985

AN ISOTOPIC STUDY OF THE INHALATION TOXICOLOGY OF OXIDANTS

John M. Hayes and Jeffrey Santrock

Indiana University
Department of Chemistry
Bloomington, IN 47405

Cooperative Agreements CR807322 and CR811261

HEALTH EFFECTS RESEARCH LABORATORY
OFFICE OF RESEARCH AND DEVELOPMENT
U.S. ENVIRONMENTAL PROTECTION AGENCY
RESEARCH TRIANGLE PARK, NC 27711

REPRODUCED BY
NATIONAL TECHNICAL
INFORMATION SERVICE
U.S. DEPARTMENT OF COMMERCE
SPRINGFIELD, VA. 22161

NOTICE

This document has been reviewed in accordance with U.S. Environmental Protection Agency policy and approved for publication. Mention of trade names or commercial products does not constitute endorsement or recommendation for use.

This is to certify that the thesis submitted by Jeffrey Santrock has been passed by the Ph.D. Advisory Committee as satisfactory in partial fulfillment of the requirements for the Ph.D. degree.

Chairman John M. Hayes
(Research Advisor)

Dennis G. Peters

W. J. Jenkins

TABLE OF CONTENTS

TABLE OF CONTENTS v

ILLUSTRATIONS AND FIGURES viii

ACKNOWLEDGMENTS xi

CHAPTER 1 INHALATION TOXICOLOGY OF OXIDANTS 1

Inhalation Toxicology 3

Respirtory Transport and Absorption of Inhaled Oxidants 6

Airway Structure 6
Epithelial Cell Population 9
Flow Dynamics 11

Chemical Mechanisms 12

Moleculat Targets 13
Ozonolysis 14
Autoxidation 17
Mechanism of Tissue Damage 23

Isotopic Studies 24

Physiological Applications of Oxygen-18 25

References for Chapter 1 28

Chapter 2 DETERMINATION OF OXYGEN-18 IN ORGANIC SUBSTANCES . 33

Oxygen Isotopic Standards 35

Pyrolysis of Benzoic Acid 36
Isotopic Standards 46

Mathematical Model 46

Chemical Processes 46
Isotopic Mass Balance 52
Correction Parameters 57
Correction of Analytical Results 65

Oxygen Isotopic Analysis 66

Yield of Carbon Dioxide 69
Correction Parameters 69
Evaluation of the Correction Parameters 78
Standards 85

Experimental Section 89

  Isotopic Standards 89
  Oxygen Isotopic Analysis 93

References for Chapter 2 98

Chapter 3 MASS SPECTROMETRIC DETERMINATION OF CARBON-13, OXYGEN-17, AND OXYGEN-18 IN CARBON DIOXIDE 101

Development of Isotope Ratio Equations 103

  Isotopic Distribution 103
  Relationships Between ^{17}R and ^{18}R 106

    Theoretical Considerations 106
    ^{17}R and ^{18}R in Natural Samples 110

Calculation of Isotope Ratios 111

Determination of Isotope Abundances 112

  Mixed Samples Enriched in ^{18}O 113
  ^{17}R and ^{18}R in Natural Samples 117

Conclusions 123

Experimental Section 124

  Preparation of Carbon Dioxide for Isotopic Analysis 124
  Mass Spectrometric Measurement 124

References for Chapter 3 127

CHAPTER 4 DEPOSITION, DISPOSITION, AND CLEARANCE OF OZONE-DERIVED OXYGEN IN LUNG 129

Detection and Quantitation of the Isotopic Label . 131

Deposition in the Respiratory System 135

  Comparative Aspects of Ozone Uptake 135
  Distribution Within the Respiratory System . . 138

Deposition and Clearance in the Lung 143

  Deposition in the Lung 143
  Clearance from the Lung 152

Experimental Section 156

  Apparatus 156

Preparation and Purfication of $^{18}O_3$ 162
Aminal Exposures 163
Tissue Sampling and Preparation 163
Elemental and Isotopic Analysis 164

References for Chapter 4 165

CHAPTER 5 DETECTION AND QUANTITATION OF AUTOXIDATION *IN VIVO*: A STUDY OF HEPATIC AUTOXIDATION INDUCED BY CARBON TETRACHLORIDE 167

Lipid Peroxidation 168

Peroxidation of Linolenic Acid 168
Measurement of Lipid Peroxidation *In Vivo* . . . 171

Carbon Tetrachloride Hepatotoxicity 172

Microsomal Cytochrome P-450 173
Carbon Tetrachloride-Induced Autoxidation . . . 174

Conclusions 183

Experimental Section 184

Protocol 184
Tissue Sampling and Preparation 184
Elemental and Isotopic Analysis 185

References for Chapter 5 186

SUMMARY AND CONCLUSIONS 189

ILLUSTRATIONS AND FIGURES

Figure

1-1 Schematic representation of the mammalian respiratory system 8

1-2 Reaction of ozone with unsaturated fatty acids 16

1-3 Reaction of nitrogen dioxide with unsaturrated fatty acids 19

1-4 Autoxidation in the cell 21

2-1 Yield and isotopic composition of carbon dioxide produced by pyrolysis of benzoic acid 39

2-2 Equilibrium constant and equilibrium isotopic fractionation factor for the reaction $CO_2 + C \rightleftharpoons 2CO$ . . 45

2-3 Production of CO_2 from organic material 53

2-4 Results Predicted for replicate analyses of organic samples 59

2-5 Flow-chart for determination of correction parameters . . 62

2-6 Illustartion of the method for refinement of values for $^{18}F_I$ and n_Q 68

2-7 Effect of I_2O_5 temperature on yield of carbon dioxide . . 71

2-8 Determination of n_Q and $^{18}F_Q$. 75

2-9 Determination of a and b 77

2-10 Sample matrix effects 84

2-11 Calibration of working standards 91

2-12 Diagram of modifications to elemental analyzer 95

3-1 Schematic representation of isotope ratio mass spectrometer 108

3-2 Relative error in ^{18}R as a function of oxygen-18 abundance 119

3-3 Relative error in ^{18}F as a function of oxygen-18 abundance 121

4-1 Distribution of ozone-derived oxygen in the respitatory system 142

4-2 Uptake of ozone-derived oxygen in the lungs 146

4-3 Molecular distribution of ozone-derived oxygen in the lungs 148

4-4 Clearance of ozone-derived oxygen from the lungs 155

4-5 Apparatus for preparation and purification of $^{18}O_3$ . . . 158

4-6 Exposure system 161

5-1 Products formed during peroxidation of linolenic acid 170

5-2 Incorporation of O_2-derived oxygen into liver 181

Table

1-1 Isotopes of oxygen 26

2-1 Effect of pyrolysis time and temperature on yield and isotopic composition of carbon dioxide 37

2-2 Recovery and isotopic composition of carbon dioxide heated to 550°C in quatrz tubes 42

2-3 Analysis of benzoic acid 47

2-4 Analysis of heterarromatic carboxylic acids 48

2-5 Iterative determination of correction parameters 73

2-6 Comparison of isotopic analysis of benzoic acids by pyrolytic decarboxylation and by the Schutze-Unterzaucher procedure 81

2-7 Comparison of isotopic analysis of heteroaromatic carboxylic acids by pyrolytic decarboxylation and by Schutze-Unterzaucher procedure 86

2-8 Analysis of water standards and sucrose samples 88

3-1 Isotopic molecular species of carbon dixide 104

3-2 Analysis of CO_2 with oxygen derived from exchange with mixed water 115

3-3 Analysis of CO_2 with oxygen derived from exchange with distilled water 122

4-1 Contributions to the variance in ^{18}F 134

4-2 Deposition of ozone-derived oxygen in the respiratory system 136

4-3 Oxygen pools in nasopharynx, trahea, lungs, and blood . . 137

4-4 Uptake of ozone-derived oxygen in the respiratory system 140

4-5 Deposition of ozone-derived oxygen in the lungs 144

4-6 Mouse-lung oxygen pools 151

4-7 Clearance of ozone-derived oxygen in mouse lung 153

5-1 Summary of experimental protocol 175

5-2 Abundance of oxygen-18 in liver 177

5-3 Relative enrichment of oxygen-18 in liver 178

5-4 Oxygen pools in liver 179

ACKNOWLEDGEMENTS

My sincere appreciation goes to John Hayes, his commitment and guidance made this thesis possible.

Dr. Edward Baer provides much advice concerning the chemistry and preparation of ozone.

The technical support in our lab is outstanding. Steve Studley had a posative influence on my research in many, innumerable ways. A special thanks for the conscientious analysis of tissue samples, and tissue samples, and tissue samples ... by David Andrews, David Archer, and Martha J. Larsen is also well deserved.

Many of the specialized pieces of equipment required in these studies were designed and constructed by the technical staff in the department. The glass blower, Don Fowler, spent many hours building rebuilding apparatus. Each of the members of the machine shop, John Dorsett, Kenny Bastin, Dick Martin, Bill Miller, Larry Sexton, and Don Swafford, contributed to this work. Several devices had their origin in the electronics: Bob Ensman, Steve Williamson, and Andy Qualls.

This work was supported by a cooperative agreement with the Unites States Environmental Protection Agency. The physiological studies were conducted at the laboratories of the Inhalation Toxicology Division of the EPA. Their support and collaboration made this work possible. A special thanks must go to Dr. Gary E. Hatch for his efforts. He initiated this project, provided the necessary administartive support from within the EPA, and had an equal and ever present hand in these studies.

CHAPTER 1

INHALATION TOXICOLOGY OF OXIDANTS

Oxidant gases, specifically ozone (O_3) and nitrogen dioxide (NO_2), are the most important toxic components of photochemical smog. Toxicity arises from oxidation of components of biological tissue. Upon inhalation, the chemical lesion occurs in the respiratory system, at the interface between inspired air and blood in the lung. Damage to tissue can occur by two processes: direct reaction of the inhaled oxidant with molecular components of the cell and free radical-induced oxidation (autoxidation) of cellular components. Although autoxidation is a secondary process, initiated by free radicals produced in the initial chemical insult, it is thought to account for the majority of damage to tissue. Moreover, a complex series of biochemical, physiological, and anatomical events in the lung ensues, and it is difficult to distinguish dysfunction resulting from oxidation from the response of the organism.

A major emphasis of current research is the establishment of relationships between effects in laboratory animals and in humans. A realistic assessment of the risk to humans must involve, not only an understanding of the chemical mechanisms of oxidant injury to tissue, but an understanding of the chemical and physiological factors which influence transport, absorption, and reactivity of oxidants in the respiratory system. A unified approach to the study of the inhalation toxicology of oxidants utilizing oxygen-18 as a physiological tracer of inhaled oxidants will be presented. This approach relies on techniques, developed in this work, for the quantitation of excess oxygen-18 in complex organic material (physiological samples). Two questions of immediate concern are addressed directly:

1. What is the retained dose of a specific oxidant, both in the lung and at specific sites within the respiratory system?

2. What are the target molecules for inhaled oxidants in the lung and the chemical mechanisms of oxidant injury in tissue?

This approach can be used to determine the influence of various biochemical and physiological factors on the retained dose and oxidant injury in the lung, and to provide a sound basis for extrapolation of dose-response relationships from laboratory animals to humans. Although the primary focus of this research has been study of the inhalation toxicology of photochemical oxidants, the experimental protocol developed in the course of these investigations is generally applicable to the study of any agent or pathological condition that causes aberrant oxidation of the molecular components of tissue.

Inhalation Toxicology

The physiological function of the lung is to provide a medium for gas exchange between inspired air and the blood, while maintaining the integrity of the organism. Any process which impairs the ability of the lung to mediate exchange of respiratory gases is detrimental. In the case of inhaled oxidants, pulmonary distress results mainly from tissue damage in the respiratory regions of the lung.

An important conclusion, derived from cytologic and biochemical observations of lung tissue, is that the peak concentration of an oxidant in the atmosphere, as opposed to exposure time or the time-weighted-average concentration, correlates most closely with changes in lung structure and biochemistry that are associated with toxicity (1). Although it is difficult to establish a distinction between an acute and a chronic dose of a particular oxidant or, more precisely, the concentration which elicits an acute or a chronic response, the oxidant levels typically found in highly polluted urban areas (ozone < 1 ppm and nitrogen dioxide < 0.5 ppm) are well within the chronic range, except for a small group of high-risk individuals (2). Exposure to high concentrations of oxidants for prolonged periods of time results in extensive destruction of epithelial tissue in the lung and can be lethal (3). Symptoms of acute toxicity include chest pains, severe respiratory distress, and accumulation of edemata in the lung (4). If the exposure is not lethal, prolonged structural and biochemical changes are observed (5). Since chronic toxicity is most prevalent, however less obvious, in the general population, the effects of low levels of inhaled oxidants are currently of greatest interest.

Chronic effects encompass a complex sequence of events. Exposure to sub-lethal concentrations of ozone or nitrogen dioxide results in an increase in breathing frequency with decreases in minute volume, total ventilation, and oxygen consumption (6). This rapid, shallow breathing is accompanied by an increase in pulmonary resistance and a decrease in pulmonary compliance (6). Respiratory function is impaired and stressed.

Susceptibility to infection is also increased. Increased risk of respiratory infection is a result of decreased phagocytyzing capacity of the alveolar macrophage (7). This effect has been observed in mice exposed to concentrations of ozone as low as 0.08 ppm (7). Furthermore, the immune response of T and B lymphocytes (8) and the phagocytic rate of polymorphonuclear leukocytes (9) are suppressed in humans exposed to low concentrations of ozone. These effects persist for at least two weeks after the exposure (1-9).

Decreases in the activities of enzymes which are particularly susceptible to attack by oxidants, such as membrane proteins and sulfhydryl-containing enzymes, are observed initially (10-14). As regenerative processes begin, biosynthesis increases, as do the activities of typical microsomal and mitochondrial marker enzymes (10,11). A certain degree of adaptation to oxidant injury occurs upon repeated exposure (12,15), but prolonged changes in lung structure (16,17), cell population (18), enzyme activity (13,14), and pulmonary function (19) occur. The degree to which the organism is affected is, in part, a function of the dose of oxidant to tissue. Tissue damage is greatest in the centriacinar* region of the lung (20-22) and, therefore, exchange of respiratory gases is greatly impaired.

Attempts to assess the dose of inhaled oxidants to specific regions within the respiratory system have relied on mathematical models which account for factors controlling the transport and absorption of reactive gases in the respiratory system (23). Though predictions of these models (24) are generally consistent with observations that the major sites of damage are the respiratory bronchioles and the alveolar ducts (20), direct experimental verification of the predicted dose is lacking. Since, in principle, such models can be used to extrapolate doseresponse relationships from laboratory animals to humans, it is imperative that direct measurements of the retained dose in tissue be made and that the mechanisms of respiratory transport and absorption of inhaled oxidants be understood.

---

*The centriacinar region collectively refers to the structural units in the lung where exchange of gases between inspired air and blood occurs. See pages 6-9.

Respiratory Transport and Absorption

The transport and absorption of gases such as nitrogen and oxygen in the respiratory system is well understood (25). In contrast, theories which describe the behavior of low concentrations of highly reactive gases in the respiratory system are not well developed, even though this issue is of central importance to understanding the toxic effects of inhaled pollutants. The dose of a reactive gas to various regions of the respiratory system and the resulting tissue damage depend on airway structure, the cellular morphology of the lung, and dynamics of gas flow in the respiratory system.

Airway Structure. Conceptually, the respiratory system can be divided into three functional zones: a conducting zone, a transitory zone, and a respiratory zone (26,27). The conducting zone comprises the nasal pharynx, the trachea, the bronchi, and the bronchioles, and functions to distribute inspired gases into the lower lung. The transitory zone forms the link between the conducting zone and the respiratory zone, and consists primarily of terminal and respiratory bronchioles. The respiratory zone, consisting of alveolar ducts and the alveoli, is the site of exchange of gases between inspired air and the blood. A schematic representation of the lung is shown in Figure 1-1.

The airways in the respiratory system form a series of bifurcated tubes terminating in small sacs in the periphery of the lung. Each airway is approximately cylindrical with flattened ends in the dimension perpendicular to the plane of the bifurcation (28). Systematic measurements of the size and branching angles of airways have shown that the lung exhibits a regular, asymmetric branching pattern (25-30). If the trachea is designated as the "zero-th generation" in the sequence of

Figure 1-1. Schematic representation of the mammalian lungs

The conducting zone consists of the the trachea, bronchi (br), and bronchioles (bl). The transitory zone consists of terminal bronchioles (tbr) and respiratory bronchioles (rbl). The respiratory zone consists of the alveolar ducts (ad) and alveoli (ad). Each bifurcation of the airway is assigned a generation number N, where the trachea is designated as the "zero-th generation" (26,27). Human lungs typically contain 23 generations between the trachea and the alveoli.

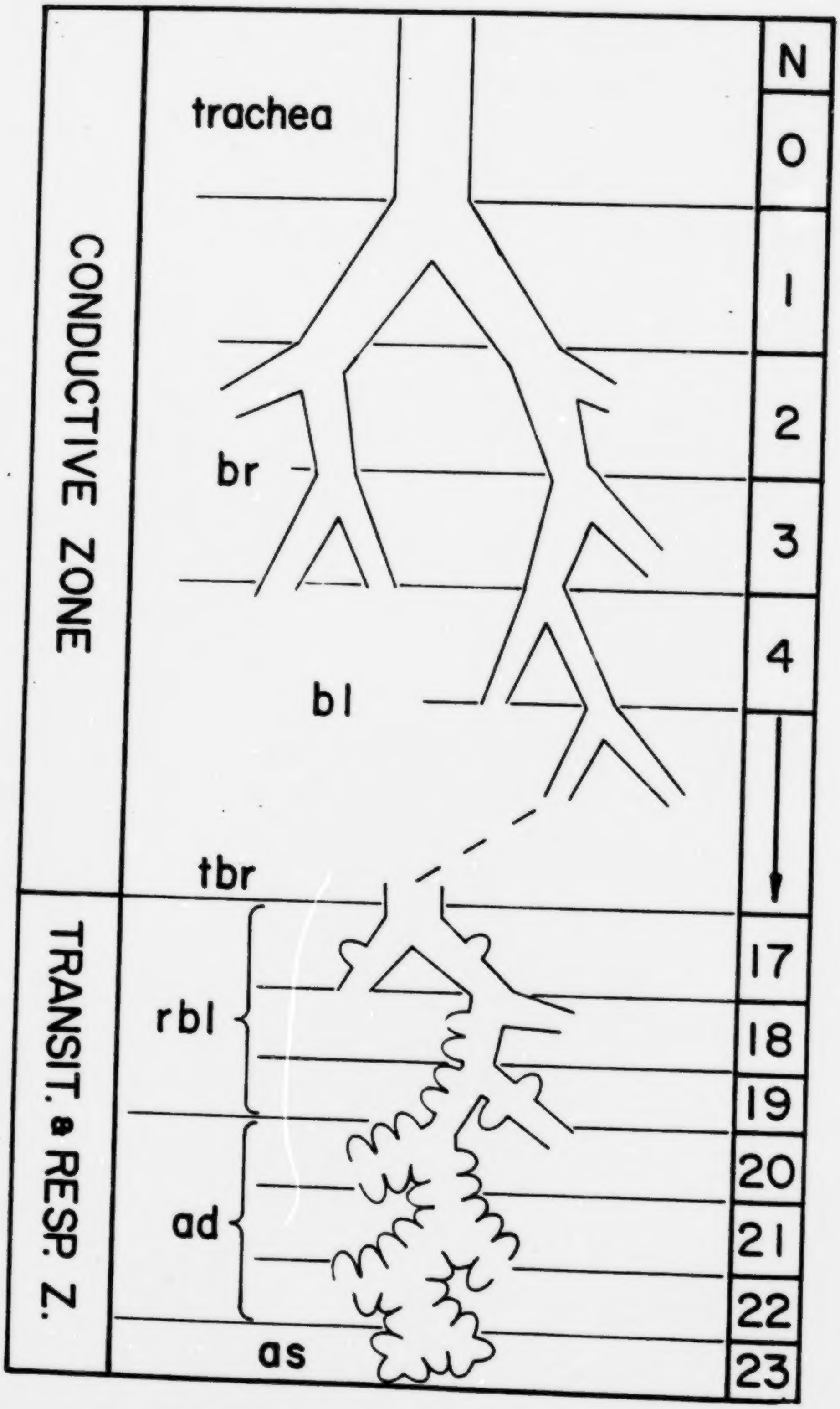
CONDUCTIVE ZONE
TRANSIT. & RESP. Z.
trachea
br
bl
tbr
rbl
ad
as
N
0
1
2
3
4
17
18
19
20
21
22
23

bifurcations, the mean length and radius of each airway decreases exponentially with generation number, whereas total lung volume and total surface area increase exponentially with generation number (24). Although variations in the branching pattern, the size, and the geometric shape of the conducting airways, thought to be a consequence of evolutionary adaptation, are observed in different species (29), lung structure is similar in mammals. Body mass is the single most important factor which determines morphometric and physiological respiratory parameters in mammals. Linear relationships between body mass and total lung volume, total lung weight, compliance, resistance, diffusing capacity, oxygen consumption, airway diameter, and alveolar surface area have been established (25). The systematic morphometry of the mammalian lung has been utilized in the development of a single convection-diffusion model to describe the mass transport of inspired gases in the lungs of mammalians (23).

Cell Population. Cell types with highly specialized functions are found in epithelial tissue of the respiratory system. The epithelium of the conducting airways contains ciliated and nonciliated cells, and receptor cells (25). The nonciliated cells synthesize and secrete onto the surface of the epithelium an aqueous fluid which becomes the mucous layer. Mucus is cleared through the epiglotus into the gastrointestinal tract by ciliary action. This is a major mechanism by which particles and aerosols are removed from the lung (30). The function of the receptor cells is not entirely clear. It is suspected that they serve as neuronal receptors for irritants.

Transition to a different population occurs in the alveolar ducts. The alveolar epithelium is composed of three cell types: Type I, Type

II, and Type III pneumocytes (25). The majority of the alveolar epithelium consists of type I cells. The function of these cells is to form the boundary between the alveolar lumen and the capillary endothelium while contributing minimally to the barrier for diffusion of gases between blood and inspired air. Type I cells extend laterally, up to 50 um, from a single nucleus to form a thin cytoplasmic layer (0.1 um) populated with relatively few organelles (25). Type II cells are cuboidal with no lateral cytoplasmic extensions. They have a high concentration of mitochondria, a well-developed endoplasmic reticulum, a Golgi complex, and numerous multivesicular bodies (25). These cells account for most of the metabolic activity of the lung, their main activity being the synthesis and secretion of a phospholipid surfactant onto the surface of the alveolar epithelium. Type III cells are very rare and their importance to lung function is unknown. It has been proposed that their characteristic brush microvilli extending into the alveolar lumen serve as neuronal receptors, in a fashion similar to the receptor cells found in the bronchi.

A consequence of the low metabolic activity and large surface area of the Type I alveolar epithelial cells is a high susceptibility to damage by inhaled oxidants (11). Cell damage progresses from severe cytoplasmic swelling to a complete disintegration of Type I cells, thus exposing the basement membrane of the intersitium (20). Early stages of tissue repair proceed by a proliferation of Type II cells, which apparently give rise to the normal population of Type I cells (17). Prolonged exposure to oxidants can result in a permanent increase in the number of type II cells (16,17), together with fibrous intrusions into the alveolar lumen, thickening of the respiratory bronchiolar and proximal alveolar walls, and partial or complete occlusion of the alveolar ducts (17,21).

Flow Dynamics. In cases of chronic exposure, localization of injury primarily to the centriacinar region is thought to be, in part, a consequence of the flow characteristics of gases in the lung. The driving force for the transport of gases in the respiratory system is a pressure gradient created by expansion (inhalation) and contraction (exhalation) of the pleural cavity. Convective flow predominates in the conducting airways. A transition from convection to diffusion occurs as the flow front penetrates the lower portions of the lung. Although the average diameter of lung airways decrease exponentially as a function of generation number, the total lung volume increases so that the velocity of the flow front decreases as inspired air expands into the lung. Air in the alveolar ducts and in the individual alveoli is stagnant. Gases diffuse along a concentration gradient between the airway lumen and the capillary lumen (25). Therefore, mass transport of gases in the lung has both convective and diffusive components.

Transport processes almost certainly play an important role in the expression of toxicity. The dose of trace reactive gases to the airway epithelium is determined by the specific modes of transport which persist in different regions of the respiratory system. If fully developed laminar flow existed in the conducting airways, then radial diffusion would be the only mechanism for transport of gases to the airway wall. Turbulent flow is common in the trachea and in the first several bronchial generations (31). The asymmetric branching structure creates nonlaminar flow profiles which are initiated at the bifurcations and propagated along the daughter branches (32,33). Increased transport of reactive gases to the airway wall would be expected where turbulent flow occurs and at the branching points, where non-laminar velocity fields predominate. As velocity decreases, the residence time of a pulse of inspired air in a single generation increases. Radial diffusion becomes more important. The transitory and respiratory regions in the lower lung are also expected to receive a high dose.

Although some protection is provided by the mucus and surfactant layers, a large dose may penetrate the airway coating, with a maximum local deposition to tissue at the bifurcations and in the respiratory bronchi, alveolar ducts, and the proximal alveoli. This view is consistent with cytologic observations that cell damage accompanying inhalation of oxidants is greatest at the branching points and in the centriacinar region. Not only is quantitation of the dose to the total lung essential, it is important to assess non-uniform distribution of inhaled oxidants in the respiratory system, as the local dose to specific epithelial sites may be disproportionately high.

Chemical Mechanisms

Studies of the reactions of ozone and of nitrogen dioxide with organic molecules *in vitro* have provided a substantial framework from which the present theories of damage to tissue have been developed. Although it has been shown that ozone and nitrogen dioxide can react with a number of compounds found in the cell, toxicity is thought to be the result of destruction of the bronchiolar and alveolar epithelium, associated with autoxidation of unsaturated fatty acids in the cell membrane (34,35). There are two essential features to this scheme. Initially, ozone or nitrogen dioxide reacts directly with carbon-carbon double bonds in the fatty acid found in membrane lipids and possibly in certain aromatic residues in membrane proteins. These reactions, in turn, generate free radicals which initiate autoxidation in the cell membrane. Autoxidation is, however, not limited to membrane lipids. Uncontrolled free-radical reactions in the cell may involve other oxidizable compounds, causing changes in membrane fluidity and membrane-bound protein structure, thus disrupting the normal function of the membrane. In fact, autoxidation may produce a chemical amplification of initial oxidative damage caused by the inhaled toxicant, and, in that way, account for most of the cell damage.

Molecular Sinks for Ozone and Nitrogen Dioxide. Studies of the reactions of ozone and of nitrogen dioxide with organic solutes and macromolecules in vitro have indicated molecular components of the cell which are susceptible to direct oxidation by inhaled pollutants. In aqueous solution, ozone was found to add across the carbon-carbon double bound in tryptophan and histidine, to oxidize the sulfhydryl group in cytosine to sulfone, and to cause hydroxylation of the aromatic ring in tyrosine and phenylalanine (36). These amino acid residues were also found to be susceptible to oxidation in proteins; however, the extent of oxidation was a function of the accessibility of a particular residue to the solution (36,37). Cross-linking of sulfhydryl groups in proteins and glutathione was also observed, and only a portion of the original biological activity of the oxidized compounds could be restored by enzymatic reduction (36-38). Aqueous solutions of NADH and NADPH were oxidized by ozone; however, both oxidized species were biologically active as coenzymes in the reduced form (39).

Unsaturated fatty acids are particularly susceptible to oxidation by ozone and nitrogen dioxide. Oxidation of methyl esters of unsaturated fatty acids occurs in both thin films and aqueous dispersions (40,41). The major products of ozonolysis of lipid in the presence of molecular oxygen indicate that lipid peroxidation had occurred. Further, addition of phenolic antioxidants (α-tocopherol, butylated hydroxyanisole, and butylated hydroxytoluene) decrease the rate of oxidation (40). Products of lipid peroxidation have also been detected in tissue from animals exposed to both ozone and nitrogen dioxide (42-45). The mode of initiation and the extent of autoxidation *in vivo* is, at present, unknown.

Direct Oxidation. The mechanism by which ozone reacts with carbon-carbon double bonds was first proposed by Criegee (46). In this scheme, Figure 1-2, ozone reacts directly with the carbon-carbon double bond to form an initial adduct, a 1,2,3-trioxylane π-complex (reaction 1). At room temperature it is unstable and rapidly decomposes to an aldehyde and a zwitterion (reaction 2). In a non-participating solvent, a non-polar solvent lacking active hydrogen, a resonance form of the zwitterion (reaction 3) can react with the aldehyde to form a 1,2,4-trioxylane ring system (reaction 4). However, in a participating solvent (the cell membrane) the zwitterion can react with any molecule containing active hydrogen, yielding a peroxide (reaction 5). Destruction of the lipid bilayer of the membrane by ozone alone could have disastrous consequences for the cell; however, the peroxide products of ozonolysis, including the 1,2,4-trioxylane compound, can initiate ion autoxidation in the cell producing a chemical amplification of oxidative damage.

Nitrogen dioxide reacts with unsaturated lipids by addition to the carbon-carbon double bond or by abstraction an α-hydrogen (47). The

Figure 1-2. Mechanism for the reaction of ozone with unsaturated fatty acids.

(1) reaction of ozone with carbon-carbon double bond to form a 1,2,3-trioxylane

(2) decomposition of 1,2,3-trioxylane to an aldehyde and a Criegee zwitterion

(3) resonance form of Criegee zwitterion

(4) reaction of Criegee zwitterion and aldehyde to form 1,2,4-trioxylane (molozonide)

(5) reaction of 1,2,4-trioxylane with molecular components of tissue containing active hydrogen to form a peroxide

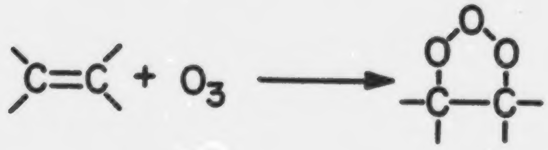

(1)

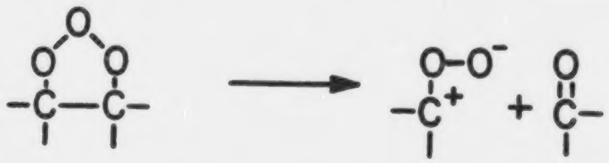

(2)

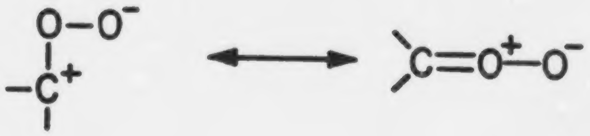

(3)

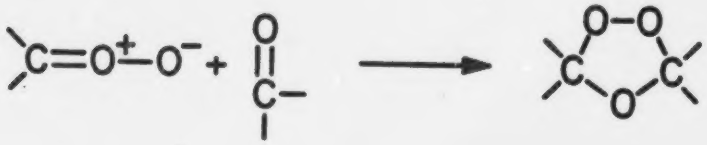

(4)

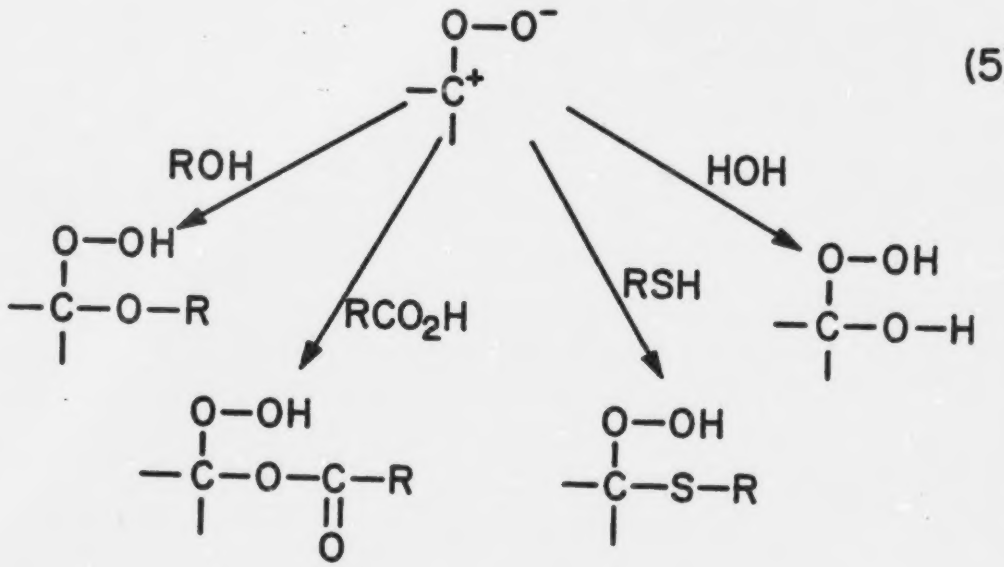

(5)

important steps in both mechanisms are shown in Figure 1-3. The addition reaction (Scheme I) predominates at extremely high concentrations of nitrogen dioxide (>1%), whereas hydrogen abstraction (Scheme II) is the predominant mode of reaction at lower concentrations. Addition of nitrogen dioxide to the carbon-carbon double bond produces a carbon-centered radical, reaction 1. In the presence of molecular oxygen, a carbon-centered radical reacts rapidly to form a peroxy radical (reaction 2). A peroxy radical can initiate autoxidation in the cell by hydrogen abstraction from an unsaturated lipid (reaction 3). Hydrogen abstraction by nitrogen dioxide produces a delocalized carbon-centered radical (reaction 4). In a similar fashion, this radical reacts with molecular oxygen to form a peroxy radical (reaction 5) thus initiating autoxidation.

Autoxidation. Lipid peroxidation in vivo is thought to be an important component of oxidant injury accompanying exposure to nitrogen dioxide (42,43) and to ozone (44,45). Presumably, carboncentered free radicals and organic hydroperoxides produced by the reaction of lipids with nitrogen dioxide and ozone, respectively, initiate autoxidation. A general scheme for autoxidation is shown in Figure 1-4. Initiation occurs by the production of carbon-centered free radicals in the cell, where an organic hydroperoxide is the precursor for the initiation process (reactions 1 and 2). At low conversions, lipid peroxidation in the membrane produces radical species which sustain the autocatalytic cycle (48-50). Propagation of the chain of free-radical induced oxidations involves the reaction of the carbon-centered radical with molecular oxygen to form a peroxy radical (reaction 3) followed by hydrogen abstraction from an organic compound to regenerate a carbon-

Figure 1-3. Mechanism for the reaction of nitrogen dioxide with unsaturated fatty acids

Scheme I: Addition mechanism

(1) addition of nitrogen dioxide to carbon-carbon double bound to form a carbon-centered radical

(2) reaction of molecular oxygen with carbon-centered radical to form a peroxy radical

Scheme II: Hydrogen abstraction mechanism

(3) abstraction α-hydrogen from unsaturated hydrocarbon to form a delocalized carbon-centered radical

(4) reaction of molecular oxygen with delocalized carbon-centered radical to form a peroxy radical

Scheme I

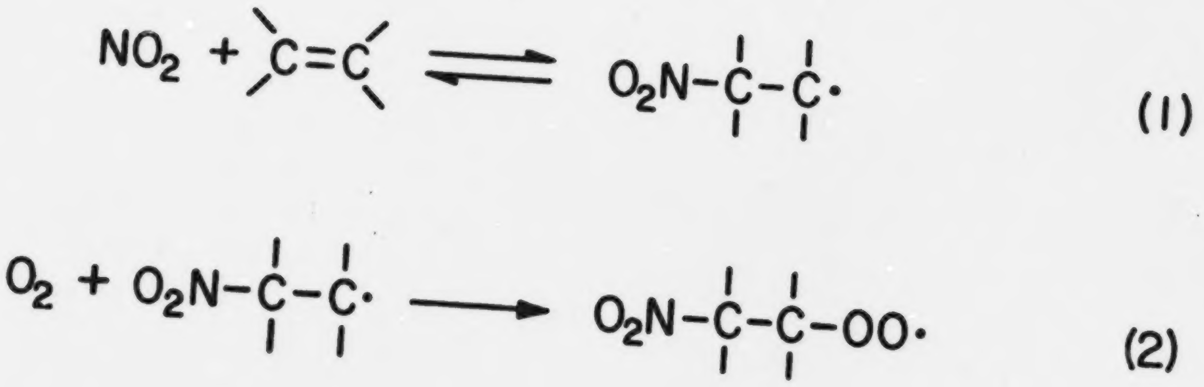

Scheme II

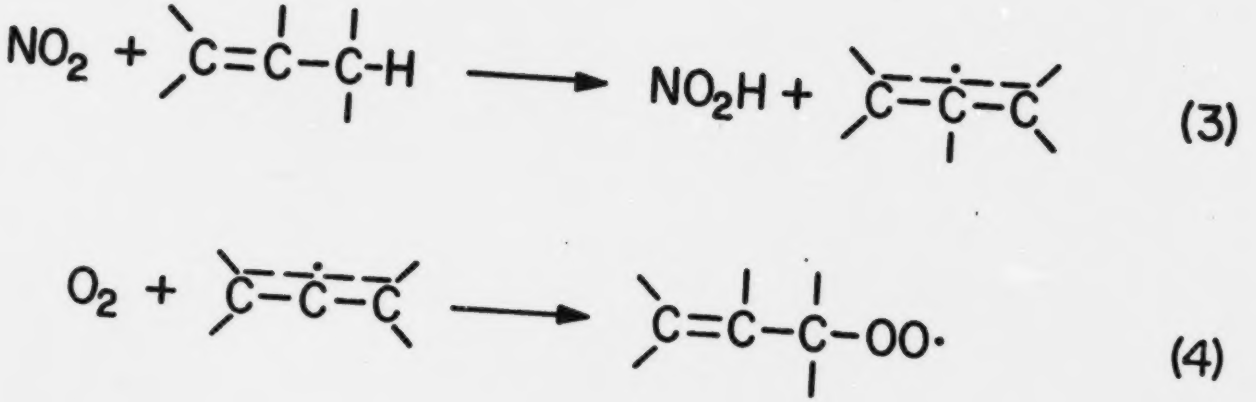

Figure 1-4. Autoxidation in the cell

(1) initiation: ferric-ion catalyzed hemolysis of hydroperoxide to yield an alkoxy radical and a hydroxide ion

(2) propagation: abstraction of hydrogen from an alkane to yield a carbon-centered radical

(3) propagation: reaction of carbon-centered radical with molecular oxygen to yield a peroxy-radical

(4) propagation: abstraction of active hydrogen to yield an organic-hydroperoxide and a free radical

(5) production of a carbon-centered radical (QH = allylic hydrogen) will result in a chemical amplification of autoxidation

(6) reduction of ferrous ion by an organic hydroperoxide to yield a peroxy radical and a hydrogen ion

RH = organic hydrogen; QH = active organic hydrogen; ROH = organic alcohol; ROOH = organic peroxide; R· and Q· = carbon centered radical; ROO = organic peroxy-radical; RO = alkoxy radical; HO^- = hydroxide ion; H^+ = hydrogen ion; Fe^{2+} and Fe^{3+} = iron ion redox couple.

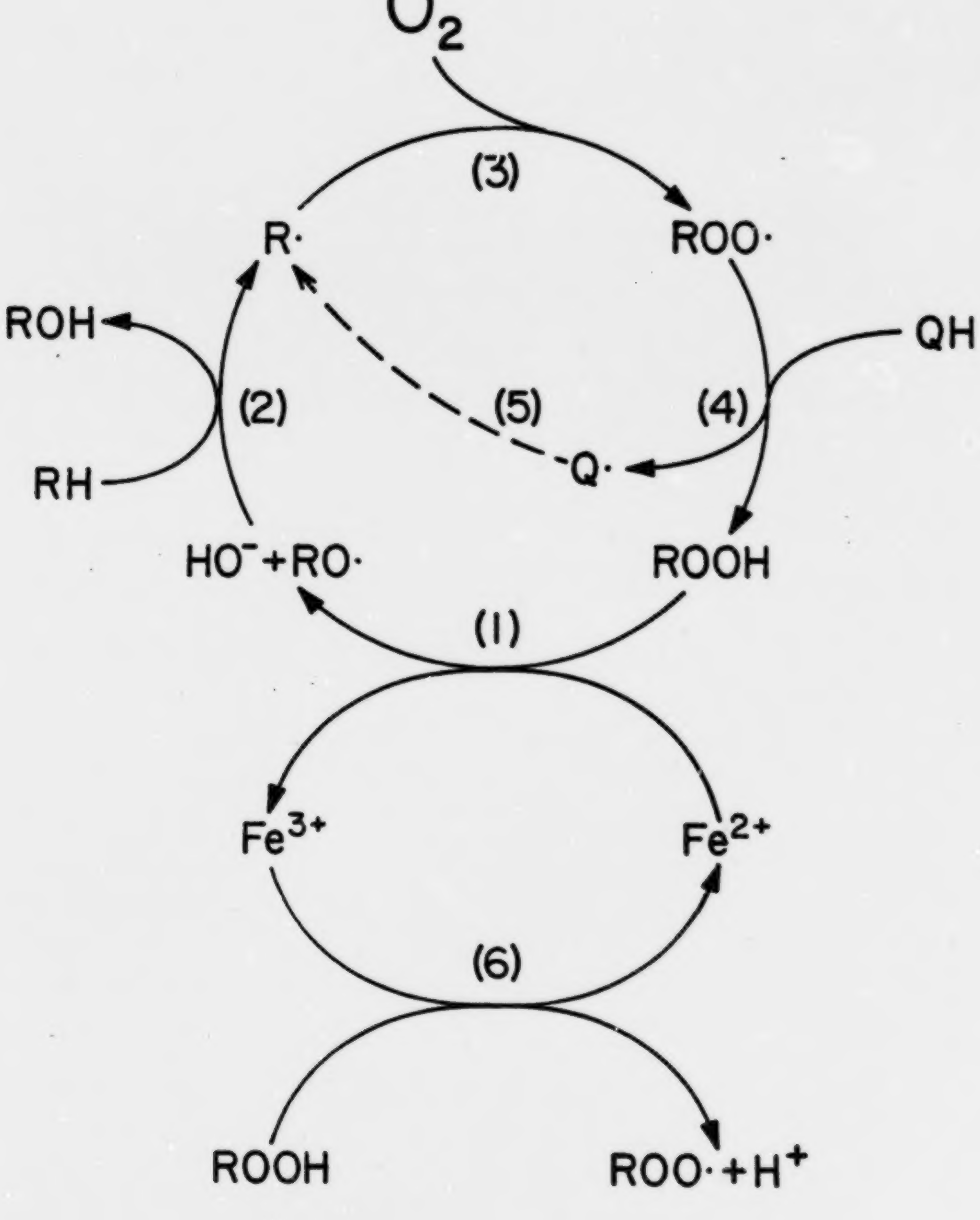
O_2
(3)
R·
ROO·
ROH
QH
(2)
(5)
(4)
RH
Q·
HO⁻ + RO·
ROOH
(1)
Fe³⁺
Fe²⁺
(6)
ROOH
ROO· + H⁺

centered radical and an organic hydroperoxide (reaction 4). Propagation can also occur by the production of alkoxy and peroxy radicals by the metal ion-catalyzed oxidation of organic hydroperoxides (reactions 1 and 5).

During the initiation phase, free radicals can be produced by thermal hemolysis of bonds, one-electron redox reactions, and highenergy radiation (49). The rate of hemolysis of organic hydroperoxides is extremely slow at physiological temperatures. However, soluble transition-metal ions (51) and transition-metal complexes such as iron protoporphyrins (52) catalyze the production of alkoxy radicals from hydroperoxides (reaction 1). Alkoxy radicals are, in general, extremely reactive so that hydrogen abstraction (even from saturated alkanes) (reaction 2) proceeds at the diffusion-limited rate. Peroxy radicals are, however, relatively stable, and can only abstract hydrogen from easily oxidizable compounds (53,54). Autoxidation in the cell is thus accelerated by reduced nucleotides, protein-thiol moieties, and polyunsaturated lipids. Termination can occur by the combination of two radical species to form nonradical products or by the formation of a stable radical. Nonradical products of termination reactions include malonaldehyde (55), conjugated dienes (56), and volatile hydrocarbons (57).

Autoxidation in tissue is limited by the concentrations of all oxidizable compounds and the rates of all initiation and termination reactions, but is independent of the partial pressure of molecular oxygen (54). As the concentrations of oxidizable compounds in the cell are fixed, the various mechanisms that have evolved to protect the cell against oxidation either limit initiation processes or increase termination reactions (58). Initiation-inhibiting antioxidants act by directing the decomposition of organic peroxides to nonradical products. This type of protective mechanism includes the glutathione peroxidase enzymes (59,60), catalase, and superoxide dismutase (61), and require NADPH, supplied by the pentose monophosphate shunt, for activity. It is therefore possible that this type of response can lead to a depletion of reducing equivalents and inhibit mitochondrial production of adenosine triphosphate. Chain-breaking antioxidants act by forming a stable radical. For example, the $\alpha,\beta,\gamma,\delta$-tocopherols (vitamin E) are found in the cell membrane and act by forming stable phenoxy radicals, thus preventing chain propagation in the lipid bilayer of the membrane (62). The reduced phenol can then be regenerated by reaction with ascorbate (vitamin C) (63). Recent evidence suggests that, at low concentrations of oxygen, β-carotene also acts as a chain-breaking antioxidant by the formation of a biologically stable radical (64).

Mechanism of Toxicity. Autoxidation is an uncontrolled branching chain reaction with potentially disastrous consequences to the cell. Studies of the effects of ozone on cultured erythrocytes suggest that toxicity is due to oxidation of the cellular membrane, and it is unlikely that ozone penetrates the cell membrane (31,38). The sequence of events is: i) free radical-induced autoxidation, initiated by ozonolysis of unsaturated phospholipids in the cell membrane; ii) cross-linking of membrane proteins, either by direct radical combination, or by formation of Schiff-base adducts between carbonyl moieties (produced by the peroxidation of unsaturated lipids) and primary amines; and iii) the formation of disulfide linkages by the oxidation of protein-sulfhydryl groups. Disruption of membrane processes, especially in the mitochondria, and utilization of reducing equivalents by the various antioxidant mechanisms may seriously inhibit cellular production of ATP. Therefore, cell death may ultimately result from depletion of the available energy sources used to maintain normal anabolic and catabolic processes.

Isotopic Studies

At present, the key issues in the study of the toxicity of inhaled oxidants fall into two categories: dosimetry and mechanisms of oxidant injury *in vivo*. The important aspects of dosimetry are quantitation of the retained dose of an inhaled oxidant to epithelial tissue and determination of depositional fine structure within the respiratory system. An understanding of the physicochemical factors controlling respiratory absorption can be developed by correlating differences in total and local dose with differences in airway structure in various mammalian species. In conjunction with dosimetry models, this information can be used to obtain an accurate prediction of absorption in the human lung.

Activity in the area of oxidant mechanisms has involved, primarily, *in vitro* studies of the oxidation of organic compounds and the effects of a specific oxidant insult on cell cultures. Although a substantial framework for tissue damage by photochemical pollutants has been proposed, the chemical mechanisms involved in oxidant injury in vivo are still speculative. While autoxidation in the cell membrane, initiated by free radicals produced by reaction of nitrogen dioxide or ozone with unsaturated lipids, has been suggested as the primary mode of oxidation *in vitro* and in cell cultures, there is no direct evidence that this mechanism is important in the toxicity of inhaled oxidants *in vivo*. The measurement of both direct oxidation and autoxidation in vivo is therefore important because cell death may be the result of a general depletion of reducing equivalents and inhibition of mitochondrial ATP production.

Inhalation of oxidants can result in tissue damage by one, or both, of two distinct processes: direct reaction with molecular components of tissue and free radical-induced oxidation of tissue involving molecular oxygen (O_2). Direct reaction of nitrogen dioxide or ozone with tissue components results in the fixation of toxicant-derived atoms in the tissue, whereas free radical-initiated oxidation leads to the uptake of O_2-derived oxygen in tissue. This is an important distinction which allows these mechanisms to be resolved and studied in vivo by the use of oxygen isotopic tracers. The isotopic label provides a means to determine the retained dose of a specific oxidant (O_3, NO_2, or O_2) in tissue, so that, by the appropriate use of labeled oxidant, questions of dosimetry and mechanism can be addressed.

Physiological Applications of Oxygen-18. All radioactive isotopes of oxygen are sufficiently short-lived (Table 1-1) that they are of limited utility as physiological tracers. Therefore, a stable isotope of minor abundance, either oxygen-17 and oxygen-18, must be employed. The natural abundance of both isotopes in biological material represents an irreducible background, and becomes especially important if only minute quantities of labeled compound enter the body (as is the case with inhaled pollutants). Although the use of oxygen-17 would offer greater sensitivity because of its lower natural abundance, the methods used to quantify oxygen isotopes in organic material are more suited to the determination of oxygen-18. Moreover, compounds highly enriched in

Table 1-1. Isotopes of Oxygen

nuclide	natural abundance[a] %	mass AU	half-life[d] s	decay process[e]
^{13}O	---	13[b]	0.0087	β+, 17.8 MeV
^{14}O	---	14[b]	71.0	β+, 5.14 MeV
^{15}O	---	15[b]	124	β+, 2.76 MeV
^{16}O	99.759	15.99491502[c]	(stable)	---
^{17}O	0.037	16.99913220[c]	(stable)	---
^{18}O	0.204	17.99915996[c]	(stable)	---
^{19}O	---	19[b]	29	β-, 4.82 MeV
^{20}O	---	20[b]	14	β-, 3.81 MeV

[a] approximate abundance in mammalian tissue

[b] nominal mass

[c] Wapstra, A. H.; Grove, N. B. 1971 atomic mass evaluation. I. Atomic mass scale. Nuclear Data, Sect. A. 9:267-301, 1971.

[d] Handbook of Chemistry and Physics , 53rd edition, Weast, R. C. (ed.), Chemical Rubber Company Press, 1973, p. B-249.

oxygen-17 are rare and expensive, whereas compounds containing greater than 99% oxygen-18 are readily available and comparatively inexpensive. Oxygen-18 is, therefore, the best choice for use as a physiological tracer.

In contrast to a radioactive isotopic tracer where quantitation is based on the detection of a specific decay product, difference in mass is the only physical property which can be used to distinguish stable isotopes of a particular element. Mass spectrometry provides the most accurate and precise determination of oxygen isotopic abundances. However, analysis of complex organic mixtures, such as physiological samples, requires that all oxygen in a sample be converted to a simple, volatile gas for mass spectrometric measurement. Techniques for preparation of carbon dioxide from organic material and for the mass spectrometric analysis of carbon dioxide will be discussed in chapters 2 and 3, respectively.

REFERENCES

1. Melton, C. E. Effects of long-term exposure to low levels of ozone: A review. Aviat. Space Environ. Med. 53:105-111, 1982.

2. Epidemiologic Appraisal of Photochemical Oxidants, Air Quality for Ozone and Other Photochemical Oxidants, Vol. II, Chapter 10, U. S. Environmental Protection Agency, Office of Research and Development, Washington, D. C., EPA-600/8-78-004, 1978.

3. Stokinger, H. E. Ozone toxicology. Arch. Environ. Health 10: 719-731, 1965.

4. Griswold, S. S.; Chambers L. A.; Motley, H. L. Report of case of exposure to high ozone concentrations for two hours. Arch. Industr. Health 15:108-118, 1957.

5. DeLucia, A. J.; Mustafa, M. G.; Cross, C. E.; Plopper, C. G.; Dungworth, D. L.; Tyler, W. S. Biochemical and morphological alterations in the lung following ozone exposure. Am. Inst. Chem. Eng. Symp. Series, 71:93-100, 1975.

6. Dungworth, D. L.; Cross, C. E.; Gillespie, J. R.; Plopper, C. G.; The effects of ozone on animals. Ozone Chemistry and Technology, Chapter 2, Murphy, J. S. and Orr, J. R. (ed.s), Franklin Institute Press, Philadelphia, 1975.

7. Coffin, D. L.; Blommer, E. J.; Gardner, D. E.; Holzman, R. Effects of air pollution on alteration of susceptibility to pulmonary infection. Proceedings of the 3rd Annual Conference on Atmospheric Contamination in Confined Spaces, Aerospace Medical Research Laboratories, Wright-Patterson Air Force Base, Ohio, p. 71, 1968.

8. Savino, A.; Peterson, M. L.; House, D.; Turner, A. G.; Jeffries, H. E.; Baker, R. The effect of ozone on human cellular and humoral immunity: characterization of T and B lymphocytes by rosette formation. Environ. Res. 15:65-69, 1978.

9. Peterson, M. L.; Harder, S.; Rummo, N.; and House, D. Effect of ozone on leukocyte function in exposed human subjects. Environ. Res. 15:485-493, 1978.

10. Ospital, J. J.; Hacker, A. D.; Mustafa, M. G. Biochemical changes in rat lungs after exposure to nitrogen dioxide. J. Toxicol. Environ. Health 8:47-58, 1981.

11. Witschi, H.; Cote, M. G. Primary pulmonary response to toxic agents. Crit. Rev. Toxicol. 5:23-65, 1977.

12. Stokinger, H. E.; Coffin, D. L. Biological effects of urban air pollution. Air Pollution, 2nd edition, Chapter 1, Stern, A. C. (ed.), Academic Press, New York, 1968.

13. Buckley, R. D.; Balchum, O. J. Enzyme alterations following nitrogen dioxide exposure. Arch. Environ. Health, 14:687-692, 1967.

14. Werthamer, S.; Penha, P. D.; Amaral, L. Pulmonary lesions induced by chronic exposure to ozone. Arch. Environ. Health, 29:164-166, 1974.

15. Frager, N. B.; Phalen, R. F.; Kenoyer, J. L. Adaptation to ozone in reference to mucociliary clearance. Arch. Environ. Health 34:51-57, 1979.

16. Stephens, R. J.;, Freeman, G.; Wright, P. G. Cytologic changes in dogs' lungs induced by chronic exposure to ozone. Am. J. Path. 73:711-726, 1973.

17. Freeman, G.; Stephens, R. J.; Coffin, D. L.; Stara, F. J. Changes in dogs' lungs after long-term exposure to ozone. Arch. Environ. Health. 26:209-216, 1973.

18. Evans, M. J.;, Cabral, L. C.;, Stephens, R. J.; Freeman, G. Transformation of alveolar type 2 cells to type 1 cells following exposure to NO_2. Exp. Mol. Pathol. 22:142-150, 1975.

19. Bates, D. V. Physiological effects on man of air pollutants. Fed. Proc., 33:2133-2135, 1974.

20. Stephens, R. J.; Sloan, M. F.; Evans, M. J.; Freeman, G. Early response of the lung to low levels of ozone. Am. J. Pathol. 74:31-44, 1974.

21. Hugod, C. Ultrastructural changes of the rabbit lung after a 5 ppm nitric oxide exposure. Arch. Environ. Health 34:12-17, 1979.

22. Plopper, C. G.; Chow, C. K.; Dungworth, D. L.; Tyler, W. S. Pulmonary alterations in rats exposed to 0.2 and 0.1 ppm ozone: A correlated morphological and biochemical study. Arch. Environ. Health 34:390-395, 1979.

23. Miller, F. J. A mathematical model of transport and removal of ozone in mammalian lungs . Ph.D. thesis, North Carolina State University, Raleigh, North Carolina, 1977.

24. Miller, F. J.; Menzel, D. B.; Coffin, D. L. Similarity between man and laboratory animals in regional pulmonary deposition of ozone. Environ. Res. 17:84-101, 1978.

25. Weibel, E. R. Morphological basis of alveolar-capillary gas exchange. Physiol. Rev. 53:419-495, 1973.

26. Weibel, E. R.; Gomez, D. M. Architecture of the human lung. Science 137:577-585, 1967.

27. Weibel, E. R. Morphometry of the human lung . Springer, Heidelberg, 1963.

28. Personal communication from Dr. R. Schreck, Biomedical Science Department, General Motors Research Center, Warren, Michigan.

29. Horsfield, K.; Cumming, G. Morphology of the bronchial tree in man. J. Appl. Physiol. 24:373-383, 1968.

30. Horsfield, K.; Cumming, G. Functional consequences of airway morphology. J. Appl. Physiol. 24:384-390, 1968.

31. Chan, T. L.; Schreck, R. M.; Lippman, M. Effect of the laryngeal jet on particle deposition in the human trachea and upper bronchial airways. J. Aerosol Sci. 11:447-459, 1980.

32. Schroter, R. C.; Sudlow, M. R. Flow patterns in models of the human bronchial airways. Respir. Physiol. 7:341-355, 1969.

33. Olson, D. E.; Sudlow, K.; Horsfield, K.; Filley, G. F. Convective patterns of flow during inspiration. Arch. Intern. Med. 131:51-57, 1973.

34. Goldstein, B. D.; Balchum, O. J. Effects of ozone on lipid peroxidation in the red blood cell. Proc. Soc. Exp. Med. 26:356-358, 1967.

35. Menzel, D. B.; Roehm, J. N.; Lee, S. D. Vitamine E: the biological and environmental antioxidant. Agr. Food Chem. 20:481-485, 1972.

36. Mudd, J. B.; Leavitt, R.; Ongun, A.; McManus, T. T. Reaction of ozone with amino acids and proteins. Atm. Environ. 3:669-682, 1969.

37. Leh, F.; Warr, T. A.; Mudd, J. B. Reaction of ozone with protease inhibitors from bovine pancrease, egg white, and human serum. Environ. Res. 16:179-190, 1978.

38. Chan, P. C.; Kindya, R. J.; Kesner, L. Studies on the mechanism of ozone inactivation of erythrocyte membrane ($Na^+ + K^+$)-activated ATPase. J. Biol. Chem. 252:8537-8541, 1977.

39. Menzel, D. B. Oxidation of biologically active reducing substances by ozone. Arch. Environ. Health 23:149-153, 1971.

40. Roehm, J. N.; Hadley, J. G.; Menzel, D. B. Oxidation of unsaturated fatty acids by ozone and nitrogen dioxide. Arch. Environ. Health 23:142-148, 1971.

41. Kesner, L.; Kindya, R. J.; Chan P. C. Inhibition of erythrocyte membrane ($Na^+ + K^+$)-activated ATPase by ozone-treated phospholipids. J. Biol. Chem. 254:2705-2709, 1979.

42. Thomas, H. V.; Mueller, P. K.; Lyman, R. L. Lipoperoxidation of lung lipids in rats exposed to nitrogen dioxide. Science 159:532-534, 1968.

43. Csallany, A. S.; Ayaz, K. L. Long-term exposure of mice in the presence and absence of vitamin E. I. Effects on body weights and lipofuscin pigments. Arch. Environ. Health 33:285-291,1978.

44. Goldstein, B. D.; Lodi, C.; Collinson, C.; Balchum, O. J. Ozone and lipid peroxidation. Arch. Environ. Health 18:631-635, 1969.

45. Dumelin, E. E.; Dillard, C. J.; Tappel, A. L. Effect of vitamin E and ozone on pentane and ethane expired by rats. Arch. Environ. Health 33:129-135, 1978.

46. Criegee, R. The Course of ozonation of unsaturated compounds. Rec. Prog. Chem. 18:111-120, 1957.

47. Pryor, W. A.; Lightsey, J. W.; Church, D. F. Reaction of nitrogen dioxide with alkenes and polyunsaturated fatty acids: addition and hydrogen abstraction mechanisms. J. Am. Chem. Soc. 104:6685-6692, 1982.

48. Demopoulos, H. B. The basis of free radical pathology. Fed. Proc. 32:1879-1861, 1973.

49. Pryor, W. A. Free radical reactions and their importance in biochemical systems. Fed. Proc. 32:1862-1869, 1973.

50. Pryor, W. A. Free Radicals. McGraw-Hill, New York, 1966.

51. Kochi, J. K. Mechanism of organic oxidation and reduction by metal complexes. Science 155:415-424, 1967.

52. Barber, A. A.; Bernheim F. Lipid peroxidation: its measurement, occurrence, and significance in animal tissues. Advan. Gerontological Res. 2:355-403, 1967.

53. Mayo, F. R. Free-radical autoxidation of hydrocarbons. Acc. Chem. Res. 1:193-201, 1968.

54. Walling, C. Limiting rates of hydrocarbon autoxidations. J. Am. Chem. Soc. 91:7590-7594, 1969.

55. Dahle, L. K.; Hill, E. G.; Holman, R. T. The thiobarbituric acid reaction and the autoxidations of polyunsaturated fatty acid methyl esters. Arch. Biochem. Biophys. 98:265-261, 1962.

56. Farmer, E. H.; Koch, H. P.; Sutton, D. A. The course of autoxidation in polyisoprenes and allied compounds. Part V. Observations on fish-oil acids. J. Chem. Soc. 1943, 122-125.

57. Dumelin, E. E.; Tappel, A. L. Hydrocarbon gasses produced during in vivo peroxidation of polyunsaturated fatty acids and decomposition of preformed hydroperoxides. Lipids 8:194-198, 1973.

58. Burton, G. W.; Ingold, K. U. Autoxidation of biological molecules. 1. The antioxidant activity of vitamine E and related chain-breaking phenolic antioxidants in vitro. J. Am. Chem. Soc. 103: 6472-6477, 1981.

59. Chow, C. K.; Tappel, A. L. An enzymatic protective mechanism against lipid peroxidation damage to lungs of ozone-exposed dogs. Lipids 8:518-524, 1972.

60. Chow, C. K.; Tappel, A. L. Activities of pentose shunt and glycolytic enzymes in lungs of ozone-exposed rats. Arch. Environ. Health 26:205- 208, 1973.

61. Fridovich, I. Superoxide radicals and superoxide dismutase. Acc. Chem. Res. 5:321-326, 1973.

62. Beri, J. G.; Farrell, P. M. Vitamine E. in Vitamine and hormones, v. 34, pp. 31-74, Academic Press, New York, 1976.

63. Parker, J. E.; Slater, T. F.; Willson, R. L. Direct observation of a free radical interaction between vitamine E and vitamine C. Nature (London) 278:737-738, 1979.

64. Beri, J. G.; Farrell, P. M. β-Carotene: an unusual type of lipid antioxidant. Science 224:569-573, 1984.

CHAPTER 2

DETERMINATION OF OXYGEN-18 IN ORGANIC SUBSTANCES

Determination of the abundance of ^{18}O in organic materials requires conversion of oxygen to a volatile gas such as CO_2 or O_2 for mass spectrometric analysis (1). Up to now, several techniques for the preparation of carbon dioxide from oxygen in organic material have been described (2-7). Two problems commonly encountered have been i) inaccuracies linked to fractionation of the oxygen isotopes between two or more intermediates in the conversion pathway and ii) interferences arising from oxygen contamination. While these problems have been successfully overcome in procedures where the sample is pyrolyzed in a sealed nickel tube (7), such methods require a great deal of skilled manipulation and, at their present state of development, are limited to the analysis of compounds containing only carbon, hydrogen, and oxygen.

A general technique for oxygen isotopic analysis of physiological samples, which utilizes the Schutze-Unterzaucher procedure (8,9) for the preparation of carbon dioxide, is described in this chapter. In this procedure, organic oxygen is converted to carbon dioxide in a sequence of reactions: i) pyrolysis of the organic sample, ii) conversion (by equilibration with solid carbon at high temperature) of the oxygen-containing pyrolysis products to carbon monoxide, and iii) oxidation of the carbon monoxide by iodine pentoxide to produce carbon dioxide. An unavoidable blank and memory (2) associated with the pyrolytic production of CO, and the addition of oxygen from iodine pentoxide during the production of CO_2, complicate the isotopic analysis. Ultimately, the abundance of oxygen-18 in the initial sample must be reconstructed from that measured in carbon dioxide contaminated with oxygen from other sources. Interferences in the isotopic analysis arising from contamination of sample-oxygen have been addressed by the development of a mathematical model based on the physical processes occurring in the conversion of organically bound oxygen to carbon dioxide. The model facilitates accurate and precise determinations of oxygen-18 in organic material.

Determination of the effects of non-sample-derived oxygen requires the use of samples with known isotopic compositions. Because there is no standard method for analysis of oxygen isotopes in organic materials, no organic compounds which could be classified as "oxygen isotopic standards" have been available. To solve this problem, a procedure for the quantitative pyrolytic decarboxylation of aromatic carboxylic acids has been developed. The isotopic composition of the pyrolytically produced carbon dioxide can be measured directly, and the isotopic composition of the organic compound thus determined independently and accurately. These new standards have allowed accurate quantitation of contaminants and sensitive tests of the performance of the method.

Oxygen Isotopic Standards

Benzoic acid has been used to define optimum conditions for pyrolysis and to test the fidelity of the isotopic analysis. The major products of the thermal decomposition of benzoic acid are benzene and carbon dioxide. At approximately 500°C, decarboxylation of benzoic acid has been shown (10) to occur predominantly by a unimolecular process

$$C_6H_5COOH \rightleftharpoons C_6H_6 + CO_2 \qquad (2\text{-}1)$$

with small quantities of CO, H_2, and biphenyl being produced by minor side reactions involving radical intermediates. The occurrence of heterogeneous catalysis cannot be excluded (10), especially when group-VIII transition metals are present (11). Further, carbon dioxide produced by reaction 2-1 can also yield carbon monoxide if excess carbon is present (12)

$$CO_2 + C \rightleftharpoons 2CO \qquad (2\text{-}2)$$

Under the conditions that prevail during pyrolysis, reaction 2-1 is irreversible, whereas reaction 2-2 is reversible and may approach equilibrium.

The yield of carbon dioxide is affected by both processes. Kinetic isotope effects (KIE) associated with reaction 2-1, with both the forward and reverse processes in reaction 2-2, and an equilibrium isotope effect (EIE) associated with reaction 2-2 can shift the isotopic composition of the carbon dioxide from that of the carboxyl group if products other than CO_2 are formed from it during pyrolysis.

Pyrolysis of Benzoic Acid. With pyrolysis of benzoic acid, the yield and isotopic composition of the CO_2 were affected by pretreatment of the quartz tubes. If the quartz tubes were used without prior treatment, yields of carbon dioxide were low and variable (90 ± 5%), and the isotopic composition of the CO_2 was irreproducible (± 3‰). Use of the cleaning procedure described in the experimental section improved both the yield of carbon dioxide and the consistency of the isotopic analysis. Only quartz tubes treated by this procedure were used to obtain the results summarized here.

Samples of benzoic acid were pyrolyzed at 500, 550, and 600°C for 5, 10, 15, and 20 minutes. The yields and isotopic compositions of carbon dioxide are given in Table 2-1 and their variation with reaction conditions is graphically summarized in Figure 2-1. A maximum yield of approximately 97% was attained in 5 min at 600°C and at longer times

Table 2-1: Effect of Pyrolysis Time and Temperature on Yield and Isotopic Composition of Carbon Dioxide

time min	yield[a] %	$\delta^{13}C_{CO_2}$ vs PDB[a] ‰	$\delta^{18}O_{CO_2}$ vs SMOW[a] ‰
500°C			
5	76.1 ± 4.0	-32.71 ± 0.92	+25.72 ± 0.09
10	94.0 ± 0.4	-26.33 ± 0.14	+25.72 ± 0.03
15	95.2 ± 0.4	-25.93 ± 0.05	+25.68 ± 0.05
20	94.9 ± 0.1	-25.74 ± 0.02	+25.62 ± 0.04
550°C			
5	94.7 ± 0.1	-26.48 ± 0.13	+25.67 ± 0.02
10	98.4 ± 1.0	-25.56 ± 0.01	+25.61 ± 0.02
15	96.1 ± 0.4	-25.67 ± 0.04	+25.57 ± 0.03
20	94.0 ± 0.5	-25.51 ± 0.04	+25.66 ± 0.05
600°C			
5	98.8 ± 0.2	-25.56 ± 0.02	+25.59 ± 0.02
10	97.7 ± 0.1	-25.62 ± 0.08	+25.61 ± 0.13
15	93.5 ± 0.3	-25.64 ± 0.04	+25.30 ± 0.02
20	92.0 ± 0.2	-25.79 ± 0.04	+25.17 ± 0.05

[a] Means and standard errors of means of 3 replicate analyses.

Figure 2-1. Yield and isotopic composition of carbon dioxide produced by pyrolysis of benzoic acid. Each point indicates the mean and standard error of the mean of 3 replicate analyses: (●) 500°C, (■) 550°C, and (▼) 600°C.

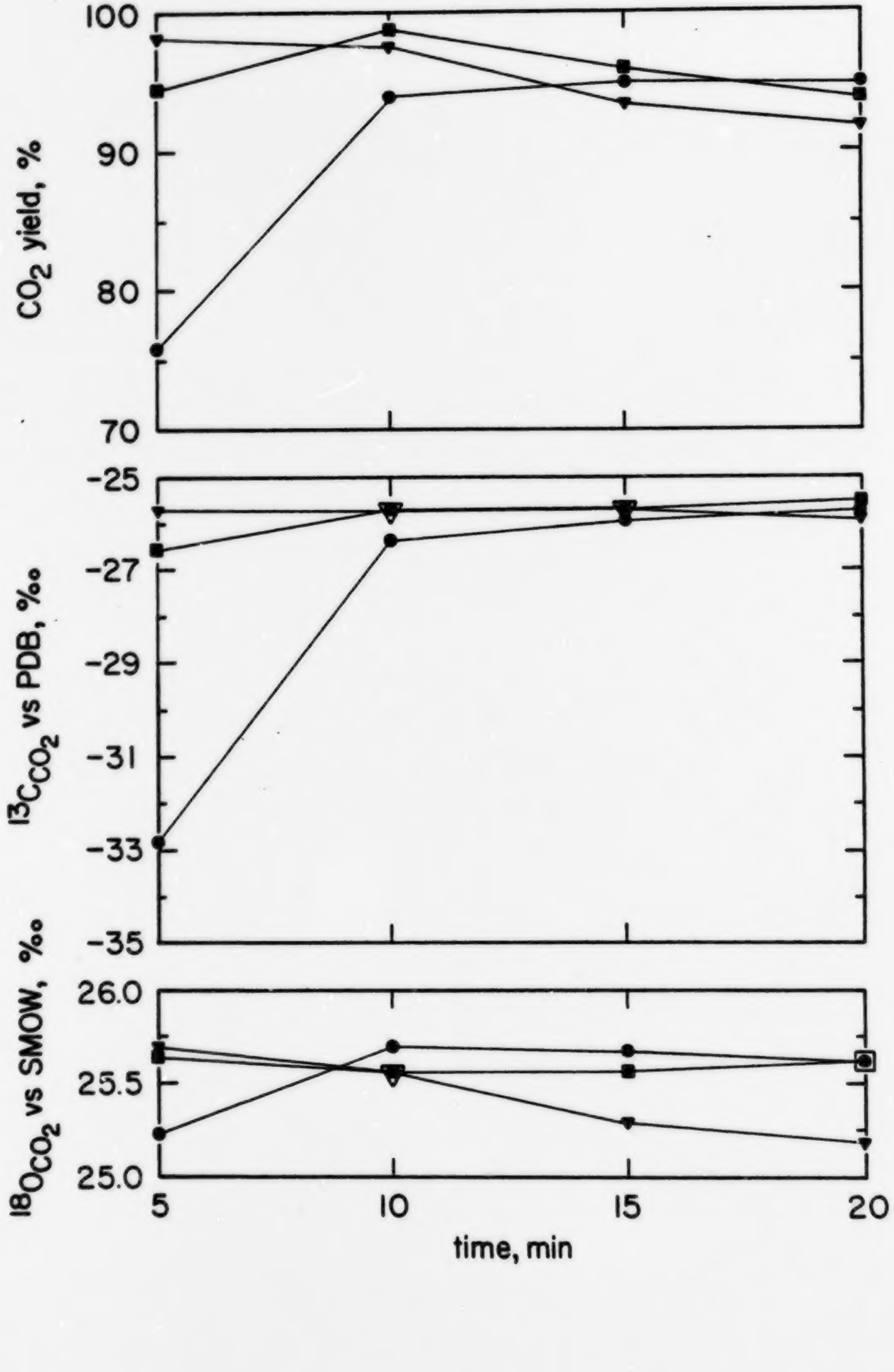
CO$_2$ yield, %
100
90
80
70
^{13}C$_{CO_2}$ vs PDB, ‰
-25
-27
-29
-31
-33
-35
^{18}O$_{CO_2}$ vs SMOW, ‰
26.0
25.5
25.0
5
10
15
20
time, min

for lower temperatures. Initial low yields of carbon dioxide were the result of incomplete decarboxylation; residual benzoic acid was observed. The systematic decrease in yield of CO_2 under more rigorous conditions was apparently associated with the partitioning of carbon and of oxygen between CO and CO_2 (reaction 2-2). In all cases, benzene (m/z 78) condensed on the inside of the quartz tube as it cooled. Carbon monoxide (m/z 27.9951) was also present in the liquid-nitrogen-noncondensible fraction of all samples.

A kinetic isotope effect is associated with decarboxylation. The decarboxylation of aromatic carboxylic acids in aqueous solution has been studied extensively (13-16). In general, the mechanism involves displacement of the carboxyl group by a proton. At low acidity, the rate-limiting step is protonation of the ring carbon to form a delocalized carbanion, and carbon isotopic fractionations are small. At high acidities, protonation is fast and the rate-limiting step is breaking of the C-C bond. Kinetic isotope effects range between 2.5 and 3.5% (13-16). For pyrolysis of benzoic acid at 500 and 550°C, initial low yields at short pyrolysis times (5 and 10 min, and 5 min, respectively) were accompanied by depletion of carbon-13 in the CO_2 (Fig. 2-1, Table 2-1). A carbon-12/carbon-13 kinetic isotope effect of approximately 1.5% was calculated from these results. The smaller value for the KIE is consistent with (i) the high temperature of the reaction and/or (ii) a concerted mechanism where the rate-limiting step involves intramolecular displacement of the carboxyl moiety by hydrogen. No secondary KIE for oxygen was observed.

The magnitude of isotopic fractionation between the carboxyl group and carbon dioxide depends on the magnitude of the isotope effect and the yield of CO_2. If decarboxylation were quantitative, no isotopic fractionation would occur, and the isotopic composition of the CO_2 would be identical to that of the carboxyl group. Isotopic fractionations diminished as decarboxylation approached completion. However, quantitative yields of CO_2 were never observed. A maximum yield was attained in 5 min at 600°C (98.8%), in 10 min at 550°C (98.4%), and in 15 min at 500°C (95.2%). At maximum yield, the carbon isotopic composition of the CO_2 was constant ($\delta^{13}C_{CO_2}$ vs PDB = $-25.65‰$). The isotopic composition of the oxygen in the CO_2 was independent of yield at 500 and 550°C ($\delta^{18}O_{CO_2}$ vs SMOW = $+25.64‰$). At 600°C, the oxygen-18 content decreased with yield. These variations in yield and oxygen-isotopic composition can be attributed to pyrolytic decomposition of CO_2 and an accompanying equilibrium isotope effect.

To examine isotopic fractionations associated with decomposition of CO_2, 30-μmole aliquots of CO_2 were transferred to quartz tubes and heated to 550°C for intervals of 5 to 30 minutes. The recoveries and isotopic compositions of the residual carbon dioxide are summarized in Table 2-2. Although small amounts of CO_2 were lost, no statistically significant isotopic shifts were observed ($p < 0.05$). However, the data in Table 2-2 suggest that decomposition of CO_2 under conditions of pyrolysis resulted in an enrichment of carbon-13 and a depletion of oxygen-18 in the residual carbon dioxide. These trends differ from those observed with pyrolysis of benzoic acid (Table 2-1, Fig. 2-1), and were probably due to a KIE associated with decomposition of CO_2 to CO (the forward process of reaction 2-2). Acceleration of reaction 2 in both directions in the presence of elemental carbon produced by decomposition of benzene during pyrolysis of benzoic acid (10) allows

Table 2-2: Recovery and Isotopic Composition of Carbon Dioxide Heated to 550°C in Quartz Tubes

time min	n	recovery[a] %	$\delta^{13}C_{CO_2}$ vs PDB[a] ‰	$\delta^{18}O_{CO_2}$ vs SMOW[a] ‰
0	5	100	-10.09 ± 0.09	+31.33 ± 0.04
10	4	99.8 ± 0.1	-9.96 ± 0.02	+31.28 ± 0.03
20	4	99.5 ± 0.2	-9.94 ± 0.03	+31.28 ± 0.02
30	4	99.4 ± 0.1	-9.92 ± 0.06	+31.27 ± 0.04

[a] Means ± standard errors of means of n replicate analyses.

this reaction to approach equilibrium. In this case, the isotopic compositions of the products are controlled by the equilibrium isotope effect associated with reaction 2-2.

Estimates of isotopic fractionations between carbon dioxide and carbon monoxide were obtained from calculations of the thermodynamic equilibrium constant and of the equilibrium oxygen isotopic fractionation factor for reaction 2-2 (Figure 2-2). The isotopic composition of the product gas mixture at 550°C was calculated using values of $^{16/18}\alpha = 1.000735$, $K = 0.12$. The temperature and pressure of the gas inside the quartz tube during pyrolysis were estimated assuming decarboxylation was quantitative. This calculation indicated that, at equilibrium, the composition of gases derived from the carboxyl group would be 94.1% CO_2 and 5.9% CO, resulting in a shift in the oxygen isotopic composition of the CO_2 from that of the carboxylic acid moiety of $\Delta\delta^{18}O_{CO_2}$ vs carboxylic acid = -0.30‰. Although the decrease in yield and the shift in isotopic composition observed during thermal decomposition of benzoic acid at 600°C (Table 2-1, Fig. 2-1) were significantly greater ($p > 0.05$) than the predicted values, the model calculations serve only to estimate isotopic fractionations arising from an EIE. The differences between the experimental and theoretical results are not serious. Since the rates of the forward and reverse steps in reaction 2-2 are temperature dependent (17), only at 600°C does this reaction approach equilibrium and do the isotopic fractionations become significant. Isotope effects associated with decarboxylation are unimportant when near-quantitative (maximum) yields of carbon dioxide are obtained. Only with pyrolysis at 600°C does the oxygen isotopic composition of carbon dioxide change significantly from that at maximum yield.

Figure 2-2. Calculated values for the thermodynamic equilibrium constant (K) and the equilibrium oxygen isotopic fractionation factor (α) for reaction 2 over the temperature range of 300 to 1500°K.

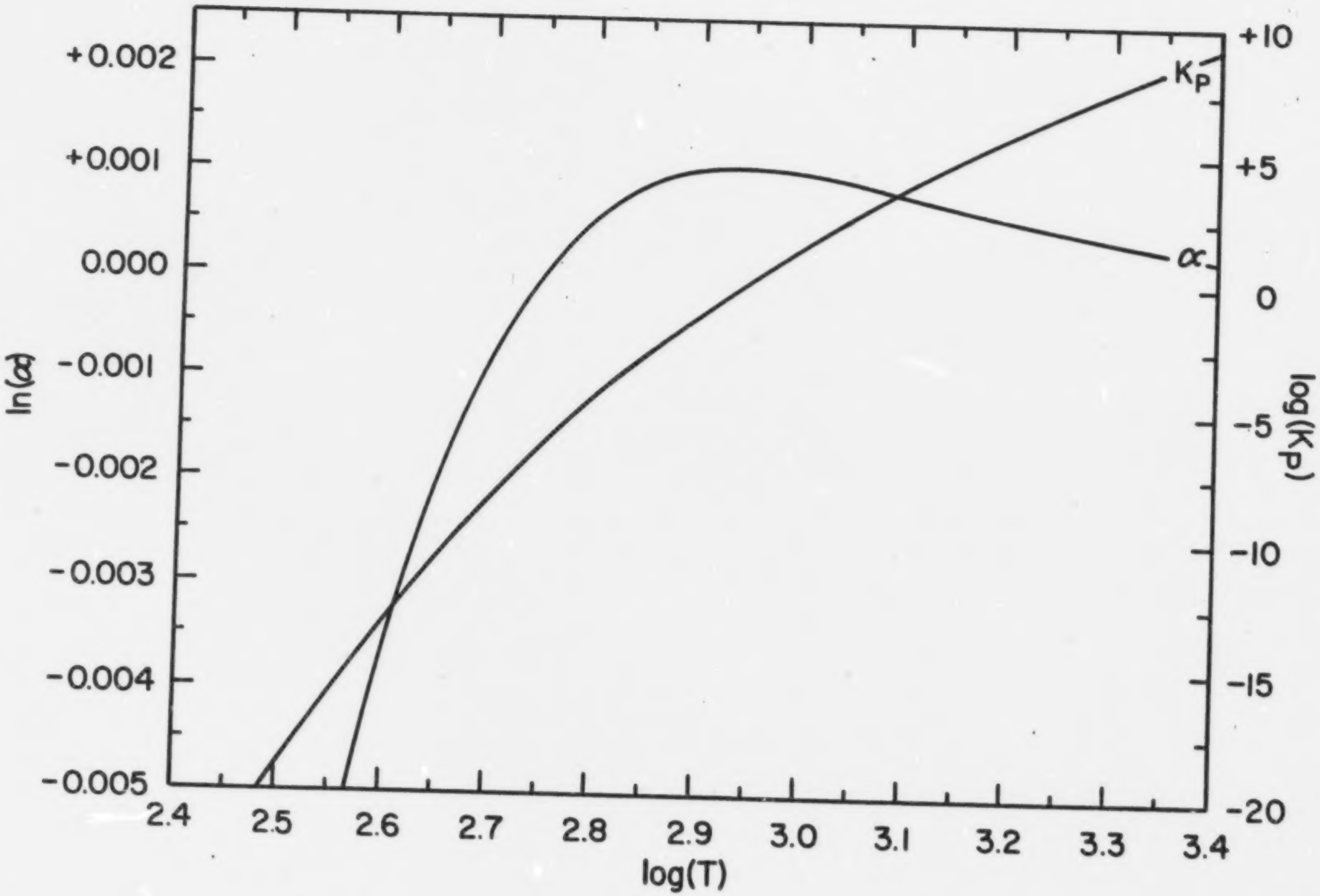
+0.002
+0.001
0.000
-0.001
-0.002
-0.003
-0.004
-0.005
ln(α)
2.4
2.5
2.6
2.7
2.8
2.9
3.0
3.1
3.2
3.3
3.4
log(T)
+10
+5
0
-5
-10
-15
-20
log(K_P)
K_P
α

Suitable conditions for isotopic analysis are those which result in no isotopic fractionation from either incomplete decarboxylation or production of carbon monoxide.. At 550°C there is a considerable range, between 10 and 20 minutes, where there is no apparent isotopic fractionation, which is ideal for isotopic analysis. Any combination of time and temperature of pyrolysis which gives a maximum, near-quantitative yield of carbon dioxide also satisfies the condition of minimal isotopic fractionation. The isotopic composition of the carbon dioxide is, therefore, identical to that of the carboxyl group.

Isotopic Standards. Results of isotopic analyses of CO_2 derived by replicate pyrolytic decarboxylations (550°C, 10 min) of five benzoic acids are summarized in Table 2-3. Isotopic analysis of CO_2 obtained by pyrolysis (550°C, 10 min) of 2,6-pyridinecarboxylic acid, pyrrole-2-carboxylic acid, and 2-thiophenecarboxylic acid are shown in Table 2-4.

MATHEMATICAL MODEL

The following description of the chemical processes involved in the production of carbon dioxide from organic material by the Schutze-Unterzaucher procedure explains the physical basis for the mathematical treatment.

Chemical Processes

Pyrolysis of organic material. Depending on the composition and the structure of the initial sample, pyrolysis products generated in the first step of the process may include CO, CO_2, H_2O, NO, COS, H_2, N_2, CH_4, and traces of H_2S and C_6H_6 (18,19). Some generalizations can be made about the pyrolytic behavior of specific oxygen functionalities. Carboxyl groups yield their oxygen predominantly in the form of carbon

Table 2-3: Analyses of Benzoic acid Standards

sample	%-yield[a]	$^{18}F_{CO_2}$ x 10^3 [a]
benzoic acid-0	97.0 ± 0.2	2.03548 ± 0.00015
benzoic acid-1	96.9 ± 0.2	2.04756 ± 0.00009
benzoic acid-2	96.5 ± 0.2	2.11813 ± 0.00015
benzoic acid-3	96.3 ± 0.3	2.18844 ± 0.00015
benzoic acid-4	96.2 ± 0.3	2.24562 ± 0.00040

[a] Means ± standard errors of means of 5 replicate analyses.

Table 2-4: Analysis of Heteroaromatic Carboxylic Acids

sample	%-yield[a]	$^{18}F_{CO_2} \times 10^3$ [a]
2,6-pyridine-dicarboxylic acid	99.1 ± 0.4	2.03740 ± 0.00017
pyrrole-2-carboxylic acid	95.6 ± 0.2	1.97134 ± 0.00006
2-thiophene-carboxylic acid	99.0 ± 0.2	1.97804 ± 0.00005

[a] Means ± standard errors of 5 replicate analyses.

dioxide, whereas aldehydes, ketones, and alcohols yield carbon monoxide. Carbohydrates are the only compounds to produce water in appreciable amounts. Traces of carbonyl sulfide are present when the sample contains organic sulfur. The interactions of the various oxygen-containing pyrolysis products with carbon in the second step are of central importance in formation of carbon monoxide and in the appearance of the blank and the memory.

Production of CO from pyrolysis products. A helium carrier gas is employed to sweep the pyrolysis products through a quartz tube packed with carbon and maintained at 1060°C. The oxygen-containing compounds react with the carbon surface to yield carbon monoxide as the thermodynamically favored product (12). This reaction proceeds through a surface-oxide intermediate. The reactions of interest are (20):

$$CO_2 + C \rightleftharpoons CO + C_x(O) \qquad \text{fast} \qquad (2\text{-}3)$$

$$2NO + 2C \rightleftharpoons N_2 + 2C_x(O) \qquad \text{fast} \qquad (2\text{-}4)$$

$$H_2O + C \rightleftharpoons H_2 + C_x(O) \qquad \text{fast} \qquad (2\text{-}5)$$

$$2COS + 2C \rightleftharpoons CS_2 + 2C_x(O) \qquad \text{fast} \qquad (2\text{-}6)$$

where $C_x(O)$ represents oxygen chemisorbed CO on the surface of the carbon and x is the number of atoms in the carbon matrix which participate in the surface-oxygen complex. The surface oxide then undergoes a unimolecular decomposition

$$C_x(O) \longrightarrow CO + C \qquad \text{slow} \qquad (2\text{-}7)$$

However, the carbon surface is microscopically heterogeneous, containing two physically distinct reaction sites (21-27): a short-lived intermediate that rapidly decomposes to yield carbon monoxide (reaction 2-3), and a more stable surface oxide (reaction 2-7) in which oxygen is strongly adsorbed to the surface (25). The activation energy for desorption at both sites is inversely proportional to the local surface coverage (23,26,27). Thus, oxygen accumulates on the carbon surface as chemisorbed carbon monoxide.

Reactions 2-3 through 2-6 mediate the exchange of oxygen between the carbon surface and the gas phase. Desorption of CO from the surface (reaction 2-7) is rate limiting in the formation of carbon monoxide, and is essentially irreversible (25), whereas reaction 2-3 is readily reversible (22-24) during the time when the pyrolysis products are in contact with carbon. Thus, any oxygen entering the system will be distributed between the surface oxide and gaseous carbon monoxide. As multiple samples are sent through the reactor, slow desorption of carbon monoxide effectively generates a sorbed-oxygen pool charged with oxygen from previous inputs. As subsequent samples are produced, exchange of oxygen with this pool can buffer the isotopic composition of the carbon monoxide produced.

The analytical blank. The blank arises from a reaction between carbon and silica (the quartz tube used to contain the carbon bed). A direct interaction

$$SiO_2 + C \longrightarrow CO + SiO + C \qquad (2\text{-}8)$$

is apparently of minimal importance (28). Significant amounts of carbon monoxide are produced by reaction 2-8 at temperatures in excess of 1200°C, but a large blank is observed at lower temperatures. A process involving a silicon-hydroxyl moiety as the active oxygen species

$$2SiO(OH) + 2C \longrightarrow 2CO + 2SiO + H_2 + 2C \qquad (2\text{-}9)$$

has a lower overall energy of activation and could explain the blank observed at lower temperatures. Surface hydroxyl groups are likely to be produced by reaction of acidic gases and H_2, produced in the pyrolysis reactor, with the walls of the quartz tube (20):

$$SiO_2 + HX \longrightarrow SiO(OH) + X \qquad (2\text{-}10)$$

Due to its lower energy requirements, a mechanism involving reactions 2-9 and 2-10 is a more likely explanation of the blank (20).

Two factors influence the magnitude of the blank: contact between carbon and the quartz tube in the pyrolysis reactor, and the temperature of the the reactor in the region of the contact. Each has been utilized by other investigators in schemes to reduce the blank. The quartz tube has been lined with platinum foil (2) to separate the carbon from the quartz, but carbon from the sample is inevitably deposited on the internal surface of the tube in the region where it undergoes volatilization and initial pyrolysis. Smaller blanks are observed at temperatures below 1200°C, but use of a metal catalyst in direct contact with the carbon is required to ensure a quantitative yield of carbon monoxide in a dynamic system (20). The metal on the carbon surface acts as a catalyst for reaction 2-7, increasing the rate of evolution of carbon monoxide at the lower temperature (26,29).

The presence of low levels of a volatile chlorinated hydrocarbon in the carrier gas has been found to improve the yield and reduce the tailing of carbon monoxide (30). The mechanism leading to this improvement is not known. However, acidic gases are adsorbed by carbon (31), and it seems likely that HCl produced by pyrolysis of the halocarbons

(19) competes successfully for sorption sites on the carbon surface. As a result, interferences arising from the sorbed-oxygen pool are reduced and stabilized.

Oxidation of CO to yield CO$_2$. Carbon monoxide produced in the pyrolysis reactor is oxidized to carbon dioxide as it is swept through a tube packed with iodine pentoxide (9) and maintained at 120°C. Under these conditions, hydrocarbons, methane in particular, are not oxidized by I_2O_5, nor is oxygen exchanged between either carbon monoxide or carbon dioxide and the reagent (2). Therefore, no interferences to the isotopic analysis other than the addition of oxygen from iodine pentoxide accompany this reaction.

Isotopic Mass Balance

An isotopic mass balance is required to understand the relationship between the isotopic composition of carbon dioxide produced by the Schutze-Unterzaucher procedure and those of the components of the carbon dioxide-oxygen pool. The mass-balance equations must reflect the specific reactions that result in the production of carbon dioxide from an organic material. As noted in Figure 2-3, oxygen in the carbon dioxide derives from several sources: the sample being analyzed, previous samples (memory effect), silica in the quartz tube which contains the carbon packing (blank), and iodine pentoxide.

Mass Balance for CO. The abundance of oxygen-18 in the total oxygen pool is the weighted sum of the abundances in each component. The mass-balance equations are

$$n_T{}^{18}F_T = n_S{}^{18}F_S + n_Q{}^{18}F_Q + \Sigma n_j{}^{18}F_j \qquad (2\text{-}11)$$

and

Figure 2-3. Schematic representation of the production of CO_2 from an organic sample. The sorbed-oxygen pool is represented by $\{C_x(O)\}$. Oxygen from the present sample, from previous samples (memory), and from the quartz tube (blank) are incorporated in the carbon monoxide through the surface-oxide. Carbon monoxide is oxidized to carbon dioxide by I_2O_5 with the addition of a single atom of oxygen to each molecule of CO.

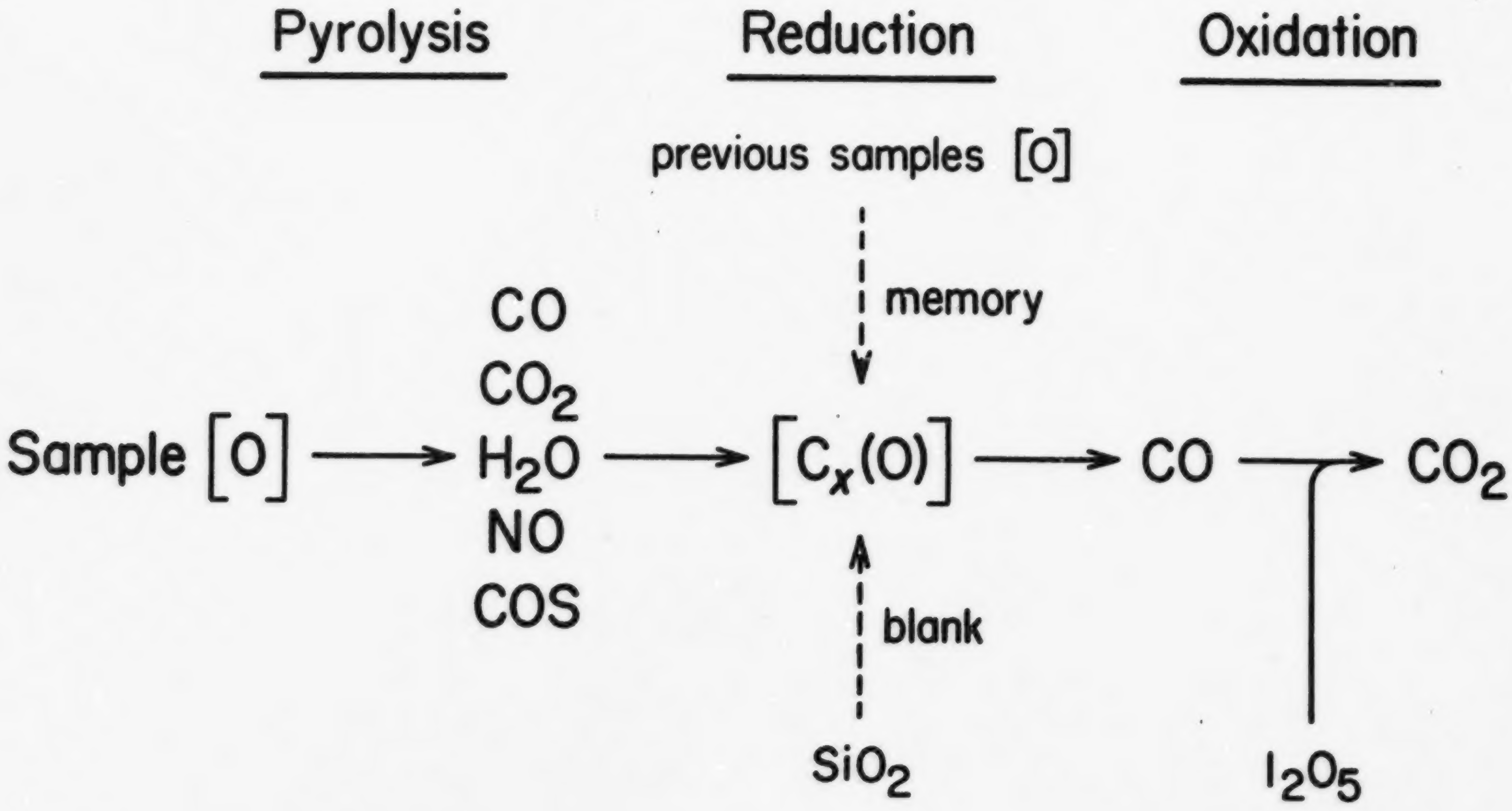
Pyrolysis
Reduction
Oxidation
previous samples [O]
memory
Sample [O]
CO
CO_2
H_2O
NO
COS
$[C_x(O)]$
CO
CO_2
blank
SiO_2
I_2O_5

$$n_T = n_S + n_Q + \Sigma n_j \tag{2-12}$$

where ^{18}F is the fractional abundance of oxygen-18 and n is the amount of oxygen (μmol O). The subscript T designates the total oxygen pool; S designates oxygen derived from the sample itself; Q is used to designate oxygen from the blank, thought to be derived largely from the quartz reactor tube; and j is used to designate oxygen derived ultimately from a previous sample carrying the index j, that is, a "memory effect" (32). Only a finite number of samples is considered to be significant in the sorbed oxygen pool.

An expression for the fractional abundance of oxygen-18 in the carbon monoxide can be obtained if it is assumed that no isotopic fractionation accompanies the partitioning of oxygen between the gas phase and the sorbed phase in the reduction reactor. The carbon monoxide is then a representative sample of the total oxygen pool, $^{18}F_{CO} = {}^{18}F_T$, and equations 2-11 and 2-12 yield the following relationship

$$^{18}F_{CO} = \frac{^{18}F_S + (n_Q{}^{18}F_Q + \Sigma n_j{}^{18}F_j)\cdot 1/n_S}{1 + (n_Q + \Sigma n_j)\cdot 1/n_S} \tag{2-13}$$

where $^{18}F_{CO}$ is the fractional abundance of oxygen-18 in the carbon monoxide oxygen pool. Equation 2-13 can be rearranged to yield the fractional abundance of oxygen-18 in the sample:

$$^{18}F_S = {}^{18}F_{CO} + \{n_Q({}^{18}F_{CO} - {}^{18}F_Q) + \Sigma n_j({}^{18}F_{CO} - {}^{18}F_j)\}\cdot 1/n_S \tag{2-14}$$

The perturbation caused by each contaminant oxygen pool is a function of i) the difference in isotopic composition between the sample and the contaminant, and ii) the mole fraction of the contaminant in the total oxygen pool.

Mass Balance for CO_2. The oxidation of carbon monoxide by iodine pentoxide results in the combination of two oxygen pools of equal size

$$n_{CO_2}{}^{18}F_{CO_2} = n_{CO}{}^{18}F_{CO} + n_I{}^{18}F_I \qquad (2\text{-}15)$$

$$n_{CO_2} = n_{CO} + n_I \qquad (2\text{-}16)$$

$$n_{CO} = n_I \qquad (2\text{-}17)$$

where the subscripts (CO_2 and I) designate the total carbon-dioxide oxygen pool and that portion of it derived from iodine pentoxide, respectively. It follows that, since the size of the oxygen pool is doubled, isotopic fluctuations in the carbon monoxide are reduced by a factor of two in the carbon dioxide:

$${}^{18}F_{CO} = 2\cdot{}^{18}F_{CO_2} - {}^{18}F_I \qquad (2\text{-}18)$$

Note that ${}^{18}F_I$ is the only quantity required for definition of the relationship between ${}^{18}F_{CO}$ and ${}^{18}F_{CO_2}$.

Combining equations 2-13 and 2-18 yields a relationship which relates the isotopic composition of the carbon dioxide to those of its component oxygen pools:

$$2\cdot{}^{18}F_{CO_2} = \frac{{}^{18}F_S + (n_O{}^{18}F_O + \Sigma n_j{}^{18}F_j)\cdot 1/n_S}{1 + (n_O + \Sigma n_j)\cdot 1/n_S} \qquad (2\text{-}19)$$

Equation 2-19 summarizes the dependence of the analytical result on experimental parameters, only one of which is the isotopic composition of the sample. The relationship between ${}^{18}F_S$ and ${}^{18}F_{CO_2}$ is complex. In particular, it will be different for each sample because the isotopic composition of the sorbed oxygen pool depends on the history of the reactor. Nevertheless, if all other terms in equation 2-19 are known, ${}^{18}F_S$ can be calculated from observed values of ${}^{18}F_{CO_2}$. In practice, it is most convenient to use equations 14 and 16 to calculate ${}^{18}F_S$.

Determination of Correction Parameters

In devising a procedure to determine ${}^{18}F_I$, ${}^{18}F_Q$, n_Q, and an expression for n_j it is helpful to consider the relationship between ${}^{18}F_{CO_2}$ and ${}^{18}F_S$ for each member in a series of analyses of a single material where each sample differs only in size. Equation 2-19 indicates the effects of each parameter on the observed results. A plot of $2 \cdot {}^{18}F_{CO_2}$ as a function of $1/n_S$ for a hypothetical series of replicate analyses of a single organic material with a true isotopic composition, ${}^{18}F_S$, is shown in Figure 2-4. Several different curves appear as a result of changes in the isotopic composition of the sorbedoxygen pool. If a sample is infinitely large ($1/n_S$ approaches zero), the effects of the blank and the memory will be insignificant. Accordingly, all curves converge to a common y-intercept at ${}^{18}F_S + {}^{18}F_I$. For samples of finite size, curve A represents the locus of all possible results of the first analysis in the series, curve B the second, curve C the third, etc.. Each curve is displaced from its predecessor because each sample changes the isotopic composition of the sorbed oxygen pool, making it more like that of the sample. A small input affects the sorbed oxygen pool less strongly than a large one; therefore, as shown in Figure 2-4, the magnitude of the shift between curves depends on the size of the previous sample (recall that a small value of 1/n corresponds to a large sample). Curve Z defines the limit reached when, after repeated analyses of a single material, the isotopic composition of the sorbed-oxygen pool differs from that of the input sample only due to

Figure 2-4. Results predicted for a plot of $2\cdot{}^{18}F_{CO_2}$ vs. 1/n for replicate analyses (A, B, C, D, ... , Z) of an organic compound with a true isotopic composition of ${}^{18}F_S$. Equation 2-17 defines the locus of all possible results for a single analysis. In this example, both the blank and the initial sorbed-oxygen pool have been assumed to be depleted in oxygen-18 relative to the sample, so all analyses fall below ${}^{18}F_S + {}^{18}F_I$, the y-intercept. Curve Z defines the limit where memory effects have been eliminated by the continuous, repetitive processing of samples of the same material.

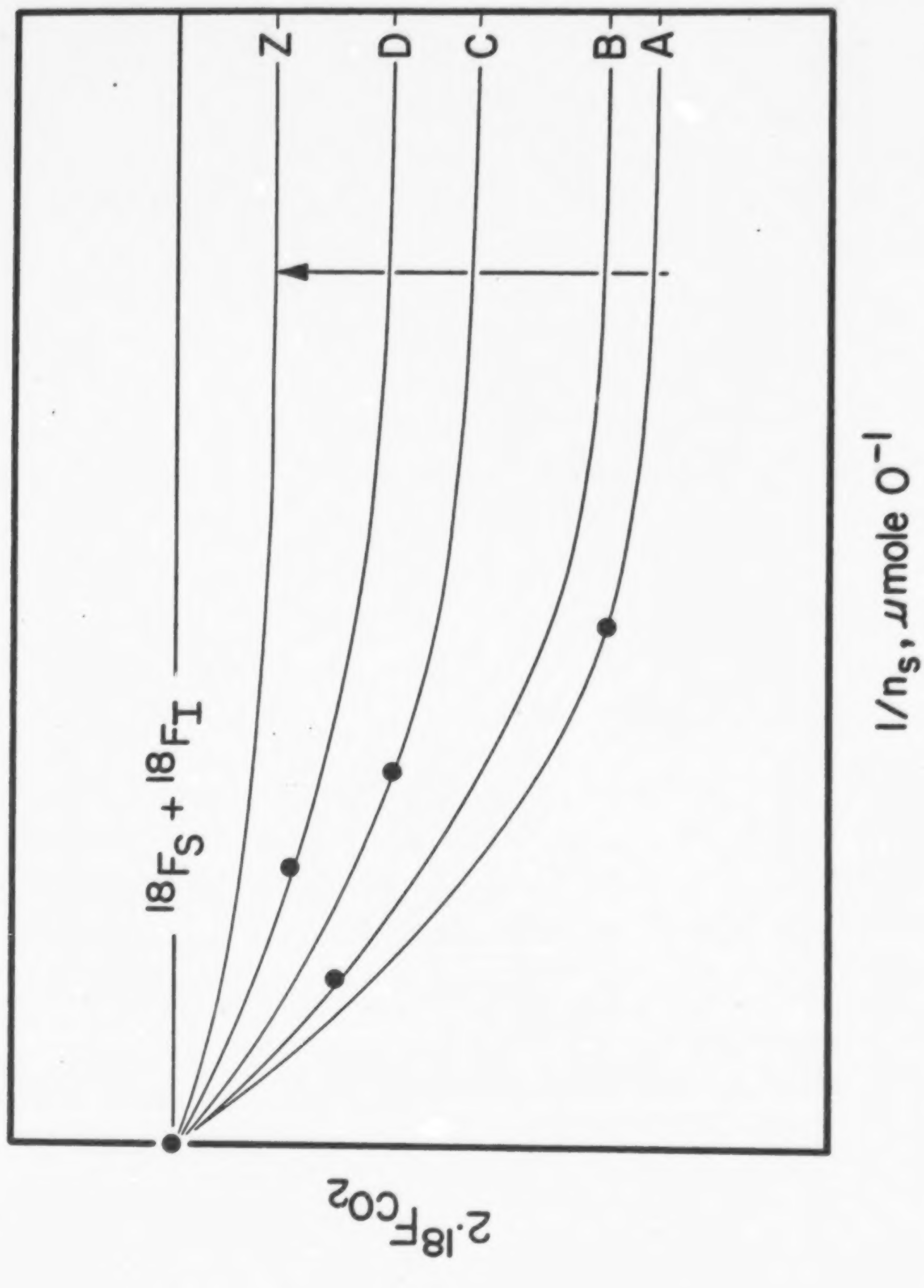
$^{18}F_S + ^{18}F_I$
Z
D
C
B
A
$2 \cdot ^{18}F_{CO_2}$
$1/n_s$, μmole O^{-1}

contributions from the blank. The condition where the effects of memory have been suppressed by saturation of the sorbed-oxygen pool with oxygen from the sample will be referred to as "memory equilibration". In the construction of Figure 2-4, it was assumed that both the isotopic composition of the blank and the sorbed-oxygen pool were depleted in oxygen-18 with respect to the sample.

Values of the correction parameters (*i. e.*, all terms in equation 2-19 except $^{18}F_I$, $^{18}F_{CO_2}$, and n_S) can be determined from results of analyses of materials for which $^{18}F_S$ is known. However, since the terms used to correct for the blank and the memory are not separable an iterative procedure is required. In practice, it is useful to manipulate experimental conditions so that the effects of the blank or the memory are maximized in a particular experiment, thus improving the precision with which the correction parameters can be determined.

An outline of the procedure used to determine $^{18}F_I$, $^{18}F_Q$, n_Q, and an expression for n_j is shown in Figure 2-5. Initial estimates of $^{18}F_I$, $^{18}F_Q$, and n_Q are obtained from a single experiment in which memory equilibrium has been established (step I). Subsequently, the effects of the memory can be quantitated in a separate experiment (step II). These estimates are then refined by a procedure of successive approximations until the values for all parameters converge within predetermined limits (step III). A detailed description of this procedure follows.

Blank and I_2O_5-added Oxygen. Under conditions of memory equilibration, the difference between $^{18}F_S$ and $^{18}F_{CO_2}$ is controlled by the isotopic composition and relative size of the blank and by the isotopic composition of the oxygen derived from the I_2O_5. The latter quantity ($^{18}F_I$) can be determined from the y-intercept of a plot of

Figure 2-5. Flow-chart of the procedure for determining the correction parameters.

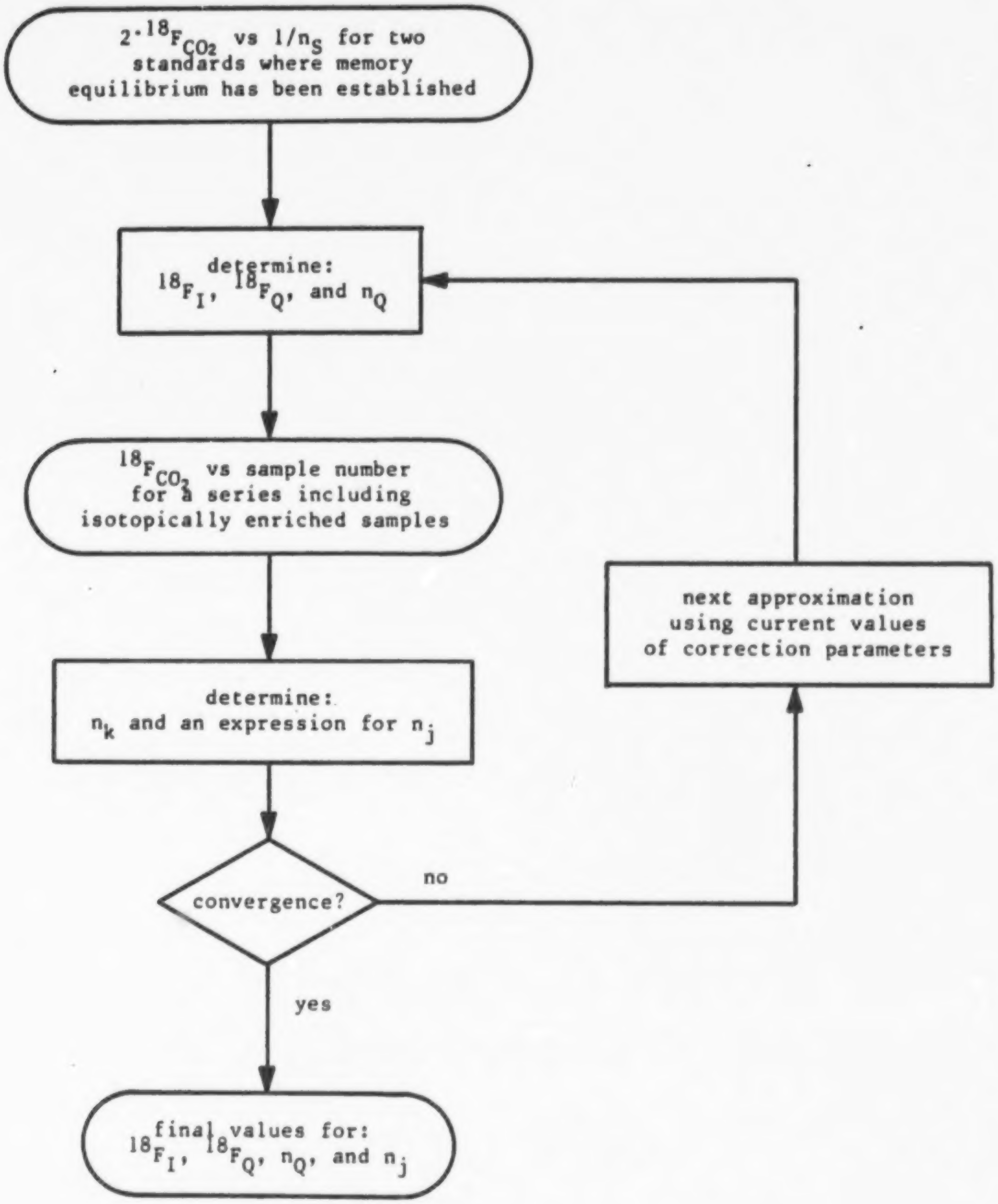
$2 \cdot {}^{18}F_{CO_2}$ vs $1/n_S$ for two standards where memory equilibrium has been established
determine: ${}^{18}F_I$, ${}^{18}F_Q$, and n_Q
${}^{18}F_{CO_2}$ vs sample number for a series including isotopically enriched samples
determine: n_k and an expression for n_j
convergence?
no
yes
next approximation using current values of correction parameters
final values for: ${}^{18}F_I$, ${}^{18}F_Q$, n_Q, and n_j

$2 \cdot {}^{18}F_{CO_2}$ vs $1/n_S$ if ${}^{18}F_S$ is known:

$$\{\text{y-intercept}\} = {}^{18}F_S + {}^{18}F_I \tag{2-20}$$

The size and the isotopic composition of the blank are determined from memory-equilibrated curves for two samples of different but known isotopic compositions. Comparison of difference between the observed and true isotopic compositions (${}^{18}F_{CO_2}$ and ${}^{18}F_S$) at a particular value of n_S gives n_Q

$$n_Q = (n_S + \Sigma n_j) \cdot \left(\frac{\Delta {}^{18}F_S}{\Delta {}^{18}F_{CO_2}} - 1 \right) \tag{2-21}$$

where Σn_j is set equal to zero in the first approximation. The isotopic composition of the blank can be determined from the slope at a particular value of n_j by differentiating equation 2-19 with respect to $1/n_S$ and setting the ${}^{18}F_j = {}^{18}F_S$ to express the condition of memory equilibration:

$$\{\text{slope}\} = \frac{n_Q({}^{18}F_Q - {}^{18}F_S)}{\{1 + (n_Q + \Sigma n_j) \cdot 1/n_S\}^2} \tag{2-22}$$

However, these solutions are not independent of n_j, a parameter whose values are, furthermore, unknown at this point. An iterative procedure can be adopted to derive a consistent set of correction parameters once the characteristics of the memory have been derived.

Memory. The amount of a previous sample which is present in the sorbed oxygen pool at any time is a function of the size of that sample and of the rate of its displacement by subsequent throughputs. As an approximation

$$n_j = n_{j,0} \cdot f(j) \qquad (2\text{-}23)$$

where $n_{j,0}$ is the initial size of the jth previous sample and f(j) is an exponential function of the index, j. The quantitative characteristics of f(j) cannot easily be derived from a specific model of the sorbed oxygen pool since the surface oxide is heterogeneous. In practice, the exponential function which best describes the wash-out of a particular sample (see below) is determined empirically (32).

The turnover of oxygen in the sorbed oxygen pool can be determined by examining the response of the system to isotopic perturbations (32). In this approach, a series of samples of known isotopic composition ($^{18}F_1$) is interrupted by an input of material highly enriched in oxygen-18 ($^{18}F_2$). If the sizes of the samples are constant, then the amount of oxygen from the enriched input appearing in the k-th sample after that input is given by

$$n_k = (n_S + \Sigma n_j)\left[\frac{^{18}F_{CO} - {}^{18}F_1}{^{18}F_2 - {}^{18}F_1}\right] + \left[\frac{^{18}F_{CO} - {}^{18}F_Q}{^{18}F_2 - {}^{18}F_1}\right] \qquad (2\text{-}24)$$

where $^{18}F_{CO}$ is calculated using equation 2-13. Since f(j) is initially unknown, values for n_j cannot be determined and, in the first approximation, are set equal to zero in equations 2-13 and 2-24. The values of n_k are then fit to an exponential function of the index (j). Further approximations are obtained by using equation 2-23 to calculate values for n_j in equations 2-13 and 2-24 and recalculating values for n_k.

It is also possible that more than one enriched sample appears in the series. In this case, equation 2-24 must be modified to account for the introduction of multiple isotopic perturbations at different times. The most recent enriched sample causes the greatest shift in $^{18}F_{CO_2}$, so its effects alone are considered explicitly. Components from all previous enriched samples are grouped in a single summed term which treats these effects as a small contribution to the observed shift

$$n_k = (n_S + \Sigma n_j)\left[\frac{^{18}F_{CO} - {}^{18}F_1}{^{18}F_2 - {}^{18}F_1}\right] + n_j \cdot \left[\frac{^{18}F_{CO} - {}^{18}F_Q}{^{18}F_2 - {}^{18}F_1}\right] - \Sigma H_j n_j \qquad (2\text{-}25)$$

where $H_j = 1$ when j corresponds to an enriched sample prior to the most recent and $H_j = 0$ for all other samples, independent of their isotopic composition. As in the previous example, initial estimates of n are obtained by setting $n_j = 0$ and only isotopic perturbations caused by the most recent enriched sample are considered in the calculation of n_k. This procedure is only an expedient adopted during study of the sorbed-oxygen pool. Once the functional form of f(j) has been specified, the effects of all previous enriched samples enter into the calculation.

To complete the procedure, the first approximations of $^{18}F_I$, n_Q, $^{18}F_Q$, and n_j are used to calculate values for all unspecified terms. The procedure is repeated until convergent values for all correction parameters are obtained.

Adjustment of Analytical Results

Application of the correction procedure can be visualized most simply in terms of equations 2-14, 2-18, and 2-23. Since $^{18}F_I$ is known, $^{18}F_{CO}$ can be determined from equation 2-18. The characteristics of the blank (n_Q and $^{18}F_Q$) and of the memory (n_j) have been determined directly by the procedure outlined above. Solution of equation 2-14 for $^{18}F_S$ requires, in addition, values for n_S and $^{18}F_j$. The size of the sample (n_j) is determined from the elemental analysis, and values for $^{18}F_j$ are given by the results of previous analyses in the series. Equation 2-23 is used to determine values for n_j, and $^{18}F_j$ is, in each case, set equal to $^{18}F_S$ for the j-th previous sample.

In the correction of a series of analytical results, equations 2-14 and 2-16 are used to calculate values of $^{18}F_S$ based on the final set of correction parameters and the observed values of $^{18}F_{CO_2}$. The initial isotopic composition of the sorbed oxygen pool is assumed to be that of atmospheric O_2 ($^{18}F_{AIR} = 2.04435 \times 10^{-3}$) because the introduction of air into the system is unavoidable when the sampling head is loaded. Values for $^{18}F_S$ are calculated sequentially. In this way, values for n_S and $^{18}F_S$ for all previous samples are available and provide the information necessary to correct for the effects of the memory. A limit of 30 is placed on the index j. Software allowing rapid completion of these calculations has been developed.

Refinement of correction parameters. The inclusion of three samples of a working standard in each sequence of analyses allows refinement of parameters initially determined using the more elaborate procedure outlined above. It is of particular interest to check the values assigned to $^{18}F_I$ and n_Q. The procedure is graphically summarized in Figure 2-6. The value assigned to n_Q is adjusted until the value calculated for $^{18}F_S$ is independent of n_S. Because the true value of $^{18}F_I$ is known, the value assigned to $^{18}F_Q$ can then be checked using equations 2-14 and 2-18.

Oxygen Isotopic Analysis

Two benzoic-acid standards (designated 0 and 1 in Table 2-3), and samples of glycine at natural abundance and enriched in oxygen-18 were used in the evaluation of the correction parameters. In subsequent

Figure 2-6. A schematic illustration of the method for refinement of values for $^{18}F_I$ and n_Q. The latter parameter is first adjusted to minimize the sum of the residuals noted here as ΔF. The value of $^{18}F_I$ is then adjusted until the calculated value of $^{18}F_S$ matches the known value.

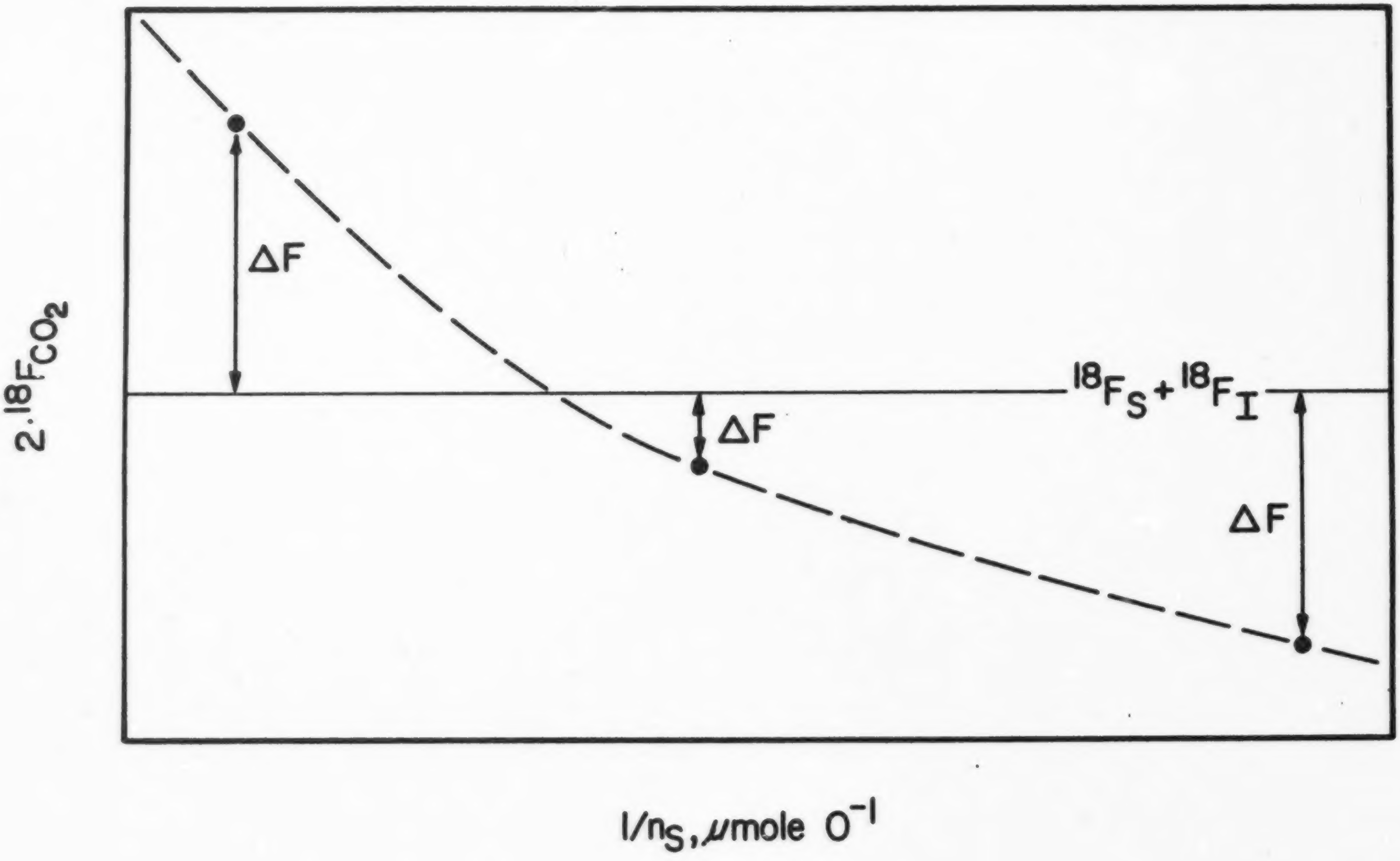

$2 \cdot {}^{18}F_{CO_2}$
ΔF
ΔF
${}^{18}F_S + {}^{18}F_I$
ΔF
$1/n_S$, μmole O^{-1}

tests, the benzoic acid samples listed in Table 2-3, the three heteroaromatic carboxylic acids (pyrrole-2-carboxylic acid, 2-thiophene carboxylic acid, and 2,6-pyridine dicarboxylic acid), and three primary standard water samples, SMOW, NBS-1, and NBS-1A, were used to determine the accuracy and precision of this technique.

Yield of Carbon Dioxide

Manometric techniques were employed to determine the yield of carbon dioxide from the Schutze-Unterzaucher procedure for samples of from 3 to 60 μmoles oxygen. Quantitative yields of carbon dioxide were obtained from samples containing less than 50 μmoles oxygen at I_2O_5-reactor temperatures above 125°C (see Figure 2-7). Incomplete yields of carbon dioxide were obtained at lower temperatures even though the thermal conductivity detector just downstream from the pyrolysis reactor indicated that quantitative yields of CO were being produced. It is evident, therefore, that oxidation of CO to CO_2 by iodine pentoxide can be slow and can lead to non-quantitative yields of carbon dioxide at the flow rate required by the analyzer (25 mL/min.). The isotopic composition of the CO_2, however, did not vary even when the oxidation of CO was incomplete. This result demonstrates that isotope effects in the oxidation of carbon monoxide by iodine pentoxide are minimal. During routine analyses, the temperature of the iodine pentoxide was maintained between 120 and 140°C to insure quantitative yields.

Correction Parameters

Blank, I_2O_5. Values of $^{18}F_Q$, n_Q, and $^{18}F_I$ were determined by five replicate analyses each of samples of benzoic acid designated 0 and 1 in Table 2-3 (step I). The sample sizes in each set of analyses varied

Figure 2-7. A plot of yield of carbon dioxide (μmole CO_2) vs oxygen input (μmole O) for sucrose at various temperatures of the I_2O_5 reactor: 25°C (●), 50°C (■), 75°C (▲), 100°C (○), and 125°C (□).

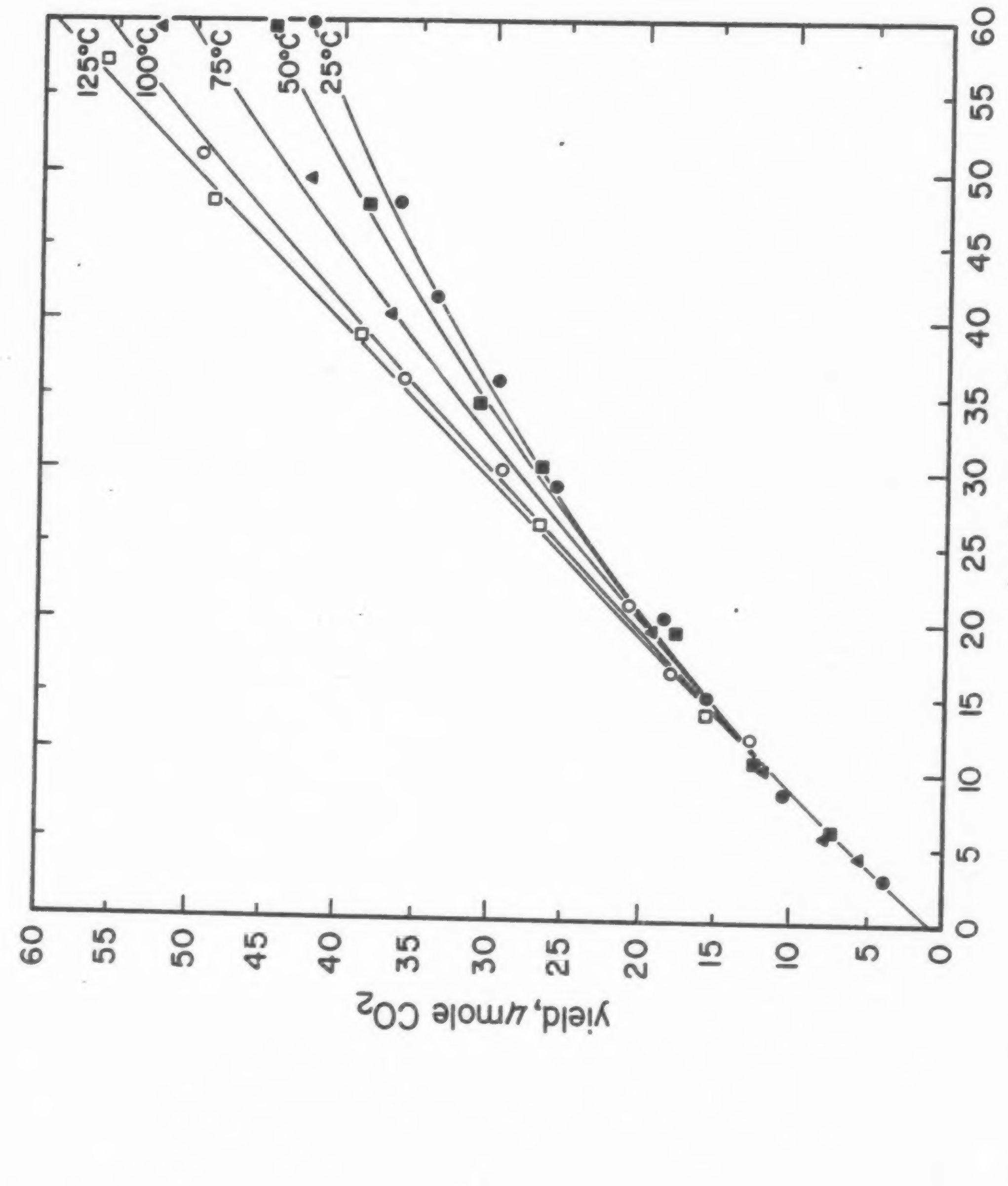
yield, μmole CO$_2$
input, μmole O
0
5
10
15
20
25
30
35
40
45
50
55
60
125°C
100°C
75°C
50°C
25°C

from 30 to 2 μmol O. Memory equilibration was obtained by processing five samples containing 40 μmol O of the same material prior to each set. A plot of $2\cdot{}^{18}F_{CO_2}$ vs $1/n_S$ for these data is shown in Figure 2-8. The curves were obtained by fitting each set of data to an equation of the form $y = \{({}^{18}F_S + Ax)/(1 + Bx)\} + C$ (that is, the form of equation 2-19).

The isotopic composition of the iodine pentoxide-derived oxygen was determined from the y-intercept of each curve (equation 2-20). The size of the blank was determined from the difference between the two curves at $1/n_S = 0.1$ $(\mu\text{mol O})^{-1}$ (equation 2-21), and the isotopic composition of the blank was determined from the slope of each curve at the same point (equation 2-22). These results are shown in the "initial estimates" column of Table 2-5.

Memory. The washout of a single contribution to the sorbed-oxygen pool was quantitated by analysis of a series of 23 samples of glycine which was interrupted at positions 9 and 16 with glycine highly enriched in oxygen-18 (step II). Results are summarized Figure 2-9. The contribution (n_j) of the enriched sample to each total oxygen pool was initially determined using equation 2-25. The values of n_j were fit to an equation of the form $f(j) = a(j)^b$ (32). Once initial estimates of a and b were established, equation 2-23 was used to calculate values for n_j in equation 2-24, and values for a and b were refined.

Values for ${}^{18}F_I$, ${}^{18}F_Q$, and n_Q were then recalculated using these values of a and b to specify n in equations 2-21 and 2-22 (step III). The results appear in the "first iteration" column in Table 2-5. Three iterations were necessary to obtain convergent values for the correction parameters (Table 2-5). For every recalculation ${}^{18}F_I$, ${}^{18}F_Q$, and n_Q,

Table 2-5: Iterative determination of correction parameters

		initial estimates	iterative determinations[a]		
			1	2	3
$10^3 \times {}^{18}F_I$		1.9895	1.9895	1.9895	1.9895
$10^3 \times {}^{18}F_Q$		2.0413	1.9766	1.9745	1.9750
n_Q		0.71	1.00	1.01	1.02
	1	0.072	0.080	0.081	
a	2	0.080	0.081	0.082	0.081
	3	0.082	0.081	0.081	
	1	-1.80	-1.56	-1.60	
b	2	-1.72	-1.61	-1.60	-1.60
	3	-1.75	-1.61	-1.60	

[a] Three iterations of the memory-correction parameters (a and b) were performed for each refinement of the blank parameters (n_Q and ${}^{18}F_Q$).

Figure 2-8. A plot of $2 \cdot {}^{18}F_{CO_2}$ vs. $1/n_S$ for five replicate analyses of two benzoic acids, ${}^{18}F_{BA-0} = 2.03547 \times 10^{-3}$ and ${}^{18}F_{BA-1} = 2.04757 \times 10^{-3}$; uncorrected: BA-0 (■), BA-1 (●); corrected for the blank and the I_2O_5-added oxygen: BA-0 (□), BA-1 (○).

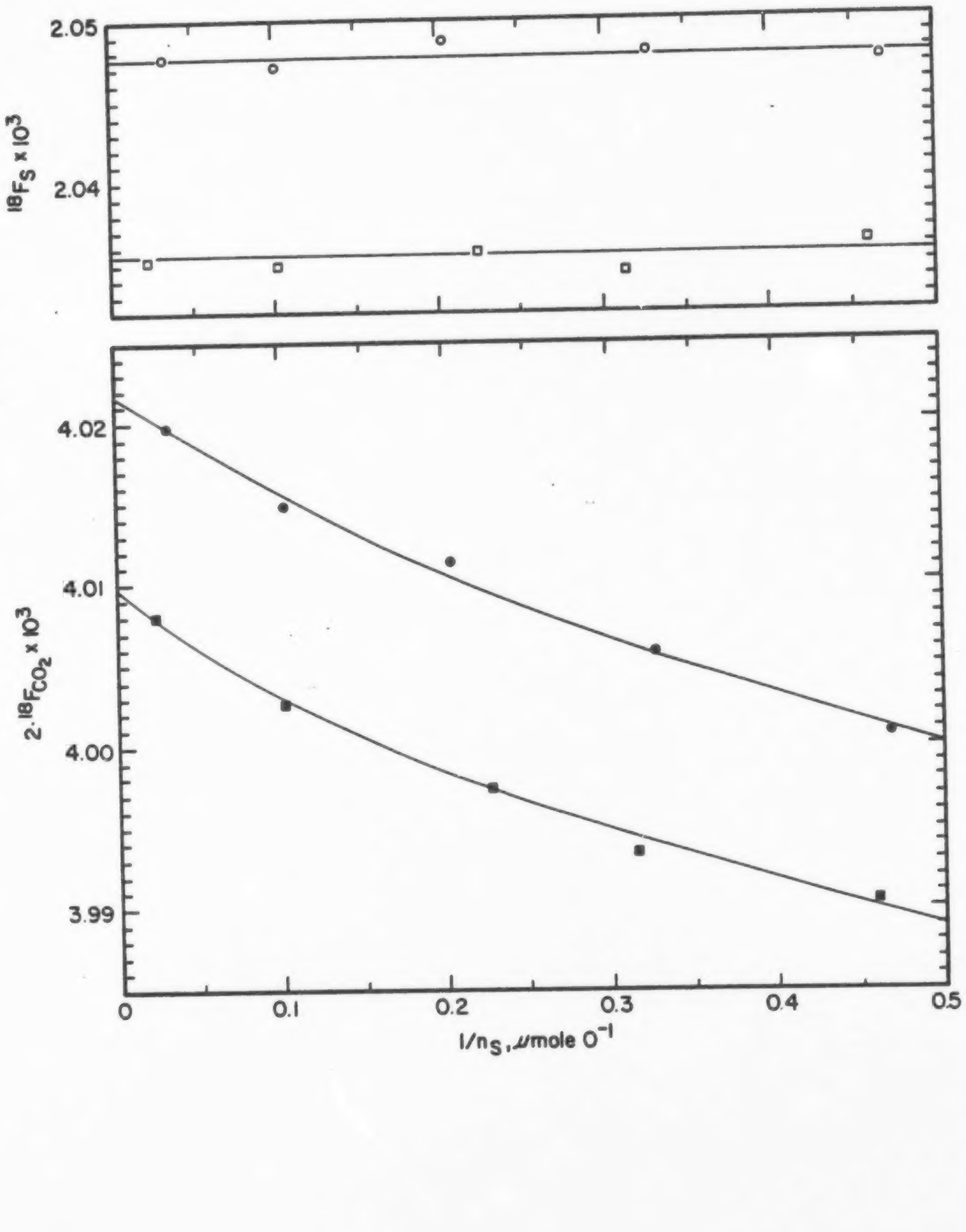
2.05
2.04
$^{18}F_S \times 10^3$
4.02
4.01
4.00
3.99
$2 \cdot {}^{18}F_{CO_2} \times 10^3$
0
0.1
0.2
0.3
0.4
0.5
$1/n_S$, μmole O^{-1}

Figure 2-9. A plot of $^{18}F_S$ vs sample number for a series of glycine ($^{18}F_1 = 2.06012 \times 10^{-3}$) analyses interrupted at positions 9 and 16 with highly enriched material ($^{18}F_2 = 4.489 \times 10^{-3}$); corrected for the blank and the I_2O_5-added oxygen (●); corrected for the blank, the I_2O_5-added oxygen, and for the memory (○). The sample size was constant at 26 μmol O. The filled symbols are the raw results corrected only for the blank and the iodine pentoxide-added oxygen.

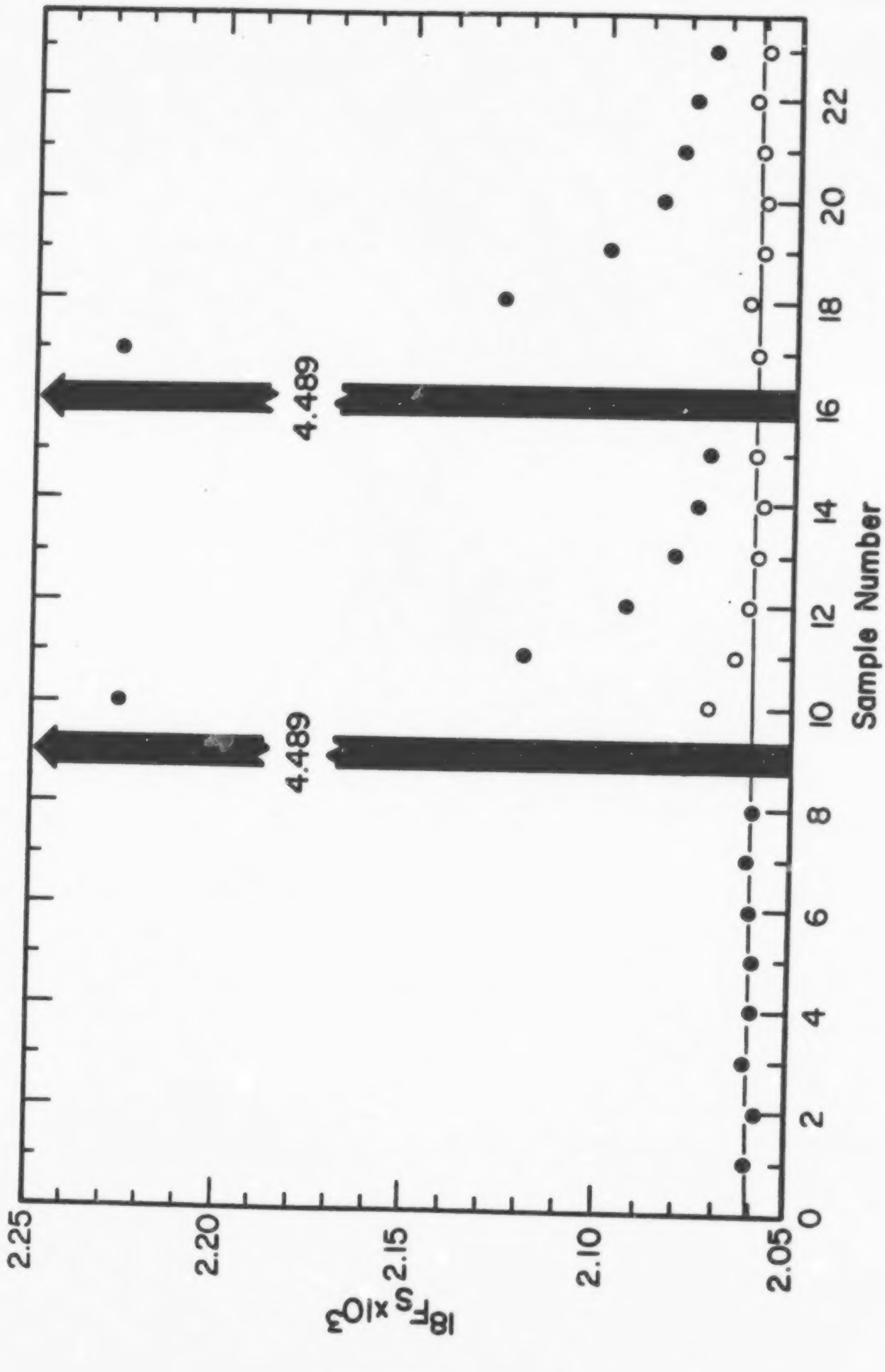

$^{18}F_S \times 10^3$
2.25
2.20
2.15
2.10
2.05
0
2
4
6
8
10
12
14
16
18
20
22
Sample Number
4.489
4.489

three successive refinements were necessary to adjust the parameters a and b. The calculated value of the isotopic composition of the iodine pentoxide-added oxygen remained constant during this calculation, whereas the other values changed substantially between the first and the second iterations (Table 2-5). Convergence was rapid once values for all terms were specified.

The limits for convergence were chosen so that the total error due to uncertainty in the correction parameters was smaller than the observed precision of repeated measurements, $s^2 = 2 \times 10^{-7}$ (see be low). Convergence limits accepted for the various correction parameters were: n_Q , 0.05 µmol O; $^{18}F_Q$, 10^{-6}; $^{18}F_I$, 10^{-7}; a, 0.002; and b, 0.02. The standard deviation of calculated values of $^{18}F_S$ will be less than 2×10^{-7} under these circumstances, provided n_S is greater than 5 µmol O and ^{18}F is within a factor of 2 of all other components. In general, the mathematical correction is most sensitive to $^{18}F_I$, and this value must be highly accurate under all conditions. Uncertainties in the terms specifying the contribution of the memory are much less important when memory effects are small. Thus, uncertainties in the values of a and b can be as large as 0.5 and 0.1, respectively, when samples within the natural abundance range are analyzed.

Evaluation of the Correction Procedure

The correction procedure outlined here incorporates some assumptions that are essentially untestable. We cannot be certain, for example, that sample-derived oxygen retained in the sorbed-oxygen pool does not differ in isotopic composition from that in the initial sample. Although it would be extremely difficult to show that all such assumptions are correct, it is possible to show at least that the correction procedure performs adequately. Three questions arise and will be discussed in sequence: i) is the functional form of the correction procedure essentially correct, ii) what levels of accuracy and precision can be obtained, and iii) are correction parameters derived with one set of test samples generally applicable?

Validation of the Model. Results summarized in Figures 2-8 and 2-9 show that the correction procedure has accurately adjusted results obtained during experimental runs designed for evaluation of correction parameters. The open symbols in both figures are the results of these calculations. The correction procedures accurately describe the contribution of the blank over a range of sample size from 2 to 30 μmol O. The means of the calculated values of $^{18}F_S$ in both sets of data (open symbols in Figure 2-8), $^{18}F_{BA-0} = 2.03512 \pm 0.00030 \times 10^{-3}$ and $^{18}F_{BA-1} = 2.04768 \pm 0.00028 \times 10^{-3}$ ($x \pm$ S.E.), do not differ significantly ($p < 0.05$) from the true isotopic compositions of both materials, as determined by the pyrolytic decarboxylation procedure. The effect of the blank on the isotopic composition of the carbon dioxide (the filled symbols) becomes more pronounced, shifting $2\cdot{}^{18}F_{CO_2}$ further from the y-intercept, as the size of the sample decreases. A comparison of the slopes for each curve also reveals that the effect of the blank is, as expected, greater for benzoic acid-1. However, the correction procedure effectively eliminates these variations.

The effects of the memory are also adequately described and taken into account by the mathematical correction. The exponential relationship, $a(j)^b$, closely described the wash-out of samples 9 and 16 in the total oxygen pool, with a correlation coefficient for a least-squares fit of $r^2 = 0.995$ (Figure 2-9). Thus, equation 2-23 can be used to estimate n_j, and to provide an accurate indication of the amount of a particular component in the sorbed-oxygen pool for the memory correction. The open symbols in Figure 2-9 are the calculated values of $^{18}F_S$ for samples 10-15 and 17-23. Only the values for samples 10 and 11 differ significantly ($p > 0.05$) from the mean of samples 1-8, which is unaffected by the memory. This example is an extreme demonstration of the memory effect, the great difference in the isotopic compositions of the two materials resulting in a large shift in the abundance of oxygen-18 in carbon dioxide produced from samples following each enriched sample. The effect of the memory will be small and more easily quantitated when samples of similar isotopic composition are analyzed.

Accuracy and Precision. Accurate results were obtained in analyses of the benzoic-acid standards (Table 2-6). The correction parameters were refined using the sample designated 0; the only value found to differ from those in the original parameter set was that for $^{18}F_0$. The mean isotopic abundances of the remaining samples (1 through 4) were compared to the results obtained by the pyrolytic decarboxylation procedure. A paired t-test indicates that the only significant difference between calculated and true isotopic compositions occurs for sample 1 ($p > 0.05$). This discrepancy, albeit small, is possibly the result of impurities in this sample, which is unique in that it was used "as supplied," and was not equilibrated with water and, consequently, was not recrystallized. If the impurities happened to yield CO_2 on pyrolysis, the pyrolytic result could have been affected.

The precision of the analyses in Table 2-6 is typical of this technique. In general, precision decreases as the sample becomes more enriched or depleted in oxygen-18 with respect to the blank and I_2O_5-

Table 2-6: Comparison of Isotopic Analyses of Benzoic Acids by Pyrolytic Decarboxylation and by the Schutze-Unterzaucher Procedure

	Pyrolytic Decarboxylation[a] $^{18}F_{BA} \times 10^3$	Schutze-Unterzaucher[b,c,d] $^{18}F_{BA} \times 10^3$ Δ
Benzoic Acid-0	2.03548 ± 0.00015	2.03544 ± 0.00022 (-0.02)
Benzoic Acid-1	2.04756 ± 0.00009	2.04957 ± 0.00018 (+0.98)
Benzoic Acid-2	2.11705 ± 0.00015	2.11782 ± 0.00087 (+0.36)
Benzoic Acid-3	2.18844 ± 0.00015	2.18976 ± 0.00095 (+0.60)
Benzoic Acid-4	2.24562 ± 0.00040	2.24429 ± 0.00066 (-0.59)

[a] mean ± S.E. of 5 replicate analyses

[b] mean ± S.E. of 4 replicate analyses

[c] The correction parameters were optimized for Benzoic Acid-0: $n_O = 1.0$ μmol O, $^{18}F_O = 1.977 \times 10^{-3}$, $^{18}F_I = 1.9740 \times 10^{-3}$, $a = 0.081$, and $b = -1.60$. All other isotopic abundances were calculated with these values.

[d] $\Delta = (^{18}F_{\text{Schutze-Unterzaucher}} / ^{18}F_{\text{pyrolysis}} - 1) \times 1000$

added oxygen. This occurs because small variations in the contaminant oxygen pools have, under these circumstances, a more pronounced effect on the calculated result. For samples in the range of natural abundance (*e. g.*, benzoic acid samples 1 and 2), the standard deviation of ^{18}F is typically 2×10^{-7} (equivalent to 0.1 ‰). The trend toward increasing standard deviations is evident in the results obtained from the more highly enriched samples.

General Applicability of Correction Parameters. Sample matrix effects have been identified. That is, the chemical form in which the oxygen is introduced can affect the analytical result. Differences in the reactivity of the initial oxygen-containing pyrolysis products with the carbon, which persist even at high temperatures (33), and interaction of non-oxygen containing gases such as N_2, H_2, and H_2S (18, 20) with the surface oxide are probable causes. Doping the carrier gas (*i. e.*, with hydrocarbons and halocarbons) minimizes these effects, but does not eliminate them completely.

An example of these effects is shown in Figure 2-10, which plots $2 \cdot {}^{18}F_{CO_2}$ vs. $1/n_S$ for a series of analyses of acetanilide, benzoic acid, and glycine (filled symbols, lower panel). Three different curves, indicative of different values for n_Q, are obtained. These differences are particularly clear in the upper panel of Figure 2-10, which plots the calculated (symbols) and the true (lines) isotopic compositions of each sample. The causes of these differences are not known in detail, but it is notable that, to obtain the corrected values in the upper panel, the correction parameters have been optimized for benzoic acid, which yields CO_2 as its principal pyrolysis product, whereas acetanilide yields CO and glycine yields a mixture of CO and CO_2. The deviations

Figure 2-10. A plot of $2 \cdot {}^{18}F_{CO_2}$ vs $1/n_S$ for benzoic acid, glycine, and acetanilide; corrected for the I_2O_5-added oxygen: benzoic acid (●), glycine (■), and acetanilide (▲); corrected for the blank, the memory, and the I_2O_5-added oxygen: benzoic acid (○), glycine (□), and acetanilide (△). The correction parameters were optimized for the benzoic acid.

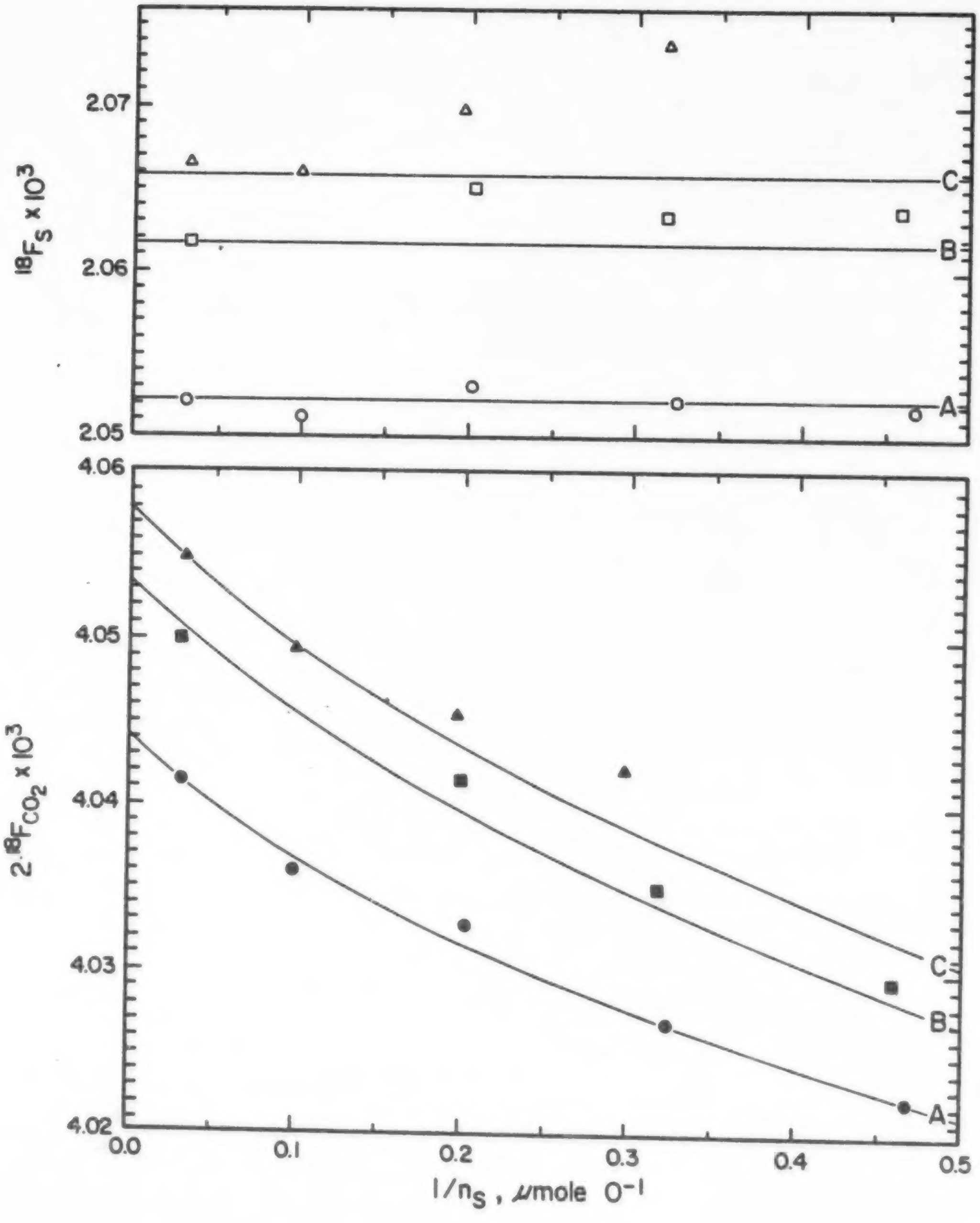

$^{18}F_S \times 10^3$
2.07
2.06
2.05
C
B
A
$2 \cdot {}^{18}F_{CO_2} \times 10^3$
4.06
4.05
4.04
4.03
4.02
C
B
A
0.0
0.1
0.2
0.3
0.4
0.5
$1/n_S$, μmole O^{-1}

for acetanilide and glycine at the smaller sample sizes are plausibly the result of differences in the size of the blank for CO and CO_2. The presence of N_2 apparently also influences the blank.

The effects of nitrogen and sulfur on analytical results are evident in the analyses of heteroaromatic carboxylic acids (Table 2-7). The correction parameters were established using benzoic acid, which, of course, yields no sulfur- or nitrogen-containing pyrolysis products. The results calculated for the Schutze-Unterzaucher procedure for the N- and S-containing materials differ significantly from the accurate values determined by pyrolytic decarboxylation. Sensitivity to heteroelement content is also observed for the blank in oxygen elemental analysis using the Schutze-Unterzaucher procedure; the blank is found to be smaller for C,H,O compounds than for C,H,N,O or C,H,O,S compounds (18-20, 33). The differences seen in Table 2-7 arise from an increase in the size of the blank due to the presence of nitrogen or sulfur in the sample. Paired t-tests indicate that all differences are significant ($p > 0.05$) if $n_Q = 1.0$ μmol O, but that the results of the two procedures do not differ significantly ($p < 0.05$) if $n = 3.0$ μmol O. The mathematical model accurately reflects dependence of the size of the blank on heteroelement content of the sample. The importance of choosing a working standard which closely matches the composition and structure of the sample in order to correctly establish the size of the blank and obtain the greatest accuracy is thus demonstrated.

Standards

Analysis of Standard Waters and Carbohydrates. The primary standard for oxygen isotopic abundances is "Standard Mean Ocean Water" (34). Samples of sucrose intended as supplementary standards for the

Table 2-7: Comparison of Isotopic Analyses of Heteroaromatic Carboxylic Acids by Pyrolytic Decarboxylation and by the Schutze-Unterzaucher Procedure

	Pyrolytic Decarboxylation[a] $^{18}F \times 10^3$	Schutze-Unterzaucher[b,c] $^{18}F \times 10^3$ Δ	
		n = 1.0[d]	n = 3.0[e]
pyrole-2-carboxylic acid	1.97134 ± 0.00006	1.97756 ± 0.00018 (+3.16)	1.97229 ± 0.00018 (+0.51)
2-thiophene carboxylic acid	1.97804 ± 0.00005	1.98241 ± 0.00018 (+2.21)	1.97771 ± 0.00020 (-0.17)
benzoic acid-0	2.03548 ± 0.00015	2.03530 ± 0.00039 (-0.09)	2.03557 ± 0.00041 (+0.04)
2,6-pyridine carboxylic acid	2.03740 ± 0.00017	2.03827 ± 0.00010 (+0.43)	2.03875 ± 0.00012 (+0.66)

[a] mean ± S.E. of 5 replicate analyses

[b] mean ± S.E. of 4 replicate analyses

[c] $\Delta = (^{18}F_{\text{Schutze-Unterzaucher}} / ^{18}F_{\text{pyrolysis}} - 1) \times 1000$

[d] n_O = 1.0 μmol O, all other correction parameters were optimized for benzoic acid: $^{18}F_O = 1.975 \times 10^{-3}$, $^{18}F_I = 1.98500 \times 10^{-3}$, a = 0.077, and b = -1.60. All other isotopic abundances were calculated using these values.

[e] n_O = 3.0 μmol O, all other correction parameters were optimized for benzoic acid-0: $^{18}F_O = 1.975 \times 10^{-3}$, $^{18}F_I = 1.98975 \times 10^{-3}$, a = 0.077 and b = -1.60. All other isotopic abundances were calculated using these values.

analysis of oxygen isotopes in organic materials have been distributed by I. Friedman (4). Because sucrose should yield water as its predominant oxygen-containing pyrolysis product (19), direct comparison of results obtained for water and sucrose standards should be possible.

Results of the analysis of cane and beet sugar (4) and standard waters (35) are shown in Table 2-8. The correction parameters were optimized for V-SMOW (34). A paired t-test indicates that the results calculated for NBS-1 and NBS-1A do not differ significantly ($p < 0.05$) from their accepted ^{18}O abundances (34). The calculated values for cane and beet sugar are both slightly greater than previous measurements (4-6,36). At least four different laboratories have analyzed these samples, each reporting a slightly higher oxygen-18 content than the previous measurement, and each accounting for the discrepancy by virtue of reduction of blank and memory effects in their respective procedures. Our measurements extend the trend. The accuracy of our results for NBS-1 and NBS-1A in the same series of analyses suggests that the effects of the blank and of the memory have been eliminated in the mathematical correction and that the isotopic abundances for cane and beet sugar reported in Table 2-8 are, in fact, correct.

Calibration of Working Standards. Although small variations in the size of the blank are unimportant if large samples are used, the effects of these variations can be minimized for samples of all sizes if working standards yielding pyrolysis products similar to those of the sample are available. The provision of such standards is always possible because the accurate isotopic composition of any sample can be determined by obtaining multiple analyses and fitting a curve similar to that shown in Figure 2-4. Such multiple analyses are tedious, but need

Table 2-8: Analysis of Water Standards and Sucrose Samples

	Accepted value[a,b] $^{18}F \times 10^3$ ($\delta^{18}O$ vs SMOW) ‰	Schutze-Unterzaucher[c] $^{18}F \times 10^3$ ($\delta^{18}O$ vs SMOW) ‰
cane sugar	2.0627 - 2.0685 (+31.3 - +34.1)	2.06978 ± 0.00073 (+34.7)
beet sugar	2.0489 - 2.0547 (+24.3 - +27.2)	2.05373 ± 0.00055 (+26.7)
V-SMOW	2.00044 (0.00)	2.00042 ± 0.00004 (-0.01)
NBS-1	1.98499 (-7.74)	1.98496 ± 0.00035 (-7.75)
NBS-1A	1.9519 (-24.3)	1.9526 ± 0.0010 (-24.0)

[a] Samples of cane and beet sugar were provided by Dr. I. Friedman (4). The range indicates results obtained by other investigators (4-6,32).

[b] The absolute abundance of oxygen-18 in V-SMOW was measured by Baertschi (30), and the abundances of oxygen-18 in NBS-1 and NBS-1A relative to V-SMOW were measured by Gonfiantini (31).

[c] Results of the triplicate analysis of samples containing approximately 50 μmol O. The correction parameters were optimized for V-SMOW: $n = 1.2$ μmol O, $^{18}F_Q = 1.977 \times 10^{-3}$, $^{18}F_I = 1.9890 \times 10^{-3}$, $a = 0.077$, and $b = -1.50$. All other isotopic abundances are calculated with these values.

not be repeated once a standard allowing adequate determination of correction parameters has been established. As an example, a plot of $2 \cdot {}^{18}F_{CO_2}$ vs. $1/n_S$ for benzoic acid, glycine, mouse lung homogenate, and mouse blood is shown in Figure 2-11. Samples of benzoic acid were used to determine ${}^{18}F_I$ and the values of ${}^{18}F_S$ for each of these materials were determined from the y-intercept. These materials can now be used as working standards in the analysis of similar tissue samples, where the values of n_Q and ${}^{18}F_I$ for a particular set of analyses are optimized by the procedure previously discussed in the section titled "Adjustment of Analytical Results".

EXPERIMENTAL SECTION

Isotopic Standards

Pyrolysis of Benzoic Acid. Benzoic acid (elemental analysis standard, Erba, Inc.) was pyrolyzed in sealed, evacuated quartz tubes. Prior to use, the quartz tubes (o.d. = 6 mm, length = 15 cm) were heated in air at 550°C for 12 hours, soaked in concentrated hydrochloric acid for 12 hours, and again heated in air at 550°C for 12 hours. Immediately before use, each tube was evacuated, heated to 800°C with a flame, and allowed to cool under vacuum. A sample of benzoic acid, approximately 3.6 mg (30 μmoles), was weighed to the nearest μg with a Cahn electrobalance. The tube was vented, the sample was added, and the tube was then evacuated for 60 to 120 sec prior to sealing. The sealed, evacuated tube was placed in a preheated muffle furnace for the specified time, removed from the furnace and allowed to cool in air.

In order to investigate reaction 2 under the conditions of this work, approximately 30-μmole aliquots of carbon dioxide (99.99%,

Figure 2-11. A plot of $2\cdot{}^{18}F_{CO_2}$ vs $1/n_S$ for benzoic acid (●), acetanilide (◆), mouse blood (■), and mouse-lung homogenate (▲). All results were corrected for the I_2O_5-added oxygen.

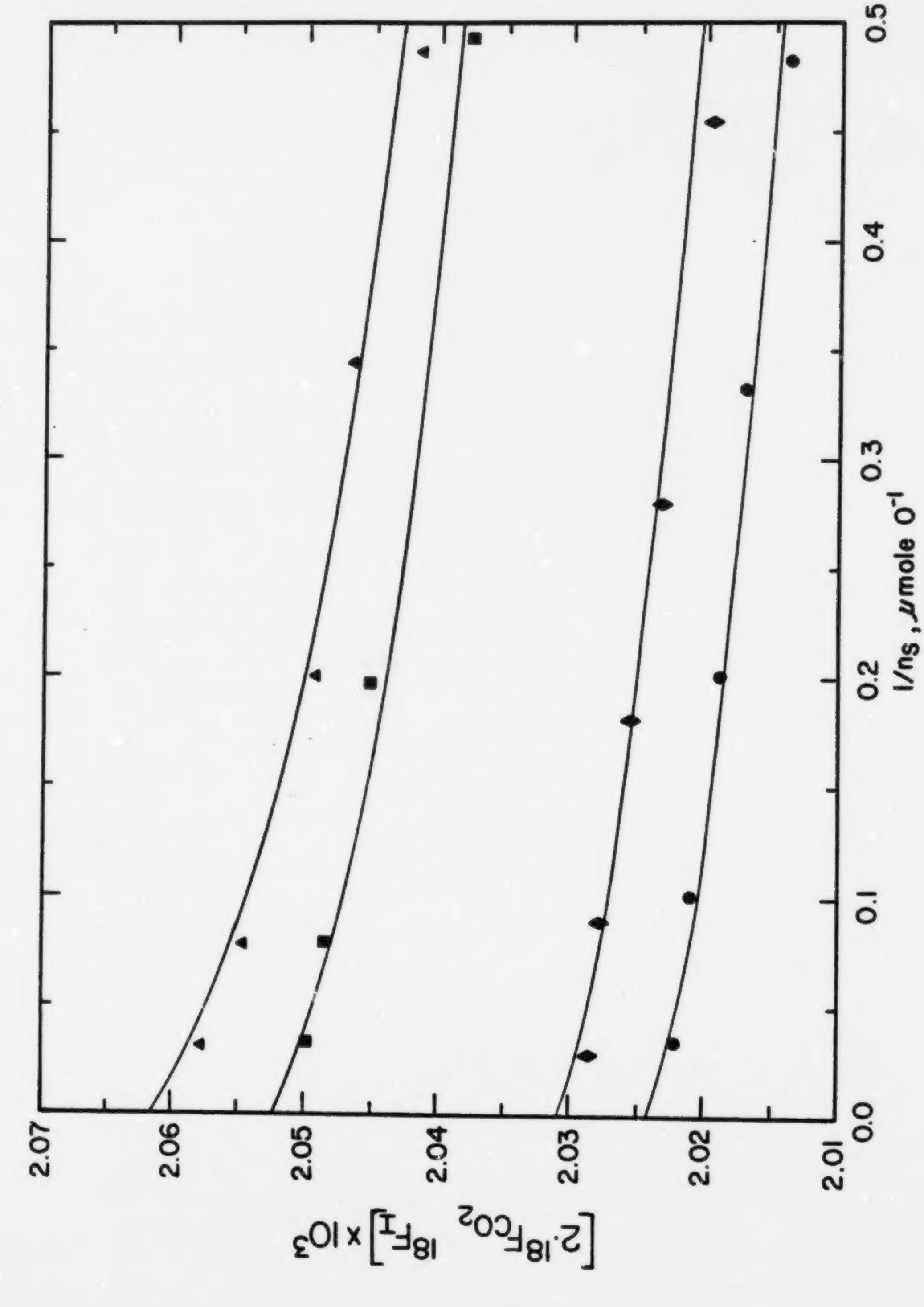
$[2 \cdot {}^{18}F_{CO_2} \; {}^{18}F_I] \times 10^3$
2.07
2.06
2.05
2.04
2.03
2.02
2.01
0.0
0.1
0.2
0.3
0.4
0.5
$1/n_S$, μmole O^{-1}

Matheson) were sealed in quartz tubes cleaned as described above and placed in a muffle furnace, preheated to 550°C, for times from 0 to 60 minutes. The tubes were removed from the furnace and allowed to cool in air.

Preparation of Carbon Dioxide. Carbon dioxide from sealed-tube experiments was purified by cryogenic distillation. The yield of CO_2 was measured using a gas buret and mercury manometer.

Mass Spectrometric Analysis. Isotopic analysis of carbon dioxide was performed with a Nuclide 6-60 RMS isotope-ratio mass spectrometer and isotopic abundances were calculated as described in Chapter 3. Pyrolysis products other than carbon dioxide were identified using a Kratos MS-80 high-resolution mass spectrometer.

Theoretical Calculations. The equilibrium constant (K) for reaction 2 for temperatures between 300 and 1500°K was calculated from values of the enthalpies and entropies of formation of CO and CO_2 (37) and values of the heat capacities of CO, CO_2, and graphite (38). The equilibrium oxygen isotopic fractionation factor for this reaction was calculated by means of the Bigeleisen-Mayer formulation (39), with literature values of the force constants for CO and CO_2 (40). These results were used to predict the yield of carbon dioxide and the shift in isotopic composition of the carbon dioxide from that of the carboxyl group.

Isotopic Standards. Five samples of benzoic acid with different isotopic compositions were prepared by exchange with water (41). For each of five isotopically different waters, approximately 4 g of benzoic acid were added to 100 mL of water. Gaseous HCl was bubbled through the mixture until the concentration of HCl was 5 N. The mixture was sealed under an atmosphere of N_2 and kept at 80°C for 120 hours. The benzoic acid was extracted in ether and the ether was removed under vacuum. Samples of 2,6-pyridinedicarboxylic acid, pyrrole-2-carboxylic acid, and 2-thiophenecarboxylic acid (Aldrich) were used as purchased. In order to determine their oxygen-isotopic compositions, the products were pyrolytically decarboxylated in sealed, evacuated quartz tubes at 550°C for 10 minutes. The carbon dioxide was purified by cryogenic distillation and the abundance of oxygen-18 in the CO_2 was measured mass spectrometrically.

Oxygen Isotopic Analysis

Apparatus. A Carlo Erba model 1106 elemental analyzer (Erba Instruments, Inc.) was modified for the preparation of organic samples for isotopic analysis (Figure 2-12). These modifications do not interfere with the normal operation of the elemental analyzer, a description of which has appeared elsewhere (42,43), and allow the preparation of CO_2 for the determination of oxygen-18 or for the preparation of CO_2, N_2 and H_2O for deternimation of carbon-13, nitrogen-15, and deuterium, respectively. Here, only procedures pertinent to oxygen isotopic analysis will be discussed.

The effluent of the chromatographic column was redirected so that it passed through an oxidation reactor before entering an auxiliary vacuum line for collection, purification, and packaging of carbon dioxide. The oxidation reactor was a pyrex tube, 10 mm o.d. x 40 cm in length, 30 cm of which were packed with an iodine pentoxide reagent (44). The remaining 10 cm were filled with dry silica gel. The I_2O_5 was heated to 135°C. A series of traps and a vacuum system were constructed so that carbon dioxide could be trapped from the effluent of

Figure 2-12. Schematic diagram of modifications to the Carlo Erba elemental analyzer used for the preparation of carbon dioxide from organic material for isotopic analysis. Details of the operation of the elemental analyzer appear elsewhere (42). Valves V2, V3, and V4 were connected to the high-vacuum system at positions A, B, and C. Carbon dioxide was trapped from the effluent of the I_2O_5 reactor in T3.

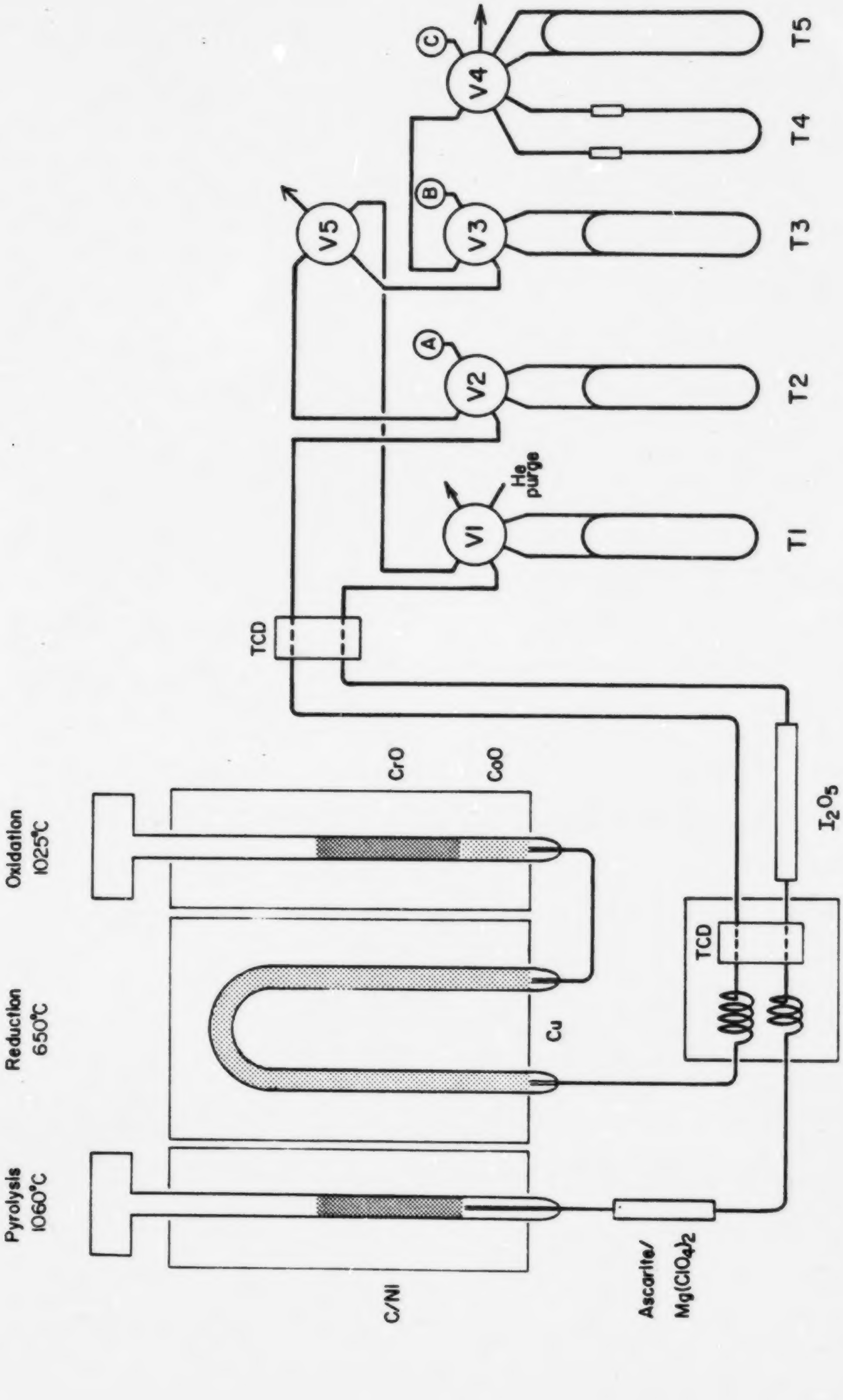
Pyrolysis
1060°C
Reduction
650°C
Oxidation
1025°C
C/Ni
Cu
CrO
CoO
Ascarite/
Mg(ClO4)2
TCD
I2O5
TCD
V1
He purge
V2
A
V3
B
V4
C
V5
T1
T2
T3
T4
T5

the oxidation reactor, purified, and transferred to a sample tube for mass spectrometric analysis. All valves were stainless steel and utilized 1/8"-low dead volume fittings (Valco Instruments Co.; V1, V2, and V3 were type HP-6a; V5 was type HP-4a; and V4 was type HP-10a). Traps T1, T2, T3, and T5 were multicoiled, containing 6 loops each, and were constructed from type 321 stainless steel tubing, 0.125" o.d. x 0.010" wall (Tube Sales). Trap T4 was constructed from 6-mm pyrex tubing and contained 0.1 g of molecular sieve 5A, 60/80 mesh (Analabs). The connections between the valves were made with teflon-lined aluminum tubing, 1/8" o.d. x 1/16" i.d. (Analabs). Connections to the highvacuum system were made using one-piece, graphite-impregnated Vespel ferrules (Supeltex M-2A, Supelco). Standard two-piece Swagelok Teflon ferrules (Crawford Fitting Co.) were used for other connections.

Reagents. High-purity helium, 99.995% (Air Products) was used as the carrier gas for the elemental analyzer. The carrier gas was doped with approximately 550 ppm of CCl_4 and 1500 ppm of C_7H_{16}. These materials were mixed with the helium by volatilization from a toroidal pyrex vessel with a 1-mm orifice, containing a 5% (v/v) solution of carbon tetrachloride (Fisher, Spectranalyzed) in n-heptane (Fisher, Spectranalyzed). The vessel was placed in the sample dispenser, just upstream from the reaction chamber.

Iodine pentoxide was prepared by mixing a solution containing 50 g of I_2O_5 (Mallinckrodt Analytical Reagent) in 100 mL of distilled water with 100 g of 8-12 mesh silica gel (Preiser Scientific, Inc.). This mixture was allowed to dry at 80°C for 96 hours. Concentrated sulfuric acid (25 mL) was added to the dried material and the mixture was again allowed to dry. Finally, the mixture was heated to a temperature of

220°C for 4 h in a dry helium stream (44). The active reagent, a coarse yellow material, was kept dry and not exposed to light.

Isotopic Analyses. Samples were weighed into silver-foil cups (Erba, Inc.) on a Cahn 25 Electrobalance (Cahn Instruments, Inc.) and placed in the sampling-head of the instrument. The analyzer was operated normally, so that oxygen elemental abundances in the samples were also obtained. A dry ice-acetone bath was placed around T1 to remove residual amounts of I_2, a byproduct of the oxidation of CO by I_2O_5, which were present in the carrier gas. To prevent aerosol formation and ensure quantitative recovery, T3 was immersed to half its length in liquid nitrogen when trapping carbon dioxide from the analyzer effluent. Valve V3 was switched to direct the effluent of the oxidation reactor through T3 60 sec after a carbon dioxide peak was detected by thermal conductivity detector D1 (the delay was determined using D2). Helium was removed and the carbon dioxide was transferred to a sample tube for mass spectrometric analysis. Isotopic analysis of carbon dioxide is described in Chapter 3.

REFERENCES

1. Mook, W. G.; Grootes, P. M. The measuring procedure and corrections for the high-precision mass-spectrometric analysis of isotopic abundance ratios, especially referring to carbon, oxygen, and nitrogen. Int. J. Mass Spectrom. Ion Phys. 12:273-298, 1973.

2. Taylor, W.; Chen, I-J. Variables in oxygen-18 isotopic analysis by mass spectrometry. Anal. Chem. 42:224-228, 1970.

3. Fong, B. J.; Smith, S. R.; Tanaka, J. Reevaluation of the preparation of organic compounds for mass spectrometric analysis for oxygen-18. Anal. Chem. 44:655-659, 1972.

4. Hardcastle, K. G.; Friedman, I. A method for oxygen isotope analysis of organic material. Geophys. Res. Lett. 1:165-167, 1974.

5. Ferhi, A. M.; Letolle, R. R.; Lerman, J. C. Oxygen isotope ratios of organic matter: Analysis of natural compositions. Proceedings of the Second International Conference on Stable Isotopes, 716-724, 1976.

6. Thompson, P.; Gray, J. Determination of $^{18}O/^{16}O$ ratios in compounds containing C, H, and O. Int. J. Appl. Radiat. Isot. 23: 411-415, 1976.

7. Brenninkmeijer, C. A. M.; Mook, W. G. A batch process for direct conversion of organic oxygen and water to CO_2 for $^{18}O/^{16}O$ analysis. Int. J. Appl. Radiat. Isot. 32:137-141 1981.

8. Unterzaucher, J. The direct micro-determination of oxygen in organic substances. Analyst 77:584-595, 1952.

9. Schutze, M. Die direkte bestimmung des Sauerstoffs in Zinkoxyd. Z. Anal. Chem. 118:241-245, 1939.

10. Winter, K.; Barton, D. The thermal decomposition of benzoic acid. Can. J. Chem. 48:3797-3801, 1970.

11. Maier, W. F.; Roth, R. V.; Thies, I.; Schleyer, P. v. R. Gass phase decarboxylation of carboxylic acids. Chem. Ber. 115:808-115, 1982.

12. Rhead, T. F. E.; Wheeler, R. V. The effect of temperature and of pressure on the equilibrium $2CO \rightleftharpoons CO_2 + CO$. J. Chem. Soc. 99: 1140-1153, 1911.

13. Stevens, W. H.; Pepper, J. M.; Lounsbury, M. The decarboxylation of anthranilic acid. Can. J. Chem. 30:529-540, 1952.

14. Dunn, G. E.; Dayal, S. K. Mechanism od decarboxylation of substituted anthranilic acids at high acidity. Can. J. Chem. 48:3349-3353, 1970.

15. Dunn, G. E.; Lee, G. K. J. Kinetica and mechanism of the decarboxylation of pyrrole-2-carboxylic acid in aqueous solution. Can. J. Chem. 49:1032-1035, 1971.

16. Dunn, G. E.; Gordon, K. J. L.; Thimm, L. Kinetics and mechanism of decarboxylation of some pyridinecarboxylic acids in aqueous solution. Can. J. Chem. 50:3017-3027, 1972.

17. Rhead, W. F.; Wheeler, R. V. The rate of reduction of carbon dioxide by carbon. J. Chem. Soc. 101:831-845, 1912.

18. Haraldson, L. An investigation of the products of pyrolysis in the determination of oxygen in sulphur-containing organic substances. Mikrochim. Acta 1962, 651-670.

19. Belcher, R.; Ingram, G.; Majer, J. R. Direct determination of organic compounds in the determination of oxygen. Mikrochim. Acta 1968, 418-426.

20. Belcher, R.; Ingram, G.; Majer, J. R. Direct determination of oxygen in organic materials-I. Talanta 16:881-892, 1969.

21. Bonner, F.; Turkevich, J. J. Study of the carbon dioxide-carbon reaction using C^{14} as a tracer. J. Am. Chem. Soc. 73:561-564, 1951.

22. Oring, A. A.; Sterling, E. Oxygen transfer between carbon dioxide and carbon monoxide in the presence of carbon. J. Phys. Chem. 58: 1044-1047, 1954.

23. Ergun, S. Kinetics of the reaction of carbon dioxide with carbon. J. Phys. Chem. 60:480-485, 1956.

24. Vastola, F. J.; Hart, P. J.; Walker, P. L. A study of carbon-oxygen surface complexes using O^{18} as a tracer. Carbon 2:65-71, 1964.

25. Menser, M; Ergun, S. Kinetics of oxygen exchange between CO_2 and CO on carbon. Carbon 5:331-337, 1967.

26. Grabke, H. J. Oxygen transfer and carbon gasification in the reaction of different carbons with CO_2. Carbon 10:587-599, 1972.

27. Tremblay, G.; Vastola, F. J.; Walker, P. L. Thermal desorption analysis of oxygen surface complex on carbon. Carbon 16:35-39, 1978.

28. Gouverneur, P.; Schreuders, M.; Degens, P. N. The direct determination of oxygen in organic compounds. Anal. Chim. Acta 5: 293-312, 1951.

29. Tamai, Y.; Watanabe, H.; Tomita, A. Catalytic gasification of carbon with steam, carbon dioxide, and hydrogen. Carbon 15:103-106, 1977.

30. Kirsten, W. J. Micro and trace determination of oxygen in organic compounds. Anal. Chim. Acta 100:279-288, 1978.

31. Freeman, G. B.; Reucroft, P. J. Adsorption of HCN and H_2O vapor mixtures by activated and impregnated carbons. Carbon 17:313-316, 1979.

32. Hartley, P. E. Corrections for memory effects in analytical instruments. Anal. Chem. 54:148-150, 1982.

33. Belcher, R.; Ingram, G. Some observations on the microdetermination of oxygen in organic materials. Microchem. J. 11:350-357, 1966.

34. Baertschi, P. Absolute ^{18}O content of Standard Mean Ocean Water. Earth Planet. Sci. Lett. 31:341-344, 1976.

35. Gonfiantini, R. Standards for stable isotope measurements in natural compounds. Nature 271:534-536, 1978.

36. Wedeking, K. W.; Hayes, J. M. unpublished results.

37. Rossini, E. D.; Wagman, D. W.; Evans, W. H.; Lavine, S.; Jaffe, I. Selected values of thermodynamic properties, National Buro of Standards Circular 500, 1952.

38. Spencer, H. M. Emperical heat capacity equations of gasses and graphite. Ind. Eng. Chem. 40:2152-2154, 1949.

39. Bigeleisen, J.; Mayer, M. G. Calculation of equilibrium constants for isotope exchange reactions. J. Chem. Phys. 15:261-267, 1947.

40. Stern, M. J.; Spindel, W.; Monse, E. V. Temperature dependence of isotope effects. J. Chem. Phys. 48:2908-2919, 1968.

41. Roberts, I.; Urey, H. C. Kinetics of the exchange between benzoic acid and water. J. Am. Chem. Soc. 61:2580-2584, 1939.

42. Pella, E.; Colombo, B. Improved instrumental determination of oxygen in organic compounds by pyrolysis-gas chromatography. Anal. Chem. 44:1563-1671, 1972.

43. Pella, E.; Colombo, B. Study of carbon, hydrogen, and nitrogen determination by combustion-gas chromatography. Mikrochim. Acta Wien 1973, 697-719.

44. Smiley, W. G. Note on reagent for oxidation of carbon monoxide. Nucl. Sci. Abstr. 3:391-392, 1949.

CHAPTER 3

MASS SPECTROMETRIC DETERMINATION OF CARBON-13, OXYGEN-17, AND OXYGEN-18 IN CARBON DIOXIDE

Measurement of the mass spectrum of a volatile molecule can quantify only the relative abundances of molecular species of differing mass. Commonly, elemental isotope ratios are not measurable directly, but must be determined by calculations based on the observed molecular spectrum (1). In the case of carbon dioxide, for example, ion currents appear at m/z 44 through m/z 49. With the exception of m/z 44 ($^{12}C^{16}O_2$), all measurable ion currents represent sums of multiple isotopic contributions (*e. g.*, $^{13}C^{17}O^{16}O$ + $^{12}C^{18}O^{16}O$ + $^{12}C^{17}O_2$, at m/z 46). A problem common to all mathematical formulations (2-4) is that a measurement of two ion-current ratios (45/44 and 46/44) does not provide sufficient information to obtain unique solutions for three isotope ratios ($^{13}C/^{12}C$, $^{17}O/^{16}O$, and $^{18}O/^{16}O$).

The oxygen-isotope ratios have, therefore, commonly been treated as functionally related; that is, an expression for $^{17}O/^{16}O$ as a function of $^{18}O/^{16}O$ has been written and used as the third equation required for solution of the problem. This approach is based on the fact that processes (other than admixture of separated isotopes) which have affected the abundance of ^{18}O must also have affected the abundance of ^{17}O, and *vice versa* (5). Recently, however, it has been shown (i) that no single, fixed relationship correctly describes the fractionation of ^{17}O relative to ^{18}O in all processes, and (ii) that the relationship commonly employed by isotopic mass spectrometrists does not correctly describe even the "average relationship" prevailing in natural systems (6). Here, we explore the significance of these findings for isotopic analysis and show that a simple system of equations for accurate calculation of isotopic abundances can be developed.

DEVELOPMENT OF ISOTOPE-RATIO EQUATIONS

Notation. The letter R is consistently used to designate the ratio of a particular isotopic species to the related isotopic species of lowest mass

$$R = \frac{\text{isotopic species of mass n}}{\text{base species related to n}} \qquad (3\text{-}1)$$

Left superscripts will be consistently used to designate isotopic species by mass. For n = 13, the base species is ^{12}C; for n = 17 or 18, ^{16}O; and, for n = 45 through 49, the base species is $^{12}C^{16}O_2$. The letter F is consistently used in the same way to designate fractional abundances

$$F = \frac{\text{isotopic species of mass n}}{\text{sum of all species related to n}} \qquad (3\text{-}2)$$

for n = 13, the denominator is the sum ($^{12}C + ^{13}C$); for n = 17 or 18, ($^{16}O + ^{17}O + ^{18}O$); and, for n= 45 through 49, the denominator is the sum of all species of carbon dioxide. The symbol α is used to designate the fractionation factor, in this case, the ratio of isotope ratios characteristic of the isotope effect associated with a physical or chemical process

$$\alpha = \frac{^{n}R_{\text{products}}}{^{n}R_{\text{reactants}}} \qquad (3\text{-}3)$$

for n = 13, 17, or 18.

Isotopic Distribution. The isotopic species present in carbon dioxide are shown in Table 3-1. Since the vibrational modes in CO_2 are nearly harmonic and coupling between modes is weak (7), the distribution

Table 3-1: Isotopic Molecular Species of Carbon Dioxide

44	45	46	47	48	49
$^{12}C^{16}O^{16}O$	$^{13}C^{16}O^{16}O$	$^{12}C^{17}O^{17}O$	$^{13}C^{17}O^{17}O$	$^{12}C^{18}O^{18}O$	$^{13}C^{18}O^{18}O$
	$^{12}C^{16}O^{17}O$	$^{12}C^{16}O^{18}O$	$^{13}C^{18}O^{16}O$	$^{13}C^{18}O^{17}O$	
	$^{12}C^{17}O^{16}O$	$^{12}C^{18}O^{16}O$	$^{13}C^{16}O^{18}O$	$^{13}C^{17}O^{18}O$	
		$^{13}C^{16}O^{17}O$	$^{12}C^{18}O^{17}O$		
		$^{13}C^{17}O^{16}O$	$^{12}C^{17}O^{18}O$		

a particular isotopic species is accurately described by a simple probability function (1). The abundances of the various molecular species are, therefore, related to the isotopic abundances by the following equations

$$^{44}F = {^{12}F}\cdot{^{16}F}\cdot{^{16}F} \tag{3-4}$$

$$^{45}F = {^{13}F}\cdot{^{16}F}\cdot{^{16}F} + 2\cdot{^{12}F}\cdot{^{16}F}\cdot{^{17}F} \tag{3-5}$$

$$^{46}F = {^{12}F}\cdot{^{17}F}\cdot{^{17}F} + 2\cdot{^{12}F}\cdot{^{16}F}\cdot{^{18}F} + 2\cdot{^{13}F}\cdot{^{16}F}\cdot{^{17}F} \tag{3-6}$$

$$^{47}F = {^{13}F}\cdot{^{17}F}\cdot{^{17}F} + 2\cdot{^{13}F}\cdot{^{16}F}\cdot{^{18}F} + 2\cdot{^{12}F}\cdot{^{17}F}\cdot{^{18}F} \tag{3-7}$$

$$^{48}F = {^{12}F}\cdot{^{18}F}\cdot{^{18}F} + 2\cdot{^{13}F}\cdot{^{17}F}\cdot{^{18}F} \tag{3-8}$$

$$^{49}F = {^{13}F}\cdot{^{18}F}\cdot{^{18}F} \tag{3-9}$$

In practice, it is most convenient to express these relationships in terms of ratios. Dividing equations 3-5 through 3-9 by equation 3-4 yields

$$^{45}R = {^{13}R} + 2\cdot{^{17}R} \tag{3-10}$$

$$^{46}R = 2\cdot{^{18}R} + 2\cdot{^{13}R}\cdot{^{17}R} + {^{17}R^2} \tag{3-11}$$

$$^{47}R = {^{13}R}\cdot{^{17}R^2} + 2\cdot{^{13}R}\cdot{^{18}R} + 2\cdot{^{17}R}\cdot{^{18}R} \tag{3-12}$$

$$^{48}R = {^{18}R^2} + 2\cdot{^{13}R}\cdot{^{17}R}\cdot{^{18}R} \tag{3-13}$$

$$^{49}R = {^{13}R}\cdot{^{18}R^2} \tag{3-14}$$

For samples with isotopic abundances near natural levels, ion currents large enough to allow precise, rapid measurement occur only at masses 44, 45, and 46. Modern instruments employ a triple-collector system to facilitate simultaneous measurement of ^{45}R and ^{46}R (Figure 3-1).

Relationships Between ^{17}R and ^{18}R

Theoretical Considerations. Fractionations of multiple isotopes of the same element are proportional to differences in mass (5). A quantitative relationship between the values of ^{17}R and ^{18}R for two oxygen pools (designated by subscripts 1 and 2) linked by a single, mass-dependent process has been presented by Clayton and coworkers (6)

$$\left(\frac{^{17}R_1}{^{17}R_2}\right) = \left(\frac{^{18}R_1}{^{18}R_2}\right)^a \tag{3-15}$$

where $a = \ln(^{17}\alpha)/\ln(^{18}\alpha)$. Note, however, that (i) a is not constant and (ii) equation 3-15 refers to instantaneous precursor-product relationships, not to the integrated compositions of separated or mixed isotopic pools. Both of these points are significant in the isotope-analysis problem.

The value of α depends on the process causing the isotopic fractionation. Further, variations of $^{17}\alpha$ and $^{18}\alpha$ are not linked in a way that leads a to assume a constant value. As a result, relative fractionations of the oxygen isotopes can depend on the molecular species involved or on the mechanism of a particular reaction. In general, $0.50 < a < 0.53$ (6). For a series of reactions, the value of a for the overall process is the weighted average of the values for each step

$$a_\Sigma = \frac{\Sigma\{a \ln(^{18}\alpha_i)\}}{\Sigma \ln(^{18}\alpha_i)} \tag{3-16}$$

where a_i is the exponent and $^{18}\alpha_i$ is the oxygen-18 fractionation

Figure 3-1. Schematic representation of an isotope ratio mass spectrometer. Reference and sample gases are alternatively introduced into the mass spectrometer, and ion-currents at m/z 44, m/z 45, and m/z 46 are measured for each gas.

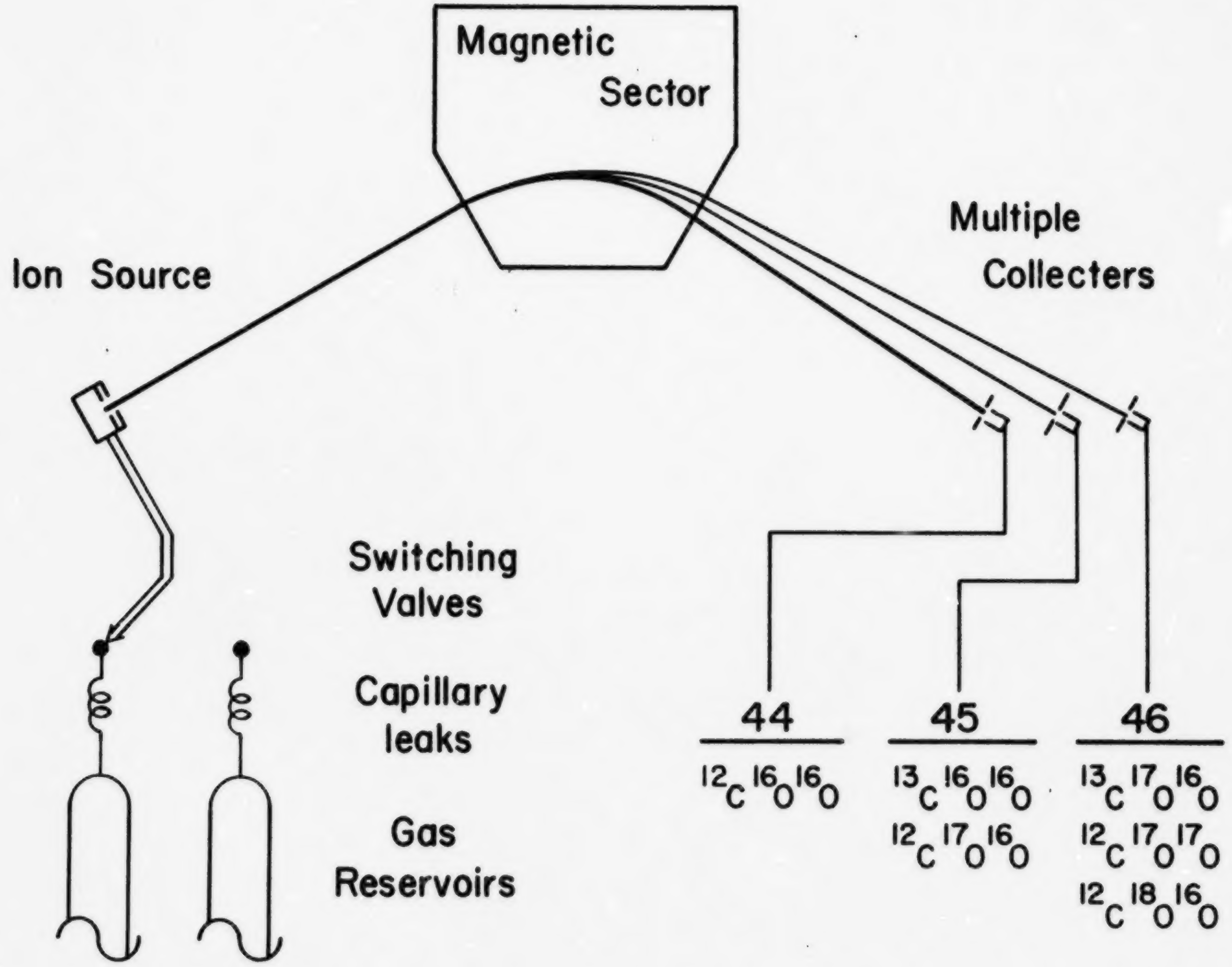
Magnetic Sector
Ion Source
Multiple Collecters
Switching Valves
Capillary leaks
Gas Reservoirs
44
$^{12}C^{16}O^{16}O$
45
$^{13}C^{16}O^{16}O$
$^{12}C^{17}O^{16}O$
46
$^{13}C^{17}O^{16}O$
$^{12}C^{17}O^{17}O$
$^{12}C^{18}O^{16}O$

factor for each step in the series of n reactions. In cases where a reaction sequence imparts a large net change in the relative abundance of one heavy isotope and a small net change in the abundance of the other heavy isotope, the value of a_Σ is not restricted to the range defined by the a_Σ, and may be very large or very small. Moreover, if a net enrichment in one isotope accompanies a net depletion in the other, then a_Σ will be negative.

Natural samples are never the products of a discrete process, or even a single sequence of processes. For polyisotopic elements, isotopic variations associated with mixing processes are complex. On the one hand, relationships governing isotopic fractionations associated with mass-dependent isotope effects are correctly cast in terms of ratios. On the other hand, accurate calculation of the composition of mixed pools must be based on fractional abundances. Even if a is known accurately, equation 3-15 will only approximately describe isotopic relationships associated with the mixing of oxygen pools with similar isotopic compositions (i. e., natural samples of terrestrial origin). In general, a will be some average of the ai weighted by the relative contribution of each component to the total oxygen pool. If one or more of the oxygen pools involved in a mixture has been selectively enriched or depleted in a single isotope, serious inaccuracies can result from application of equation 3-15 (6).

Given these considerations, it is evident that there is no basis on which an equation exactly relating ^{17}R and ^{18}R in all pools of oxygen might be developed. In particular, the relationship underlying most oxygen-isotopic analytical calculations:

$$\left(\frac{^{17}R_{\text{unknown}}}{^{17}R_{\text{standard}}}\right) = \left(\frac{^{18}R_{\text{unknown}}}{^{18}R_{\text{standard}}}\right)^{\frac{1}{2}} \qquad (3\text{-}17)$$

where "unknown" and "standard" refer to a sample of unknown isotopic composition and to some primary isotopic standard, is inexact and, because 0.50 represents a minimal value for a, may not be the most satisfactory approximation.

^{17}R and ^{18}R in Natural Samples. Independent measurements of $\delta^{17}O$ and $\delta^{18}O$ in lunar and terrestrial silicate minerals and samples of natural waters quite closely define a single relationship (6,8,9)

$$\delta^{17}O_{SMOW} = 0.52\cdot\delta^{18}O_{SMOW} \qquad (3\text{-}18)$$

As indicated by use of the d notation, this relationship is based on measurements of differences between isotopic compositions of unknown samples and isotopic standards. As such, it carries no direct information regarding absolute values of isotope ratios. Calculations of ^{17}R and ^{18}R for unknown samples -- and, for that matter, accurate calculations based on equations 3-10 and 3-11 -- require knowledge of ^{17}R and ^{18}R for the isotopic standards. Although there have been recent measurements of the absolute value of $^{18}R_{SMOW}$ (and they are in good agreement, see refs 2,10,11), there have been no direct determinations of $^{17}R_{SMOW}$.

It is, therefore, of great interest that the isotopic compositions of all natural terrestrial and lunar oxygen pools appear to be related by equation 3-18, which is closely related to equation 3-15. The δ terms are identical to the first terms in the series expansions of the ln terms in:

$$\ln\left(\frac{{}^{17}R_{\mathrm{unknown}}}{{}^{17}R_{\mathrm{SMOW}}}\right) = a\cdot\ln\left(\frac{{}^{18}R_{\mathrm{unknown}}}{{}^{18}R_{\mathrm{SMOW}}}\right) \qquad (3\text{-}19)$$

Higher-order terms are negligible when ${}^{17}R_{\mathrm{unknown}}$ and ${}^{18}R_{\mathrm{unknown}}$ are close to ${}^{17}R_{\mathrm{SMOW}}$ and ${}^{18}R_{\mathrm{SMOW}}$. It is evident that equation 3-19 is a more general form of equation 3-18, which can be recast as

$${}^{17}R = {}^{18}R^{a}\cdot K \qquad (3\text{-}20)$$

where K is a constant characteristic of the relationship between ${}^{17}R$ and ${}^{18}R$ in the terrestrial oxygen pool. Because the isotopic compositions of all samples appear to be related by this equation, evaluation of K requires only that both ${}^{17}R$ and ${}^{18}R$ be known accurately in a single, representative sample.

There has been only one set of measurements of the absolute abundances of oxygen-16, oxygen-17, and oxygen-18 in samples of terrestrial origin. Nier determined values of the ratios ${}^{17}O{}^{16}O/{}^{16}O_2$ (${}^{33}R$) and $({}^{18}O{}^{16}O + {}^{17}O_2)/{}^{16}O_2$ (${}^{34}R$) for samples of air and of O_2 from a commercial gas cylinder (12). Discordant results were obtained for the atmospheric sample (perhaps because total air, not purified atmospheric O_2, was admitted to the ion source), but, for the latter analysis, Nier reports (corrected mean and probable error) ${}^{33}R = 7.55 \pm 0.01 \times 10^{-4}$ and ${}^{34}R = 4.103 \pm 0.005 \times 10^{-3}$, which yield isotope ratios (mean and standard error of mean) of ${}^{17}R_{O_2} = (3.775 \pm 0.074) \times 10^{-4}$ and ${}^{18}R_{O_2} = (2.0514 \pm 0.0037) \times 10^{-3}$. It follows that, for $a = 0.52$, $K = (9.43 \pm 0.18) \times 10^{-3}$.

Calculation of Isotope Ratios

Combining equations 3-10 and 3-11 and substituting equation 3-20 for ^{17}R yields an expression for ^{18}R in terms of ion-current ratios, K, and a. Apart from uncertainties in K and a, the equation is exact.

$$-3 \cdot K^{2} \cdot {}^{18}R^{2a} + 2K \cdot {}^{45}R \cdot {}^{18}R^{a} + 2 \cdot {}^{18}R - {}^{46}R = 0 \qquad (3\text{-}21)$$

Rearrangement of this equation to yield an explicit solution of the form $^{18}R = f(a, K, {}^{45}R, {}^{46}R)$ is not possible except where a is exactly 0.5. An accurate value for ^{18}R can, however, be easily and rapidly obtained using numerical techniques. A value for ^{17}R can be determined from equation 3-20 or, if a direct solution in terms of ion-current ratios is required, a derivation similar to that of equation 3-21 yields

$$-3 \cdot {}^{17}R^{2} + 2 \cdot {}^{45}R \cdot {}^{17}R + ({}^{17}R/K)^{1/a} - {}^{46}R = 0 \qquad (3\text{-}22)$$

The calculation of ^{13}R follows directly from ^{45}R using equation 3-10.

For clarity in subsequent discussions, we will refer to the following sequence of calculations as "routine:"

1. ^{18}R is calculated from ^{45}R and ^{46}R (eq. 3-21).
2. ^{17}R is calculated from ^{18}R (eq. 3-20).
3. ^{13}R is calculated from ^{17}R and ^{45}R (eq. 3-10).

DETERMINATION OF ISOTOPE ABUNDANCES

The accuracy of calculated isotope ratios will depend on how well equation 3-20 actually describes the linked variations of ^{17}R and ^{18}R and on the development of representative values for a and K. Here, we will explore, by means of the application of equations 3-20 - 3-22 to calculation of results from analytical data, two particularly interesting cases:

(i) oxygen pools derived by mixing natural-abundance material with material highly enriched in ^{18}O

(ii) natural-abundance material with a range of oxygen-isotopic compositions wide enough that correct assignment of the values of a and K will be important

Mixed Samples Enriched in ^{18}O. If a sample has been selectively enriched in ^{18}O, inaccuracies will result from use of the routine sequence of calculations. Because ^{46}R is primarily dependent on ^{18}R, solution of equation 3-21 will yield a roughly correct value for ^{18}R. The value of ^{17}R will, however, be overestimated by equation 3-20. Insertion of that overestimate in equation 3-10 will lead to an incorrectly low value for ^{13}R. Further, use of equation 3-20 in the derivation of equation 3-21 causes the initially calculated value of ^{18}R (termed "roughly correct" above) to be low. Because the relative contribution of the term $\{2\cdot{}^{17}R\}$ to ^{45}R is greater than that of $\{2\cdot{}^{13}R\cdot{}^{17}R + {}^{17}R_2\}$ to ^{46}R, the error in ^{13}R will be greater than the error in ^{18}R.

Clearly, this cascade of errors can be most appropriately prevented by "uncoupling" ^{17}R and ^{18}R (that is, by not using equation 3-20 to express the relationship between ^{17}R and ^{18}R). Two approaches are possible. If ^{13}R is known independently, the sequence of calculations that we will term "^{13}C-known" can be employed:

1. ^{17}R is calculated from ^{45}R and ^{13}R (eq. 3-10).

2. ^{18}R is calculated from ^{46}R, ^{13}R, and ^{17}R (eq. 3-11). If ^{17}R is known independently, or if it is expedient to adopt an estimated value in order to reduce systematic errors in the analysis of samples for which neither ^{13}R nor ^{18}R is known, but in which ^{18}O has been enriched well above natural abundance, a sequence of calculations that might be

termed "^{17}O-known" can be employed:

1. ^{13}R is calculated from ^{45}R and ^{17}R (eq. 3-10).
2. ^{18}R is calculated from ^{46}R, ^{13}R, and ^{17}R (eq. 3-11).

To explore these problems and possibilities, we have prepared and analyzed mass spectrometrically a series of carbon dioxide samples enriched in the heavy isotopes of oxygen. Oxygen in these samples was derived by exchange with waters prepared by mixing 99% ^{18}O-water with distilled tap water. Because only oxygen-isotopic compositions could be affected by exchange, the true carbon-12/carbon-13 ratio in all samples was identical.

Results of the mass spectrometric analyses are summarized in Table 3-2, which includes normalized ion-current ratios as well as two different sets of calculated isotopic compositions. The columns headed "R" tabulate apparent isotopic compositions derived from the routine sequence of calculations. Samples bearing higher numbers have higher abundances of ^{18}O, and it can be seen that, as the oxygen-18 content of the samples increases, the apparent value of $\delta^{13}C_{PDB}$ does not remain constant, but, instead, decreases systematically. For samples enriched in ^{18}O by approximately 300‰, the error amounts to almost -10‰ (see sample 21: the routine calculation yields -19.11‰ even though the correct result must still be -10.17‰).

Use of the "^{13}C-known" sequence of calculations is appropriate in this case. Columns headed "CK" in Table 3-2 tabulate results. Because routine analysis of the unexchanged material indicated a carbon-isotopic composition of -10.17‰ vs PDB, this value was assigned to all samples in which ^{18}O had been enriched by exchange. Comparison of oxygen-isotopic compositions reported for each sample in the "R" and "CK"

Table 3-2: Carbon Dioxide-Oxygen Derived From Mixed Waters

sample	$^{45}Q^{a}$	$^{46}Q^{b}$	$\delta^{13}C_{PDB}$, ‰		$\delta^{17}O_{SMOW}$, ‰		$\delta^{18}O_{SMOW}$, ‰	
			R^{c}	CK^{d}	R^{c}	CK^{d}	R^{c}	CK^{d}
0^{e}	0.999857	1.001108	-10.17		16.95		32.56	
1	0.999835	1.004370	-10.24	-10.17	18.68	17.65	35.92	35.93
2	0.999900	1.018367	-10.66	-10.17	20.06	18.70	50.38	50.40
3	0.999952	1.036724	-11.19	-10.17	34.58	18.64	69.72	69.77
4	0.999913	1.045923	-11.66	-10.17	40.44	19.82	78.84	78.90
5	0.999982	1.061658	-12.06	-10.17	48.57	20.00	95.08	95.14
6	0.999935	1.074606	-12.56	-10.17	55.22	20.38	108.46	108.52
7	1.000006	1.090567	-13.02	-10.17	63.36	19.25	124.93	125.02
8	0.999960	1.102645	-13.48	-10.17	69.48	19.65	137.40	137.50
9	0.999973	1.116238	-13.92	-10.17	76.34	19.84	151.44	151.55
10	1.000012	1.131351	-14.38	-10.17	83.91	20.48	167.04	167.17
11	0.999940	1.140809	-14.77	-10.17	88.63	19.33	176.81	176.95
12	1.000060	1.159847	-15.27	-10.17	98.06	21.25	196.47	196.62
13	1.000009	1.174993	-15.81	-10.17	105.48	20.51	212.03	213.39
14	0.999982	1.187568	-16.25	-10.17	111.67	20.00	225.09	225.28
15	1.000003	1.201021	-16.67	-10.17	118.21	20.32	238.98	239.18

Table 3-2 continued:

sample	$^{45}Q^{a}$	$^{46}Q^{b}$	$\delta^{13}C_{PDB}$, ‰		$\delta^{17}O_{SMOW}$, ‰		$\delta^{18}O_{SMOW}$, ‰	
			R^{c}	CK^{d}	R^{c}	CK^{d}	R^{c}	CK^{d}
16	1.000048	1.215488	-17.08	-10.17	125.21	21.05	253.92	254.13
17	1.000046	1.229741	-17.54	-10.17	132.07	21.02	268.64	268.86
18	1.000050	1.242293	-17.94	-10.17	138.08	21.09	281.60	281.84
19	1.000078	1.258186	-18.41	-10.17	145.65	21.53	298.01	298.26
20	1.000106	1.270707	-18.77	-10.17	151.58	21.97	310.94	311.20
21	1.000184	1.284294	-19.11	-10.17	157.98	23.22	324.97	325.24

[a] $^{45}Q = {}^{m45}R_{unknown}/{}^{m45}R_{standard}$. $^{45}R_{standard} = 0.01188158$.

[b] $^{46}Q = {}^{m46}R_{unknown}/{}^{m46}R_{standard}$. $^{46}R_{standard} = 0.004149577$.

[c] R indicates routine sequence of calculations.

[d] CK indicates "^{13}C-known" sequence of calculations.

[e] Sample 0 was initial, unexchanged CO_2.

columns shows (i) that differences in the abundance of ^{18}O determined by the routine sequence and the "^{13}C-known" sequence of calculations are, indeed, small, and (ii) that much larger changes in the calculated abundance of ^{17}O result from uncoupling its abundance from that of ^{18}O.

To generalize these observations, the difference between the solution to equation 3-21 and the true value of ^{18}R was determined for all possible values of ^{18}F (^{17}O and ^{13}C were assumed to be at natural abundance). Results are summarized in Figure 3-2. More important in tracer studies, the relative difference between the calculated and true values of ^{18}F was also determined and is shown in Figure 3-3.

^{17}R and ^{18}R in Natural Samples. To examine relationships between ^{17}R and ^{18}R typical of those found in natural systems, a series of water samples was produced by fractional distillation. Subsequent exchange of oxygen between these samples and carbon dioxide yielded a series of samples of CO_2 with widely varying ^{18}O content. Because the same stock of CO_2 was used to prepare all samples, the carbon-isotopic compositions of all samples were identical.

Results of mass spectrometric analyses of these samples are summarized in the first two columns of Table 3-3. The third column, based on routine calculations with $a = 0.52$ and $K = 0.0094330$ (although the number of significant figures exceeds the precision with which K can presently be estimated, the value specified exactly reflects the mean isotopic abundances reported in ref. 14, and was employed in these calculations), indicates the range of oxygen-isotopic compositions. The fourth column tabulates carbon-isotopic abundances as determined in the same set of calculations. Inspection of the latter results shows that

Figure 3-2. Relative error in ^{18}R as a function of oxygen-18 enrichment: $^{13}R_{CO_2} = 1.12372 \times 10^{-2}$ and $^{17}R_{CO_2} = 3.73 \times 10^{-4}$. Exact solutions to equations 14 and 15 are obtained only at natural abundance ($^{18}R_{CO_2} = 2.00520 \times 10^{-3}$).

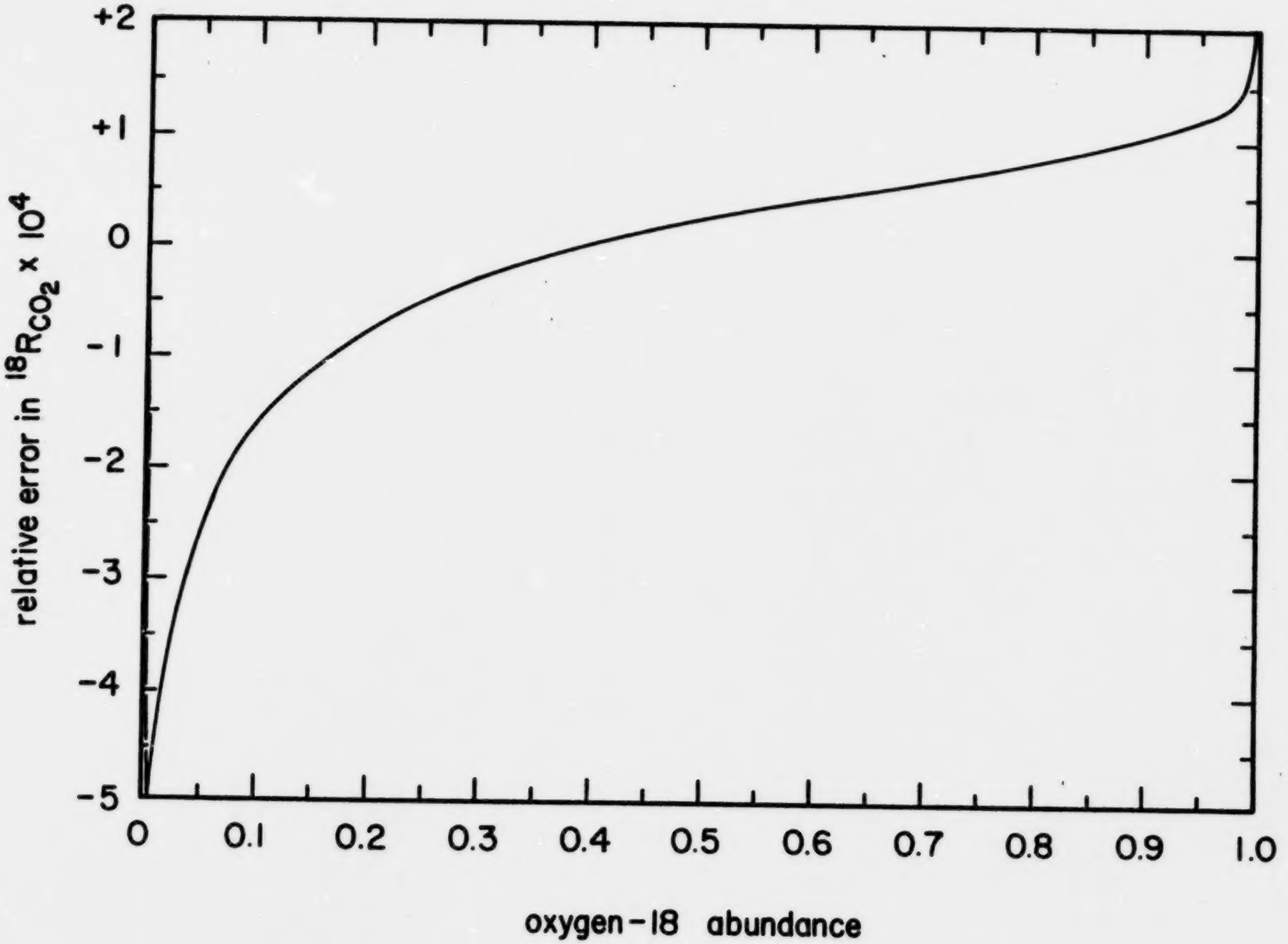
+2
+1
0
-1
-2
-3
-4
-5
relative error in $^{18}R_{CO_2}$ x 10^4
0
0.1
0.2
0.3
0.4
0.5
0.6
0.7
0.8
0.9
1.0
oxygen-18 abundance

Figure 3-3. Relative error in ^{18}F as a function of oxygen-18 abundance: $^{13}R_{CO_2}$ = 1.12372 x 10^{-2} and $^{17}R_{CO_2}$ = 3.73 x 10^{-4}. Values of $^{18}F_{CO_2}$ were calculated from equation 18 using solutions to equations 14 and 15. Exact solutions to equations 14 and 15 are obtained only at natural abundance ($^{18}F_{CO_2}$ = 2.000443 x 10^{-3}).

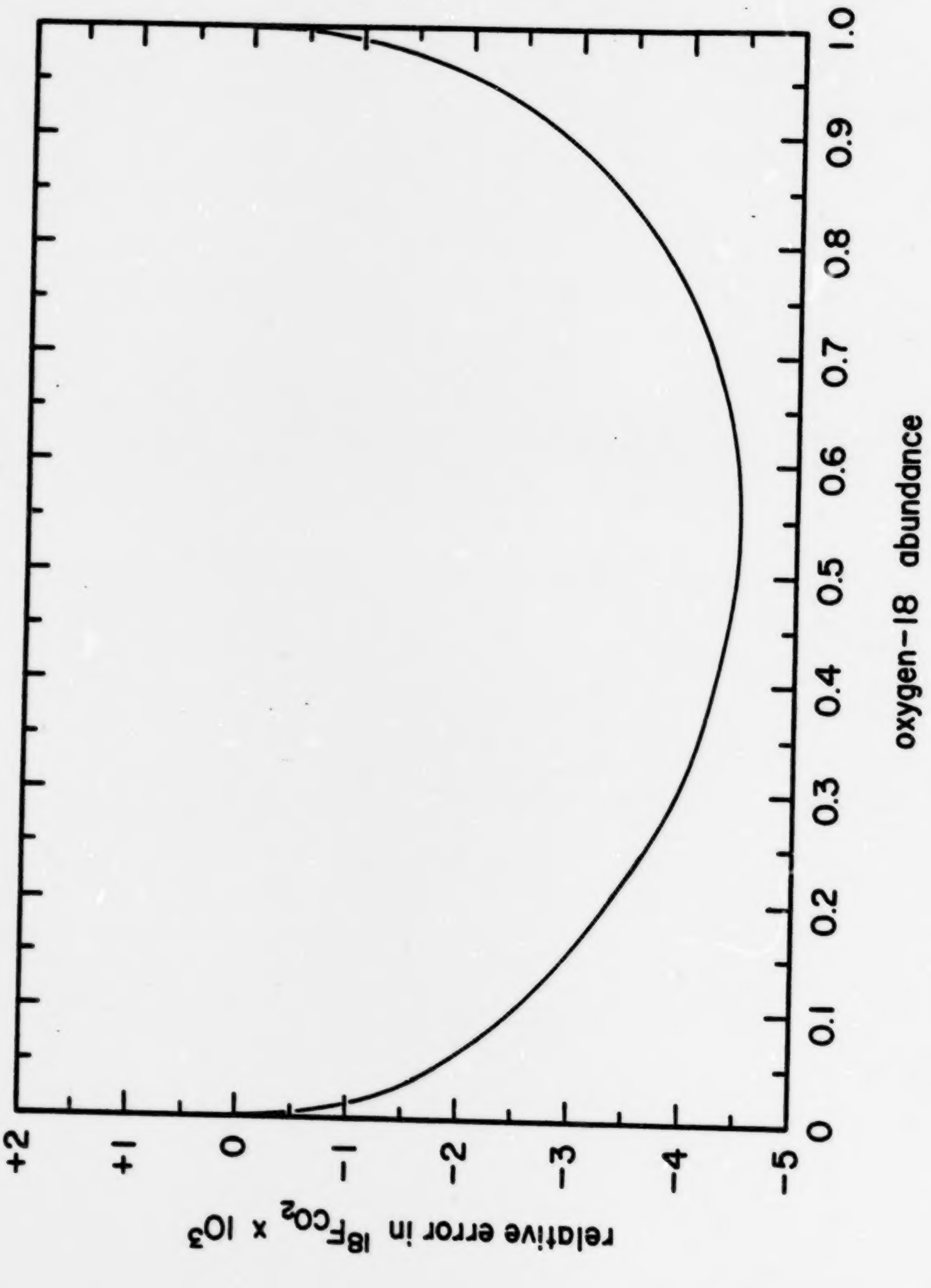
relative error in $^{18}F_{CO_2}$ x 10^3
+2
+1
0
−1
−2
−3
−4
−5
0
0.1
0.2
0.3
0.4
0.5
0.6
0.7
0.8
0.9
1.0
oxygen-18 abundance

Table 3-3: Carbon Dioxide-Oxygen Derived From Distilled Waters

sample	$^{45}Q^{a}$	$^{46}Q^{b}$	$\delta^{18}O_{SMOW}$, ‰	$\delta^{13}C_{PDB}$, ‰		
				0.52 .009433	0.50 .008335	0.52 .010090
0[c]	0.999857	1.001108				
1	0.996008	0.888515	-82.30	-10.18	-10.28	-10.03
2	0.996375	0.897943	-72.56	-10.14	-10.23	-10.02
3	0.996499	0.900305	-70.11	-10.09	-10.19	-9.98
4	0.996168	0.900698	-69.71	-10.46	-10.55	-10.34
5	0.996495	0.901266	-69.12	-10.13	-10.22	-10.02
6	0.996647	0.906725	-63.48	-10.17	-10.26	-10.07
7	0.996855	0.912028	-57.99	-10.15	-10.23	-10.06
8	0.997078	0.915067	-53.92	-10.06	-10.13	-9.98
9	0.997128	0.916327	-53.55	-10.02	-10.09	-9.94
10	0.997114	0.916420	-53.45	-10.04	-10.11	-9.96
11	0.997289	0.919115	-50.67	-10.12	-10.19	-10.05
12	0.997242	0.919410	-50.36	-10.01	-10.08	-9.94
13	1.000050	0.999867	+32.83	-9.93	-9.88	-10.04
14	1.000953	1.026080	+59.93	-9.89	-9.81	-10.06

[a] $^{45}Q = {}^{45}R_{unknown}/\ {}^{45}R_{standard}$. $^{45}R_{standard} = 0.01188158$.

[b] $^{46}Q = {}^{46}R_{unknown}/\ {}^{46}R_{standard}$. $^{46}R_{standard} = 0.004149577$.

[c] Sample 0 was initial, unexchanged CO_2.

the calculated carbon-isotopic composition is not independent of the oxygen-18 abundance, as it should be. In fact, regression of $\delta^{13}C$ on $\delta^{18}O$ indicates a slope of 0.0023‰C/‰O, a result which differs significantly ($p < 0.008$) from zero.

Small variations in assigned values of a and/or K have almost no effect on calculated values of $\delta^{18}O$, but can substantially affect the apparent variations in $\delta^{13}C$. As an example, the fifth column in Table 3-3 summarizes apparent carbon-isotopic compositions determined by use of the routine sequence of calculations with $a = 0.50$ and $K = 0.008335$. This corresponds to the present conventional approach (e. g., ref. 4). Regression of $\delta^{13}C$ on $\delta^{18}O$ in this case yields a slope of 0.0036 ‰C/‰, a systematic error even greater than that encountered in the preceding calculation. The sixth column in Table 3-3 reports apparent carbon-isotopic compositions determined by use of the routine sequence of calculations with $a = 0.52$ and $K = 0.010090$. In this case, K was adjusted to eliminate covariance between $\delta^{13}C$ and $\delta^{18}O$.

CONCLUSIONS

We have presented a simple approach to the calculation of isotope ratios from the mass spectra of carbon dioxide. A rigorous examination of the effect of assuming a quantitative relationship between ^{17}R and ^{18}R has shown (i) that determination of isotope ratios by the routine sequence of calculations for carbon dioxide highly enriched in oxygen-18 will result in errors in the isotopic analysis, and (ii) when $a = 0.52$ is used in the routine sequence of calculations, a value of $K = 0.010090$ more accurately describes the mass-dependent fractionations of oxygen isotopes by distillation and exchange. In the first case, errors in the isotopic analysis can be eliminated by decoupling ^{17}R and ^{18}R in the calculation, either with the "^{13}C-known", or the "^{17}O-known" sequence of calculations. In the second case, the value of K which eliminates covariance between δ^{13}C and δ^{18}O when a = 0.52 requires that $^{17}R_{SMOW} = 3.99 \times 10^{-4}$. It is, however, necessary to reevaluate the oxygen-17 content of SMOW by more direct methods. A systematic study of oxygen-17 and oxygen-18 abundances in many different natural samples and determination of values of a characteristic of representative processes in nature are also suggested.

EXPERIMENTAL SECTION

Preparation of Carbon Dioxide for Isotopic Analysis. A series of samples of water selectively enriched in oxygen-18 was prepared by mixing varying amounts of 99%-$H_2{}^{18}O$ (Stohler Isotopic Chemicals) with distilled, deionized water. A second series of water samples with mass-dependent enrichment of both ^{17}O and ^{18}O was produced by fractional distillation of tap water. For the exchange of oxygen between water and carbon dioxide, 200 µL of thoroughly degassed water and 20 µmoles of carbon dioxide were placed in a sealed, evacuated Pyrex tube (6 mm o.d.). The tubes were allowed to stand at 25°C for 48 hours to ensure that exchange of oxygen between water and carbon dioxide was complete (13). The carbon dioxide was purified by cryogenic distillation.

Mass Spectrometric Measurement. Values of ^{45}R and ^{46}R used in equations 3-16 and 3-17 must be numerically equivalent to the ratios of molecular species in the sample. There are two sets of reasons why recorded ion-current ratios may differ from absolute molecular ratios. Specific corrections are required in both cases.

First, there is a set of measurable phenomena such as background ion currents, amplifier-zero offsets, scattering of major-beam ions into minor-beam collectors, leakage of gas-switching valves, etc. Optimal procedures for measurement and correction of the effects of these artifacts have been extensively discussed (2-4). In the present work, only corrections for background ion currents and amplifier-zero levels have been required, and these have been applied prior to the calculation of ion-current ratios.

Second, the efficiency of the production of ions varies for the different isotopic species of carbon dioxide. If, however, this "mass-discrimination" is constant over time, then this problem can be eliminated using a reference measurement using carbon dioxide with a known isotopic composition as a working standard. Reference and sample gases are alternatively introduced into the mass spectrometer, and ion-currents at m/z = 44, m/z = 45, and m/z = 46 are measured for each gas (Figure 3-1). The true molecular-isotope ratios of the sample are determined as follows

$$ {}^{n}R_{\mathrm{sample}} = \frac{{}^{m}R_{\mathrm{sample}}}{{}^{m}R_{\mathrm{standard}}} \times {}^{n}R_{\mathrm{standard}} \qquad (3\text{-}23) $$

where ${}^{m}R$ refers to the ratio of recorded ion currents, ${}^{n}R$ refers to the true ratio of molecular species as defined in equations 3-7 through 3-11, and m and n = 45 or 46. Calibration of the working standard requires only determination of ${}^{45}R_{\mathrm{standard}}$ and ${}^{46}R_{\mathrm{standard}}$. A primary reference provides a sample of carbon dioxide with a known isotopic composition. Values of ${}^{45}R$ and ${}^{46}R$ for the primary reference are calculated from the known ${}^{13}R$, ${}^{17}R$, and ${}^{18}R$ using equations 3-7 and 3-8.

The fractional abundance of a particular isotope (j) is calculated directly from the isotope ratios

$$^{j}F = \frac{^{j}R}{\Sigma\,^{i}R} \qquad (3\text{-}24)$$

where the index i is an integral value indicating all stable isotopes of a particular element; in the case of carbon i = {12, 13} and in the case of oxygen i = {16, 17, 18}. For example, $^{18}F = {}^{18}R/(1 + {}^{17}R + {}^{18}R)$. Delta values are calculated from their definition (14)

$$\delta = \frac{R_{sample}}{R_{standard}} - 1 \quad x \quad 1000 \qquad (3\text{-}25)$$

Values of delta determined in this way do not incorporate mathematical approximations.

Mass spectrometric measurements were made using a Finnigan MAT Delta E isotope ratio mass spectrometer (Finnigan Corp.). Ion currents at m/z = 44, m/z = 45, and m/z = 46 were measured for the sample and a working standard. The contribution of instrumental background was subtracted from the ion current and the molecular ratios ^{45}R and ^{46}R for both gases were determined. The working standard was calibrated using carbon dioxide produced by phosphorolysis of K-2 and TKL-1 (15).

REFERENCES

1. Margrave, J. L.; Polansky, R. B. Relative abundance calculations for isotopic molecular species. J. Chem. Ed. 39:789-793, 1962.

2. Craig, H. Isotopic standards for carbon and oxygen and correction factors for mass-spectrometric analysis of carbon dioxide. Geochim. Cosmochim. Acta 12:133-149, 1957.

3. Deinis, P. Mass spectrometric correction factors fot the determination of small isotopic composition variations of carbon and oxygen. Int. J. Mass Spectrom. Ion Phys. 4:283-295, 1970.

4. Mook, W. G.; Grootes, P. M. The measuring procedure and corrections for the high-precision mass-spectrometric analysis of isotopic abundance ratios, especially referring to carbon, oxygen, and nitrogen. Int. J. Mass Spectrum. Ion Phys. 12:273-298, 1973.

5. Bigeleisen, J. The effects of isotopic substitution on the rates of chemical reactions. J. Phys. Chem. 56:823-828, 1952.

6. Matsuhisa, Y.; Goldsmith, J. R.; Clayton, R. N. Mechanisms of hydrothermal crystallization of quartz at 250°C and 15 kbar. Giochim. Cosmochim. Acta 42:173-182, 1978.

7. Bigeleisen, J.; Ishida, T.; Lee, M. W. Correlation of the isotopic chemistry of hydrogen, carbon, and oxygen with molecular forces by the WIMPER (2) method. J. Chem. Phys. 74:1799-1816, 1981.

8. Clayton, R. N.; Grossman, L.; Mayeda, T. K. A component of primitive nuclear composition in carbonaceous meteorites. Science 182:485-487, 1973.

9. Clayton, R. N.; Onuma, N.; Mayeda, T. K. A classification of meteorites based on oxygen isotopes. Earth Planet. Sci. Lett. 30:10-18, 1976.

10. Craig, H. Standard for reporting concentrations of deuterium and oxygen-18 in natural waters. Science 133:1833-1835, 1961.

11. Baertschi, P. Absolute ^{18}O content of standard mean ocean water. Earth Planet. Sci. Let. 31:341-344, 1976.

12. Nier, A. O. A redetermination of the relative abundances of the isotopes of carbon, nitrogen, oxygen, argon, and potassium. Phys. Rev. 77:789-793, 1950.

13. O'Neil, J. R.; Epstein, S. A method of oxygen isotope analysis of milligram quantities of water and some of its applications. J. Geophys. Res. 71:4955-4961, 1966.

14. McKinney, C. R.; McCrea, J. M.; Epstein, S.; Allen, H. A.; Urey, H. C. Improvements in mass spectrometers for the measurement of small differences in isotope abundance ratios. Rev. Sci. Inst. 21:724-730, 1950.

15. Blattner, P.; Hulston, J. R. Proportional variations of geochemical $\delta^{18}O$ scales. An interlaboratory comparison. Geochim. Cosmochim. Acta 42:59-62, 1978.

CHAPTER 4

DEPOSITION, DISTRIBUTION, AND CLEARANCE OF OZONE-DERIVED OXYGEN IN THE RESPIRATORY SYSTEM

In order to provide experimental measurements of the dose of ozone to the respiratory system, the retention and clearance of ozone-derived oxygen in the respiratory system has been examined using oxygen-18 as a tracer for inhaled ozone. Extrapolation of health effects from laboratory animals to humans begins with a prediction of the uptake of ozone in the human respiratory system based on mathematical dosimetry models which describe the transport and absorption of reactive gases in the lung (1). This approach requires an understanding of the origin of species differences in the dose of ozone to tissue and an understanding of the factors controlling the distribution of ozone-derived oxygen in the respiratory system. Correlation of systematic differences in airway structure and ventilation patterns (2) with quantitative differences in local tissue dose in different mammalian species will provide a more complete understanding of the factors controlling transport and removal of ozone in the respiratory system. The first two studies discussed in this chapter were designed to assess i) the feasibility of utilizing $^{18}O_3$ to determine species differences in deposition and ii) the ability to resolve depositional patterns within the respiratory system.

The primary events of injury to the lung must involve interaction of oxidants with biological molecules. Following the initial insult, molecules altered by ozonolysis may fail to fulfill their biological function (3). Products of ozonolysis may initiate autoxidation directly or may mediate cell damage as chemotactic agents for alveolar macrophages and polymorphic neutrophile (4-8), both events resulting in changes in cellular function, and possibly cell death. Mechanisms of protection against oxidant injury (9,10) and of extrapulmonary effects (11) have only recently been considered. The dependence of dose on exposure time at a single concentration has been examined. The distribution of ozone-derived oxygen in proteins, lipids, and organic solutes and the clearance of ozone-derived oxygen from the lung also have been determined.

Detection and Quantitation of the Oxygen-18 Label

Stable isotopes are ubiquitous in nature. Approximately 0.2% of oxygen in biological material is oxygen-18. Detection and quantitation of tracer-derived oxygen in tissue therefore requires precise knowledge of the isotopic composition of i) the initial tissue-oxygen pool and ii) the tissue-oxygen pool after incorporation of the tracer. An isotopic mass balance of oxygen in tissue from an animal exposed to labeled ozone yields an expression which can be used to determine the dose of ozone-derived oxygen to tissue. For ozone labeled with oxygen-18, the mole fraction of ozone-derived oxygen in the tissue oxygen pool is

$$\frac{n_{TR}}{n_{TI}} = \frac{{}^{18}F_{TI,E} - {}^{18}F_{TI,NA}}{{}^{18}F_{TR} - {}^{18}F_{TI,NA}} \qquad (4\text{-}1)$$

where ${}^{18}F$ is the fractional abundance of oxygen-18 and n is the quantity of oxygen (*e. g.*, micromoles O) in the i-*th* oxygen pool; the subscripts designate the oxygen pools {tissue, natural abundance (TI,NA); tissue, enriched (TI,E); and tracer (TR)}. The numerator in the right-hand side of equation 1 is the enrichment of oxygen-18 in the tissue-oxygen pool, the amount in excess of the natural background. The denominator in the right-hand side of equation 1 quantifies the potential of the tracer to produce an enrichment in the tissue. This mathematical formalism can be used in studies employing ozone which is less than 100% oxygen-18.

In this work, "dose" will refer to the total amount of ozonederived oxygen in a tissue sample, whereas "relative enrichment" refers to the mole fraction of ozone-derived oxygen in the tissue-oxygen pool. Dose is determined from relative enrichment and the size of the tissueoxygen pool

$$\text{dose} = (\text{relative enrichment}) \times (\text{oxygen pool}) \qquad (4\text{-}2)$$

where oxygen pool refers to the amount of atomic oxygen (moles) in the tissue. Utilization of oxygen-18 as a physiological tracer (in fact, utilization of any stable isotope which is normally present in biological material as a physiological tracer) requires both elemental and isotopic analyses to quantify dose.

A fundamental limitation on detection and quantitation of an isotopic tracer is imposed by variations in the natural abundance of oxygen-18, which include both variations in individual animals with time and variations among animals in the same population. These variations appear as unavoidable "noise" on the "stable isotopic signal" in any biological system. The precision of the measurement of oxygen-18 derived from labeled material in a physiological sample is a function of i) the precision of the mass spectrometric measurement, ii) isotopic variations introduced by sample preparation (including conversion of oxygen to carbon dioxide), and iii) naturally occurring variations in the abundance of oxygen-18 in the sample material. Mathematically, this can be expressed as a sum of variances

$$s_T^2 = s_M^2 + s_P^2 + s_N^2 \qquad (4\text{-}3)$$

where s_T^2 is the total analytical variance, s_M^2 is the variance associated with the mass spectrometric measurement, s_P^2 is the variance arising from sample preparation, and s_N^2 expresses natural variations in oxygen isotopic abundance as a variance. The level of isotopic enrichment also affects the precision (enrichments just above natural abundance can be measured more precisely than large enrichments), but the exact relationship between enrichment and analytical precision has not been determined.

Ideally, sample preparation and mass spectrometric measurement procedures should contribute insignificantly to uncertainty in the isotopic analysis. In practice, this condition is rarely achieved. Contributions to the variance in ^{18}F from these sources are summarized in Table 4-1. Each entry represents the variance obtained from five replicate analyses. The contribution of the mass spectrometric measurement (s_M^2) was determined from analysis of identical samples of carbon dioxide. The variance associated with sample preparation (s_P^2) has two sources: preparation of carbon dioxide from organically bound oxygen and sampling of an inhomogeneous powder (tissue homogenate). The first contribution was determined by analysis of carbon dioxide prepared from crystalline glycine and the second contribution was determined from analysis of carbon dioxide prepared from samples of a single lung homogenate. Variations in the abundance of oxygen-18 between animals (s_N^2) were examined by analysis of lung homogenates from different animals. Temporal variations of oxygen-18 were not considered here. The preparation of carbon dioxide from organic material is the greatest single source of uncertainty in the isotopic analysis, accounting for 36% of the analytical variance. Tissue sampling and variations among animals account for 34% and 29% of the analytical variance, respecively. The

Table 4-1. Contributions to the Variance in ^{18}F

source	s^2 x 10^{15}	Σs^2 x 10^{15}	detection limit[f] ppm
mass spectrometer[a]	6	6	0.10
sample preparation[b]	157[e]	163	0.50
tissue sampling[c]	146[e]	309	0.69
natural abundance[d]	126[e]	435	0.82

[a] replicate analyses of carbon dioxide.

[b] replicate analyses of glycine.

[c] replicate analyses of a single lung homogenate.

[d] replicate analyses of lung homogenates from different animals.

[e] individual contributions to the variance were calculated sequentially from the total variance (Σs^2).

[f] 95% confidence limit for relative enrichment, where $s^2 = 4.35 \times 10^{-3}$ for $^{18}F_{TI,NA}$ and $^{18}F_{TI,E'}$ $^{18}F_{TR} = 0.99$, and $N = 5$.

mass spectrometric measurement contributes only 1% of the observed variance. Detection limits corresponding to the cumulative variance at each step were calculated. A detection limit of < 1 ppm (that is, one atom of excess oxygen-18 per 10^6 atoms of oxygen in the tissue-oxygen pool) is expected if no sources of uncertainty other than those considered are present. However, differences in physiological states of individual animals can cause differences in the retention of label in tissue. Variations in the abundance of oxygen-18 observed in an apparently homogeneous test population may be significantly greater than predicted. The detection limit for excess oxygen-18 in a given test population will be effected by experimental conditions and must be evaluated in each case.

Deposition in the Respiratory System

Comparative Aspects of Ozone Uptake. This study comprises a comparison of the uptake of ozone-derived oxygen in the respiratory system of the rabbit (6.5 kg), the rat (380 g), and the mouse (21.5 g). Tissue samples included head (nasopharynx), trachea, lungs, and blood. In two separate exposures, three animals (one of each species) were placed in an exposure chamber containing 1 ppm of $^{18}O_3$ for 60 minutes. Unexposed animals (two of each species) were used to establish the natural abundance of oxygen-18 in each sample.

Results of isotopic analysis are shown in Table 4-2. Relative enrichments were calculated using equation 1, where $^{18}F_{TI,NA}$ was the abundance of oxygen-18 in tissue from unexposed animals, $^{18}F_{TI,E}$ was the abundance of oxygen-18 in tissue from exposed animals, and $^{18}F_{TR} = 0.99$. Dose was determined from the relative enrichment and an estimate of the size of the oxygen pool in each tissue, shown in Table 4-3.

Table 4-2. Deposition of Ozone-Derived Oxygen in the Respiratory System

tissue species	$^{18}F_{TI,NA}$[a] x10³	$^{18}F_{TI,E}$[a] x10³	enrichment[b] x10⁴	dose[c] nanomoles
head				
mouse	2.0286	2.0341	5.5	8.0 ± 0.8
rat	2.0302	2.0339	3.7	36 ± 6
rabbit	2.0330	2.0334	0.3	0
trachea				
mouse	2.0302	2.0463	16.4	6.2 ± 1.7
rat	2.0322	2.0489	19.9	111 ± 32
rabbit	2.0296	2.0373	7.7	63 ± 34
lung				
mouse	2.0326	2.0520	19.6	8.6 ± 0.8
rat	2.0323	2.0454	13.2	51.7 ± 2.9
rabbit	2.0335	2.0438	10.4	286 ± 22
blood				
mouse	2.0243	2.0245	0.2	0
rat	2.0235	2.0237	0.2	0
rabbit	2.0220	2.0225	0.5	0

[a] x, SE = 0.0003 x 10^{-3}, and N = 2.

[b] enrichments were calculated using the following equation 1, where $^{18}F_{TR}$ = 0.99, $^{18}F_{TI,NA}$ was the fractional abundance of oxygen-18 in the unexposed animals, and the $^{18}F_{TI,E}$ was the fractional abundance of

[c] oxygen-18 in the exposed animals, SE = 0.7 x 10^{-4}.

[d] dose is total tissue uptake, uncertainty is propagated SE.

isotopic enrichment was not statistically significant ($p < 0.05$).

Table 4-3. Oxygen Pools in Nasopharynx, Trachea, Lungs, and Blood

tissue species	weight g	% oxygen wt/wt	oxygen pool millimoles
head			
mouse	0.126 ± 0.012	16.1 ± 0.5	1.27 ± 0.12
rat	0.90 ± 0.15	17.3 ± 0.9	9.7 ± 1.7
rabbit	5.89 ± 0.10	19.5 ± 1.3	72 ± 5
trachea			
mouse	0.003 ± 0.001	20.5 ± 0.9	0.38 ± 0.13
rat	0.045 ± 0.013	19.8 ± 0.4	5.6 ± 1.6
rabbit	0.673 ± 0.029	19.6 ± 0.6	8.2 ± 4.4
lung			
mouse	0.032 ± 0.003	21.9 ± 0.7	0.44 ± 0.04
rat	0.289 ± 0.018	21.7 ± 0.5	3.92 ± 0.24
rabbit	2.03 ± 0.14	21.7 ± 0.7	27.5 ± 2.1
blood			
mouse	-----	19.3 ± 0.1	-----
rat	-----	19.3 ± 0.2	-----
rabbit	-----	19.4 ± 0.1	-----

Species differences in the uptake of ozone have their origin in differences in respiratory rate, lung size, total surface area, and ventilation. Since these parameters are proportional to body mass (13), isotopic enrichment and dose also should be a regular function of body mass. When relative enrichment is considered, the mole fraction of ozone-derived oxygen in the tissue-oxygen pool decreases with body mass. The size of the tissue-oxygen pool in each sample increases with body mass (Table 4-3), so that, with the exception of tissue from the nasopharynx, the total amount of ozone-derived oxygen in each sample increases with body mass (Table 4-2).

Measurements of the tracheal concentration of ozone in rats, guinea pigs, rabbits (14), and dogs (15,16) indicate that approximately 50% of inhaled dose is removed in the head. Nasopharyngeal deposition is therefore related to minute volume and should be directly proportional to body mass. In this study, however, an inverse trend was observed. Measurement of isotopic enrichment in the nasopharynx was complicated by the sampling procedure. Head samples included portions of extraneous muscle and skeletal material which was more difficult to remove reproducibly from the larger samples. Incorporation of small amounts of label into an increasingly large oxygen pool composed of oxygen from unexposed tissue (extraneous material) resulted in an apparent decrease in the amount of ozone-derived oxygen retained in the nasopharynx. Problems of dilution in larger animals have been circumvented with the use of different sampling techniques.

Distribution Within the Respiratory System. The distribution of ozone-derived oxygen in the respiratory system was determined in rabbits. One animal was exposed to 1 ppm $^{18}O_3$ for 60 minutes and one animal was retained to establish natural abundance. Results of isotopic analysis of airway epithelium from both animals are shown in Table 4-4. The relative enrichment in each sample was calculated using equation 1; $^{18}F_{TI,NA}$ was the oxygen-18 abundance in tissue from the unexposed animal, $^{18}F_{TI,E}$ was the oxygen-18 abundance in tissue from the exposed animal, and $^{18}F_{TR} = 0.99$ (Table 4-4). The dose to various epithelial regions was determined using equation 2, where the size of the oxygen pool was determined from the elemental analysis and the weight of the sample. Dose is expressed as picomoles of ozone-derived oxygen per milligram of dry epithelial tissue (Table 4-4).

As expected, the dose is highest in areas of greatest turbulence, the nasal turbinates and the trachea immediately below the laryngeal jet (17), and in the conducting airways of the lung (refer to Figure 4-1 for proper anatomical orientation). A small, but statistically significant ($p > 0.05$) isotopic enrichment is observed in the peripheral parenchyma of the lung. Based on the preceding discussion of variance, the detection limit is 20 picomoles of ozone-derived oxygen per milligram of epithelium. Although the dose is greatest in the nasopharynx and the conducting airways of the lung, a small amount of ozone does reach the centriacinar region. Since oxidant injury to respiratory tissue is responsible for pulmonary toxicity, the ability to measure the dose to peripheral regions of the lung is necessary in establishing a valid dose-response relationship for inhaled pollutants. However, the finding that the dose to the centriacinar region of the lung is extremely small, even with a high atmospheric concentration of ozone, brings into question the ability of ozonolysis alone to account for injury to tissue. It is therefore likely that other mechanisms of tissue damage occur.

Table 4-4. Uptake of Ozone-Derived Oxygen in the Respiratory System

tissue		$^{18}F_{TI,NA}$ x 10^3	$^{18}F_{TI,E}$ x 10^3	enrichment[a] x 10^4	dose[b] picomole/mg
nasal turbinates		2.0402	2.1359	96.9	1150
nasal septum		2.0377	2.1179	81.2	930
nasal pharynx		2.0311	2.1124	82.3	930
olfactory mucosa		2.0344	2.0651	31.1	440
trachea	1	2.0301	2.3518	325.6	3660
	2	2.0301	2.2251	197.4	2220
	3	2.0301	2.1782	149.9	1690
	4	2.0301	2.1554	126.9	1430
	5	2.0301	2.1869	158.7	1790
lung 2mm airway		2.0262	2.1267	101.8	1590
lung parenchyma		2.0312	2.0365	5.3	70

[a] enrichments were calculated using equation 1, where $^{18}F_{TR} = 0.99$, $^{18}F_{TI,NA}$ was the fractional abundance of oxygen-18 in the unexposed animals, and the $^{18}F_{TI,E}$ was the fractional abundance of oxygen-18 in the exposed animals.

[b] dose is the amount of ozone-derived oxygen/milligram of dry epithelium.

Figure 4-1. Distribution of ozone-derived oxygen in the respiratory system. The dose in a rabbit exposed to 1 ppm $^{18}O_3$ for 60 minutes is expressed as picomoles/milligram dry epithelial tissue (refer to Table 4-2).

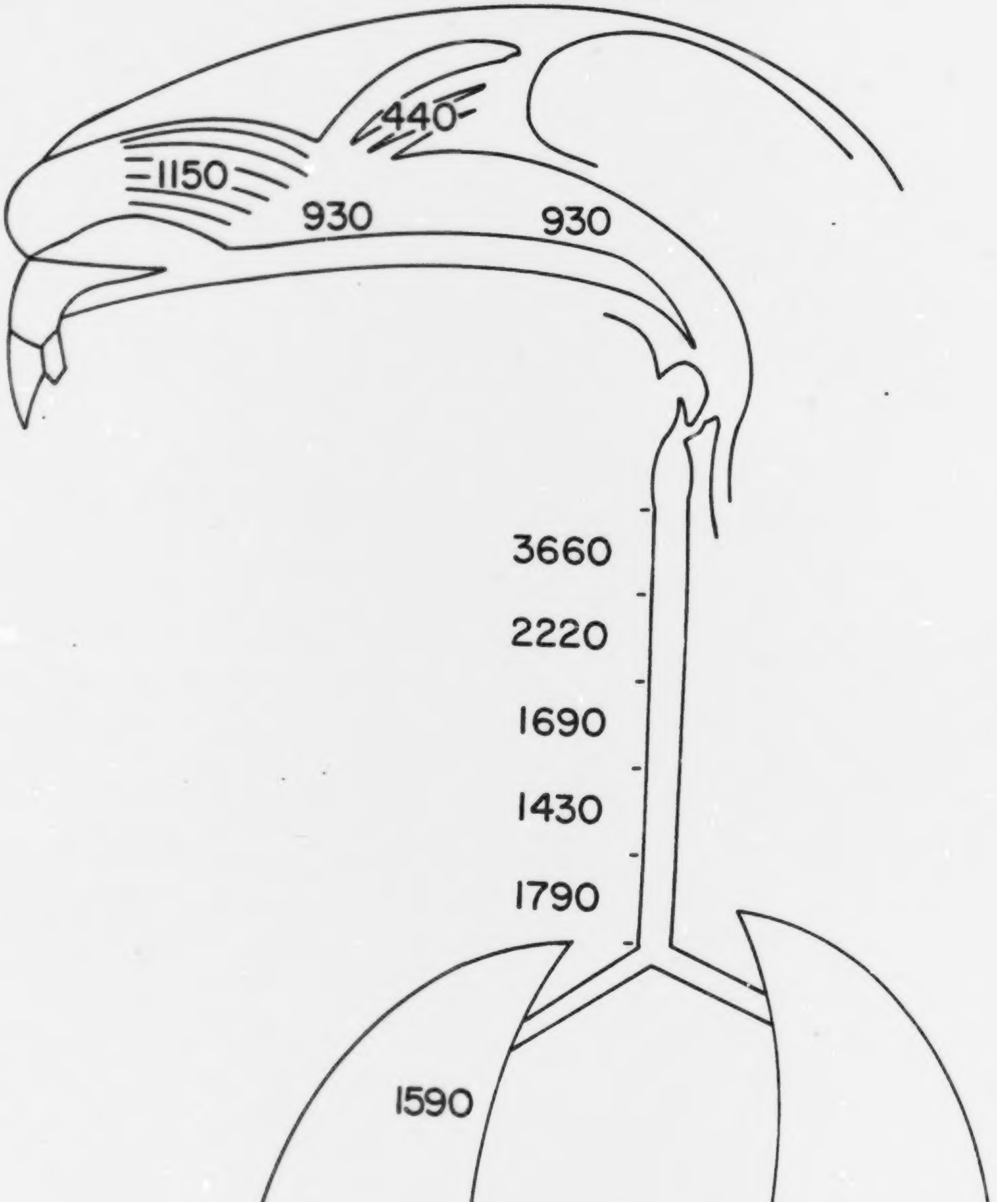
1690
1790
1590

Finally, the demonstrated ability to resolve spatial distributions of ozone-derived oxygen within the respiratory system by this technique offers great promise in the validation and definition of mathematical dosimetry models.

Deposition and Clearance in the Lung

Deposition in the Lung. To determine the effect of exposure time on retained dose in the lungs, groups of five mice were exposed to 1 ppm $^{18}O_3$ for times up to 60 minutes. A portion of the lungs from each animal was retained for analysis. The remaining tissue from the five animals in an exposure group was pooled and chemically fractionated into an acid precipitable fraction (macromolecules), chloroform extractable fraction (lipids), and a water:methanol soluble fraction (solutes). The natural abundance of oxygen-18 in each of these samples was established using five unexposed animals.

Results of isotopic analysis are shown in Table 4-5. All variables were analyzed within a linear regression framework. The dependent variable was ^{18}F and the independent variables were exposure time, the actual concentration of ozone, and their interaction. There was no indication that body weight (21.2 ± 0.7 g), lung wet weight (144 ± 8 mg), or lung dry weight (30 ± 2 mg) varied significantly ($p < 0.05$) by exposure group. Although there was some evidence of lack of fit ($p = 0.01$), this appears to be due primarily to the anomalously high average isotopic composition of the group at the 30-minute exposure. Polynomial fits did not suggest the existence of anything but a linear trend. The least-squares fit for ozone-derived oxygen in whole lung vs exposure time is shown in Figure 4-2 and those for each chemical fraction are shown in Figure 4-3. The uncertainty indicated in Figure 4-3 is the 95%

Table 4-5. Deposition of Ozone-Derived Oxygen in the Lungs

exposure time min	^{18}F x 10^3			
	lung homogenate[a]	acid precipitate[b]	chloroform extract[b]	water:methanol extract[b]
0	2.0339 ± 0.0007	2.0323 ± 0.0003	2.0353 ± 0.0004	2.0442 ± 0.0004
6	2.0350 ± 0.0001	2.0336 ± 0.0012	2.0351 ± 0.0003	2.0435 ± 0.0006
17	2.0398 ± 0.0015	2.0352 ± 0.0013	2.0388 ± 0.0006	2.0546 ± 0.0007
21	2.0395 ± 0.0014	2.0352 ± 0.0011	2.0448 ± 0.0005	2.0476 ± 0.0009
30	2.0486 ± 0.0014	2.0444 ± 0.0017	2.0569 [c] ± 0.0007	2.0527 ± 0.0006
32	2.0412 ± 0.0019	2.0346 ± 0.0019	2.0469 ± 0.0007	2.0505 ± 0.0006
35	-----	2.0363 ± 0.0014	2.0473 ± 0.0003	2.0503 ± 0.0008
44	2.0453 ± 0.0017	2.0449 ± 0.0020	2.0493 ± 0.0004	2.0570 ± 0.0010
60	2.0521 ± 0.0024	2.0466 ± 0.0022	2.0579 ± 0.0006	2.0554 ± 0.0009
intercept[d]	2.0337	2.0315	2.0342	2.0451
slope [d]	0.0003	0.0002	0.0004	0.0002
r^2 [d]	0.663	0.726	0.767	0.669

[a] x ± SE for five animals in a single exposure group.

[b] x ± SE for triplicate analyses of pooled samples.

[c] excluded form the linear regression.

[d] values of linear regression

Figure 4-2. Uptake of ozone-derived oxygen in the lung. A plot of oxygen-18 abundance in lung tissue vs exposure time for mice exposed to 1 ppm $^{18}O_3$ is shown. Each point is the mean and standard error of the mean for analysis of tissue from five mice in an exposure group. The regression line with 95% confidence limit for the regression estimate is also indicated.

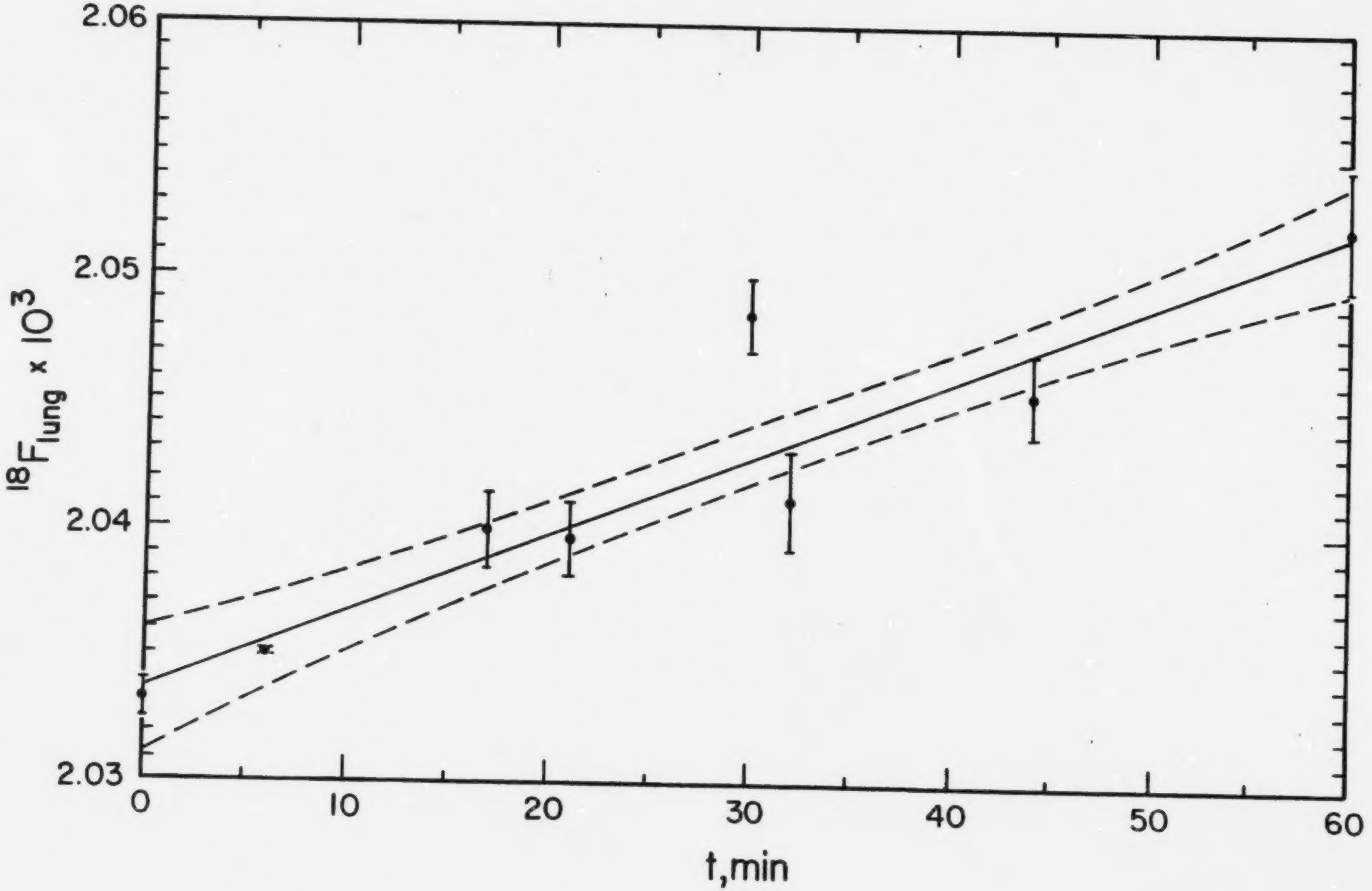
$^{18}F_{lung} \times 10^3$
2.06
2.05
2.04
2.03
0
10
20
30
40
50
60
t,min

Figure 4-3. Molecular distribution of ozone-derived oxygen in the lung. Plots of oxygen-18 abundance in the water:methanol extract, the acid precipitate, and the chloroform extract vs exposure time are shown. Each point is the mean and standard error of the mean for three replicate analyses of fraction obtained from pooled lung tissue. The regression lines and 95% confidence limits for the regression estimates are indicated.

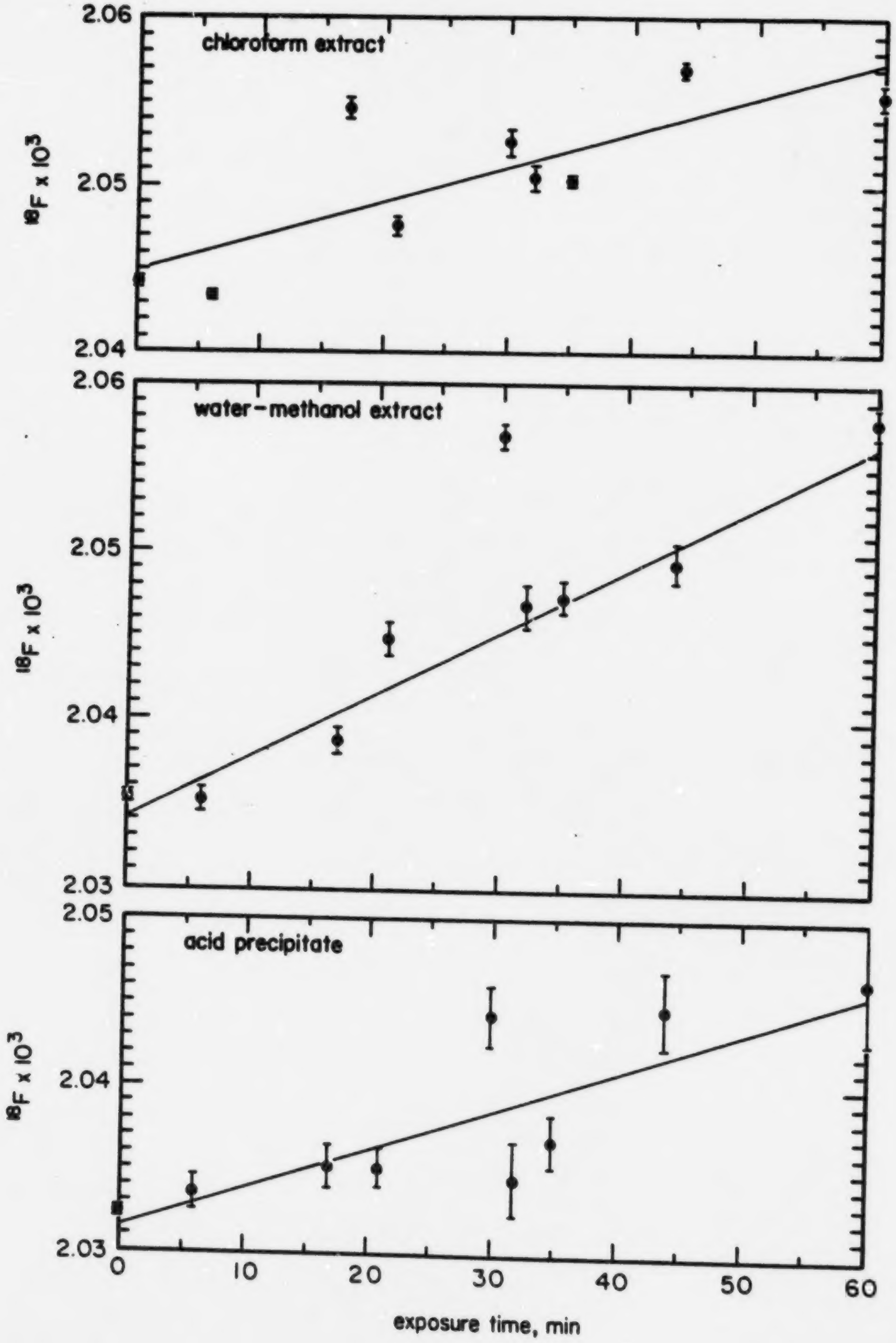
chloroform extract
water-methanol extract
acid precipitate
$^{18}F \times 10^3$
2.06
2.05
2.04
2.03
0
10
20
30
40
50
60
exposure time, min

confidence limit for the entire population, indicating real variation among individuals. Since pooled tissue samples were used to obtain the chemical fractions, uncertainties indicated in Figure 4-3 represent analytical variation.

The regression explained approximately 73% of the total variation in the fractional abundance of oxygen-18 in whole lung, 73% in the acid precipitate, 67% in the chloroform extract, and 77% in the methanolwater extract. There was evidence of an interaction ($p = 0.002$) between dose and exposure time in whole lung, but it was not significant when only exposed animals were considered. In all cases, regression of ^{18}F on the concentration-time product explained less of the total variability than did exposure time alone. Within a narrow concentration range, exposure time is the most important factor controlling uptake of ozone-derived oxygen in the lung.

In the statistical analysis, it was assumed that the variance of ^{18}F is constant for all exposure groups, a condition apparently not achieved in this case. The variance in ^{18}F of whole lung tissue seems to increase with exposure time. The statistical tests utilized are generally robust with respect to departures from this assumption, but levels of significance for specific statistical tests may be lower than if the variance were constant. A possible explanation for this heteroscedasticity is that free-breathing animals were used. Differences in minute volume among animals in the same exposure group, resulting from physiological stress, had been exacerbated over time, and could modulate the inhaled dose. Animals in groups with shorter exposure times were generally uniformly active, whereas differences in activity increased with longer exposure times. In fact, some animals appeared to sleep, burying their nose in fur, thus filtering inspired air, while others remained active throughout the entire exposure.

The dose of ozone-derived oxygen to the lungs and to each fraction was determined using regression estimates of ^{18}F as a function of exposure time. Equation 1 was used to determine the relative enrichment in each sample, where the abundance of oxygen-18 in samples from unexposed animals was used to establish $^{18}F_{TI,NA}$, the regression estimate of isotope abundance was used to determine $^{18}F_{TI,E}$, and $^{18}F_{TR} = 0.99$. Dose was determined from relative enrichment and the size of the oxygen pool. Estimates of the sizes of the oxygen pools are shown in Table 4-6. Whole lung retained approximately 100 picomoles per minute of ozone-derived oxygen. Of this amount, 63% was in the acid precipitate, 10% was in the chloroform extract, the 12% was in the methanol-water extract, and 15% was lost.

These results are somewhat surprising in light of the suggestion that membrane lipids are the primary targets for ozone (18,19). Most of the retained label appears in the acid precipitate rather than in the chloroform extract, suggesting that proteins rather than lipids are the primary targets for attack by ozone. Appearance of the isotopic label in proteins can result from termination reactions between radicals produced by ozonolysis of unsaturated lipids and proteins; however, direct attack on proteins is also a possible explanation. The unaccounted portion could have been lost by volatilization of labile molecules on acidification (small organic acids and bicarbonate) and by exchange of oxygen with water (20). Loss of the isotopic label could also have occurred during the exposure and, depending on the products of ozonolysis, resulted in selective depletion of label from one of the

Table 4-6. Lung Oxygen Pool[a]

sample	dry weight mg	% of total	% oxygen	oxygen pool micromoles
whole lung	30	100	21.9	411
chloroform extract	3	10	12.9	24
acid precipitate	20	65	31.1	288
water:methanol extract	7	25	26.8	117

[a] body weight = 20.97 ± 0.13 g, lung wet weight = 154 ± 2 mg.

x ± SE, N = 45.

chemical fractions. A complete mass balance of inhaled ozone-derived oxygen would help answer questions of tissue dose and molecular targets. Further work in this area is therefore needed.

Pulmonary toxicity is more closely related to the concentration of ozone, as opposed to exposure time or the time-weighted-average concentration (12). Future studies employing different concentrations of ozone will indicate whether tissue-dose is related to atmospheric concentration or whether saturation of the ability of the lung to protect against injury caused by oxidants occurs at higher doses.

Clearance from the Lung. To examine the characteristics of the clearance of ozone-derived oxygen from the respiratory system, 30 mice were exposed to 1 ppm $^{18}O_3$ for 45 minutes. Groups of five randomly selected animals were sacrificed at 0, 3, 6, 24, and 48 hours post exposure. The natural abundance of oxygen-18 was established using six unexposed animals.

Results of isotopic analysis are shown in Table 4-7. A plot of the natural logarithm of relative enrichment versus time post exposure is shown in Figure 4-4. A biexponential decay of ozone-derived oxygen from the lung is observed. The clearance equation, indicated by the curve in Figure 4-4, was determined using a curve-stripping procedure (21)

$$R(t) = 0.83 \cdot \exp(-0.31t) + 0.17 \cdot \exp(-0.01t) \qquad (4\text{-}4)$$

where R(t) is the fractional retention of ozone-derived oxygen in the lung and t is time in hours. The first phase accounts for the clearance of 83% of the isotopic label present in the lung at the end of the exposure (zero hours) and has a half-life of 2.2 hours. The second phase accounts for the clearance of 17% of the isotopic label initially

Table 4-7. Clearance of Ozone-Derived Oxygen in Mouse Lungs

time post exposure h	body weight[a] g	lung wet weight[a] mg	$^{18}F_{lung}$[a] x 10^3
natural abundance	24.3 ± 0.4	151 ± 7	2.0327 ± 0.0003
0	23.9 ± 0.6	143 ± 6	2.0469 ± 0.0030
3	25.6 ± 0.7	139 ± 5	2.0426 ± 0.0036
6	25.3 ± 0.8	139 ± 2	2.0369 ± 0.0019
24	25.9 ± 1.2	155 ± 15	2.0346 ± 0.0011
48	24.7 ± 1.0	150 ± 9	2.0341 ± 0.0005

[a] x ± SE for five animals in a single exposure group.

Figure 4-4. Clearance of ozone-derived oxygen from the lung. A plot of the natural logarithm of relative enrichment vs time post exposure for mice exposed to 1 ppm $^{18}O_3$ for 45 minutes is shown. Each point is the mean and standard error of the mean for analysis of tissue from five mice. The clearance equation is also indicated in the figure.

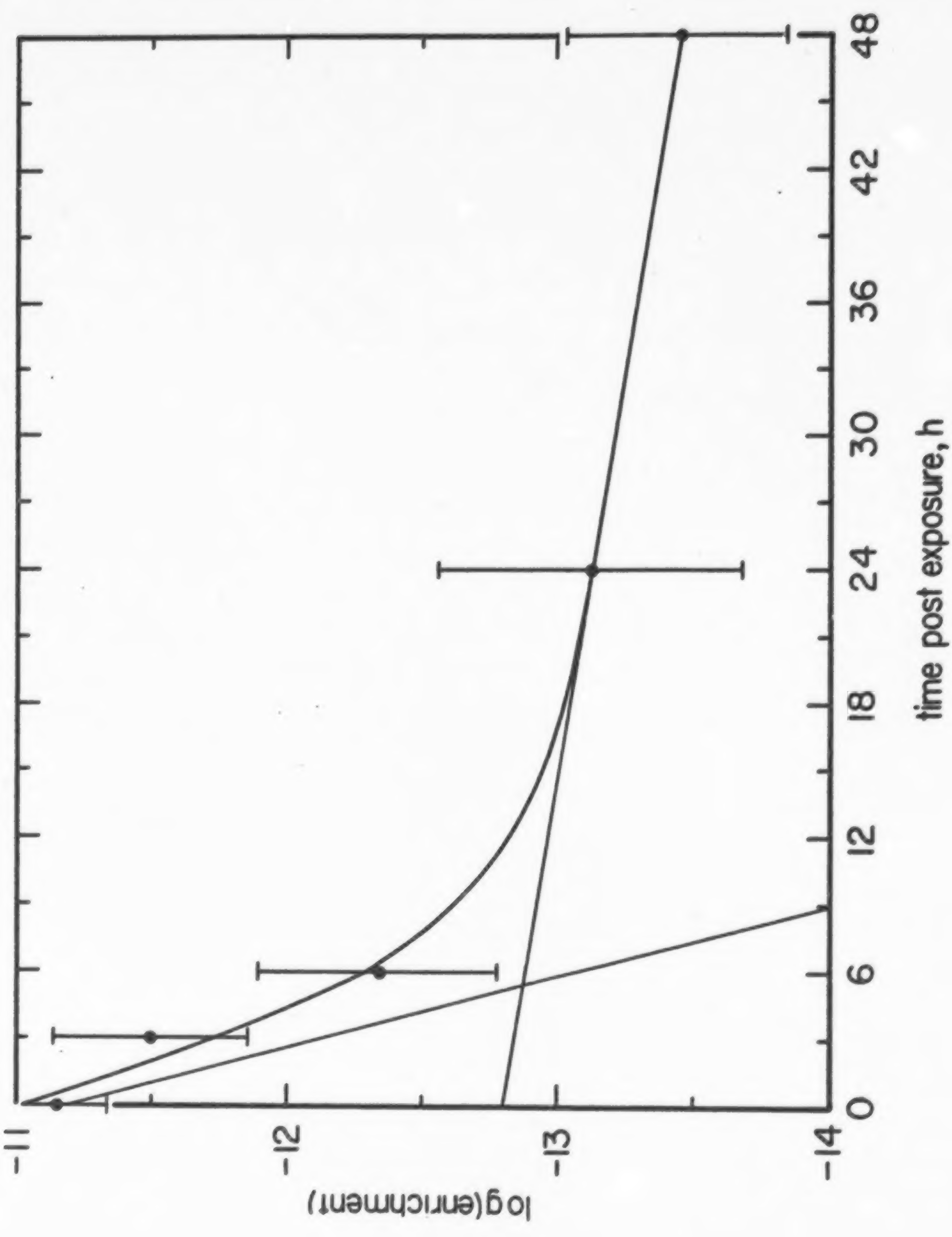
log(enrichment)
-11
-12
-13
-14
0
6
12
18
24
30
36
42
48
time post exposure, h

present and has a half live of 70 hours.

The clearance of aerosols from the lung (22) has received much attention because of the continued health risk posed by particulates lodged in the centriacinar region. Lung clearance of diesel exhaust particles is described by a three compartment model, where the three phases have half-fives of 1 day, 6 days, and 80 days (23). Particles deposited in the trachobronchial tree and the proximal bronchioles are transported to the gastrointestinal tract by the mucocillary escalator (phases 1 and 2, respectively), whereas particles reaching the alveolar region are removed by endocytosis, adsorption, dissolution, and metabolism (phase 3) (24). In contrast, clearance of ozone-derived oxygen from the lung involves catabolism of ozonolysis products and adsorption directly into the systemic and lymphatic circulation, with mucocillary clearance and phagocytosis playing minor roles. Exchange of oxygen between organic molecules and water (20) also results in removal of the isotopic label from lung tissue and could be a significant factor in lung clearance. These data indicate that ozone-derived oxygen is rapidly cleared from the lung; however, evidence for a two-compartment model is minimal. Therefore, at this time no assignment of clearance mechanisms is possible. Unambiguous definition of the phase(s) of clearance and the mechanism(s) for removal of ozone-derived oxygen from the lung require a closer examination.

EXPERIMENTAL SECTION

Apparatus. Isotopically enriched ozone was prepared from 99% oxygen-18 O_2 in the apparatus shown in Figure 4-5. The ozonizer was an annular pyrex vessel with a sealed bottom and a cold finger for condensing liquid oxygen and ozone. Cylindrical copper electrodes were

Figure 4-5. Apparatus for preparation and purification of $^{18}O_3$. Below the manifold, the apparatus consisted of an annular ozonizer and two distillation traps for the synthesis and purification of labeled ozone. Above the manifold were a 22-L ballast flask for storage of N_2 and a 2-L flask for storage of an $^{18}O_3/N_2$ mixture. See the text for details of construction and procedure.

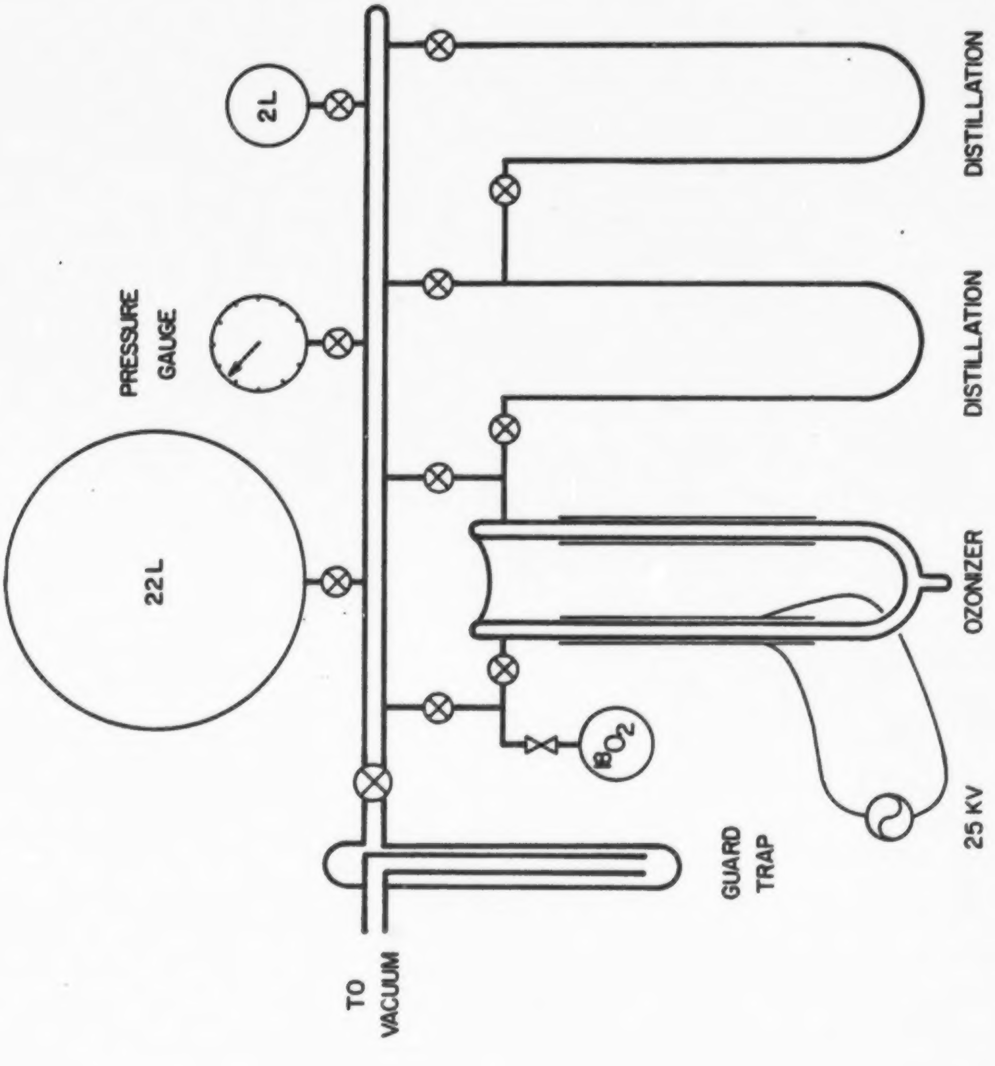
TO VACUUM
GUARD TRAP
$^{18}O_2$
25 KV
22L
OZONIZER
PRESSURE GAUGE
DISTILLATION TRAP
2L
DISTILLATION TRAP

placed on the inner- and outer-external surfaces of the ozonizer (25). The distillation traps were pyrex U-tubes. All valves were high-vacuum valves with Teflon plugs and Kel-F O-rings, with a maximum clearance of 4 mm (Kontes). The manifold was fitted with a pressure gauge which measured absolute pressure from 0 to 760 torr (Matheson) and with a thermal conductivity vacuum gauge (Varian) which operated in the range from 10-3 to 2 torr (not shown in Figure 4-5). A guard trap filled with copper turnings heated to 100°C was placed between the vacuum manifold and the pumping system to prevent ozone from reacting with oil in the mechanical pump.

Two exposure chambers and a syringe pump for metering isotopically labeled ozone into the chambers were constructed specifically for exposure of mice to $^{18}O_3$. A schematic diagram of the exposure system is shown in Figure 4-6. A small exposure chamber, which held five mice, was constructed to minimize internal volume (3 L), thus minimizing isotope consumption and expense. A larger exposure chamber (30 L) was constructed to contain up to 40 mice. Both chambers consisted of a series of plenums separated by perforated stainless steel sheets, which ensured laminar flow of gas over the animals (26). A dispersion element in the upper plenum ensured a uniform distribution of ozone in the laminar flow region. The syringe had a capacity of 500 mL (Precision Sampling). It was constructed of borosilicate glass with a Teflon cap and plunger. A stepping-motor-drive system displaced the plunger of the syringe. A variable compression rate from 0.8 to 800 mL/min was available. The transfer line from the syringe to the exposure chamber was Teflon tubing.

Figure 4-6. Exposure system. This system consisted of a 500-mL stepping-motor-driven syringe, an exposure chamber, and an ozone monitor. See the text for details of construction and procedure.

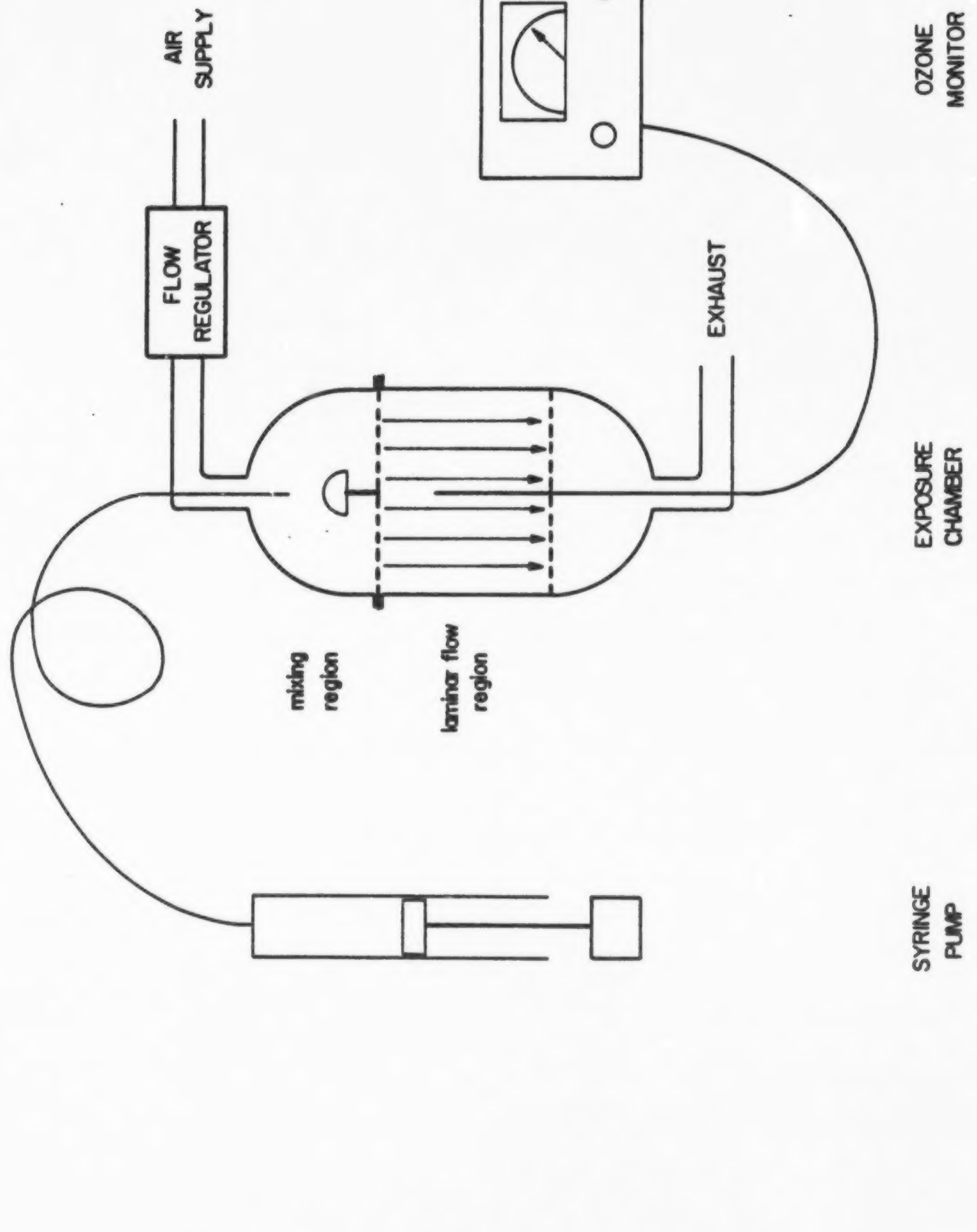
SYRINGE PUMP
mixing region
laminar flow region
EXPOSURE CHAMBER
EXHAUST
FLOW REGULATOR
AIR SUPPLY
OZONE MONITOR

Preparation and Purification of $^{18}O_3$. To synthesize $^{18}O_3$, the ozonizer was immersed in liquid nitrogen and labeled oxygen was admitted to the system. A potential of up to 25 kV was applied to the electrodes. The vapor pressure of oxygen at liquid nitrogen temperature (165 torr) was sufficient to maintain a diffuse discharge at approximately 15 kV. Ozone that formed in the discharge region immediately condensed on the walls of the ozonizer and filled the cold finger. At completion of the reaction, the pressure inside the ozonizer was that of ozone at liquid nitrogen temperature (5×10^{-3} torr) and was insufficient to maintain a diffuse discharge at full voltage. The procedure was stopped when this occurred, and a nearly quantitative yield of ozone was obtained. Residual oxygen and other possible contaminants were removed by two cryogenic distillations. The ozone was transferred to a clean 2-L pyrex flask, diluted with nitrogen from the 22-L flask at a concentration of 1% to a pressure of 740 torr, and used within 4 hours of preparation.

As ozone is both explosive and toxic, precautions to prevent injury in case of explosion and to minimize the risk of inhalation were taken. The danger of explosion is greatest when ozone is a liquid or a solid, where rapid warming or cooling of the condensed phases could cause a detonation. Rapid temperature changes should therefore be avoided. The ozonizer and distillation traps were enclosed by an explosion shield, a Plexiglas housing with a screen back. The explosion shield was designed to direct any glass fragments resulting from detonation of the ozone away from the experimenter. Two controlled explosions were performed to ensure that the explosion shield functioned adequately. A ventilation system was added to remove ozone that might escape during preparation and transfer.

Animal Exposures. Female CD mice, male Fisher 344 rats, and male New Zealand white rabbits (Charles River) were used in these studies. Animals were placed in an exposure chamber and allowed to adjust to their surroundings for 10 minutes prior to beginning the exposure. Filtered, dry air was supplied to the chamber at a flow rate of one chamber volume per minute. The syringe-pump was started, and the measurement of exposure time began when the desired ozone concentration was established in the laminar flow region of the chamber. The concentration of ozone inside the chamber was measured using a Bendix Model 8002 ozone monitor (Bendix). The stepping-rate of the syringe pump was adjusted to maintain an ozone concentration of 1 ± 0.1 ppm $^{18}O_3$ in the laminar flow region. Animals were removed promptly at the end of an exposure.

Tissue Sampling and Preparation. After removal from the exposure chamber, animals were individually anesthetized with Halothane and approximately 3 mL of blood were removed from a heart puncture. The trachea and lungs were immediately excised. The lungs were homogenized in distilled water using a Polytron homogenizer (Brinkmann Instruments). The head was skinned, muscle and skeleton not part of the nasopharyngeal region were removed, and the remaining tissue was homogenized in distilled water. Weights of all samples were obtained prior to homogenization. The tissue homogenates were immediately frozen in liquid nitrogen and lyophilized to dryness. The samples remained frozen during lyophilization. Residual water was removed by placing the samples under high vacuum for 24 hours, or until a pressure of < 10-3 torr was maintained when the samples were isolated from vacuum.

Using the following procedures, lung tissue was separated into fractions roughly corresponding to lipids, proteins, and organic solutes (27). Lung homogenates from animals in each group were pooled and resuspended in distilled water so that the final mixture was 80% (wt/wt) water and 20% (wt/wt) tissue. Volumes of solvent in the following procedure are given for one gram of tissue suspension. Ten drops of concentrated hydrochloric acid and 10 mL of methanol were added to the tissue suspension. The mixture was homogenized, 20 mL of chloroform was then added, and the mixture was again homogenized. The precipitate was removed by suction filtration through a fritted glass filtering funnel (ASTM 40-60 C), resuspended in 30 mL of chloroform-methanol (2:1 v/v), homogenized, and separated by suction filtration. This procedure was repeated and the precipitated solids were lyophilized to dryness. The three filtrates were combined, an amount of water equal to 25% of the total volume of filtrate was added, and the solution was mixed thoroughly and was centrifuged at 10,000 x g for 5 minutes to separate the two layers. The upper layer (methanol-water) was removed by aspiration and the lower layer (chloroform) was extracted twice with 1/4 volume of methanol-water (1:1 v/v). The three methanol-water fractions were pooled. Solvents were removed by evaporation in a stream of dry nitrogen. The acid precipitate contained proteins and other macromolecules, the chloroform extract contained primarily lipids, and the methanol-water extract contained polar organic solutes.

Elemental and Isotopic Analysis. Both oxygen elemental and isotopic analyses of each sample were obtained. Procedures for isotopic analysis were described in Chapters 2 and 3. Working standards (tissue identical to the samples) were calibrated as described in Chapter 2.

REFERENCES

1. Miller, F. J. A mathematical model of transport and removal of ozone in mammalian lungs. Ph.D. thesis, North Carolina State University, Raleigh, North Carolina, 1977.

2. Supplement: Comparative Biology of the Lung. Am. Rev. Respir. Dis. 128, 1983.

3. Janoff, A. Biochemical link between cigarette smoking and pulmonary emphysema. J. Appl. Physiol. 55: 285-293, 1983.

4. Tate, R. M.; Repine, J. E. Neutrophiles and the adult respiratory distress syndrome. Amer. Rev. Respir. Dis. 128:552-559, 1983.

5. Fantone, J. C.; Ward, P. A. Role of oxygen-derived free radicals and metabolism in leukocycte-dependent inflammatory reaction. Amer. J. Pathol. 107:397-418, 1982.

6. Weiss, S. J.; Lo Buglio, A. F. Phagocyte-generated oxygen metabolites and cellular injury. Lab. Invest. 47:5-18, 1982.

7. Diegelmann, R. F.; Cohen, I. K.; Kaplan, A. M. The role of macrophages in wound repair: A review. Plastic and Reconstruc. Surgery 68:107-113, 1981.

8. Transwell, A. K.; Smith, B. T. Human fetal lung type II pneumocytes in monolayer cell culture: The influence of oxidant stress, cortisol environment, and soluble fibroblast factor. Pediatric Res. 13:1097-1100, 1979.

9. Chow, C. K.; Tappel, A. L. An enzymatic protective mechanism against lipid peroxidation damage to lungs of ozone-exposed dogs. Lipids 8:518-524, 1972.

10. Chow, C. K.; Tappel, A. L. Activities of pentose shunt and glycolytic enzymes in lungs of ozone-exposed rats. Arch. Environ. Health 26:206-208, 1973.

11. Graham, J. A.; Menzel, D. B.; Miller, F. J.; Illing, J. W.; Gardener, D. E. Influence of ozone on pentobarbitol-induced sleeping time in mice, rats, and hamsters. Toxicol. Appl. Pharmacol. 61:64-73, 1981.

12. Melton, C. E. Effects of long-term exposure to low levels of ozone: A review. Aviat. Space Environ. Med. 53:105-111, 1982.

13. Weibel, E. R. Morphological basis of alveolar-capillary gas exchange. Physiol. Rev. 53:419-495, 1973.

14. Miller, F. J.; McNeal, C. A.; Kirtz, J. M.; Gardener, D. E.; Coffin, D. L.; Menzel, D. B. Nasopharyngeal removal of ozone in rabbits and guinea pigs. Toxicology 14:273-281, 1979.

15. Yokoyama, E.; Frank, R. Respiratory uptake of ozone in dogs. Arch. Environ. Health 25:132-138, 1972.

16. Morrman, W. J.; Chmiel, J. J.; Stara, J. F.; Lewis, T. R. Comparative decomposition of ozone in the nasopharynx of beagles. Arch. Environ. Health 26:153-155, 1973.

17. Chan, T. L.; Schreck, R. M.; Lippmann, M. Effect of the laryngeal jet on particle deposition in the human trachea and upper bronchial airways. J. Aerosol. Sci. 11:447-459, 1980.

18. Goldstein, B. D.; Balchum, O. J. Effects of ozone on lipid peroxidation in the red blood cell. Proc. Soc. Exp. Med. 26:356-358, 1967.

19. Menzel, D. B.; Roehm, J.; Lee, S. D. Vitamine E: The biological and environmental antioxidant. Agr. Food. Chem. 20:481-485, 1972.

20. Murphy, R. C.; Clay, K. L. Synthesis and back exchange of ^{18}O labeled amino acids for use as internal standards with mass spectrometry. Biomed. Mass Spectrom. 6:309-314, 1979.

21. Jauquez, J. A. Compartmental Analysis in Biology and Medicine . Elsevier Publishing Co., New York, pp. 103-104, 1972.

22. Morrow, P. E. Alveolar clearance of aerosols. Arch. Intern. Med. 131:101-108, 1973.

23. Lee, P. S.; Chan, T. C.; Hering, W. E. Long-term clearance of inhaled diesel exhaust particles in rodents. J. Tox. Environ. Health 12:801-813, 1983.

24. Green, G. M. Alveolobronchiolar transport mechanisms. Arch. Intern. Med. 131:109-114, 1973.

25. Myers, B. F.; Bartle, E. R.; Erickson, P. R.; Meckstroth, E. A. Laboratory generator for batch synthesis of pure ozone. Anal. Chem. 39:415-416, 1967.

26. Laskin, S.; Drew, R. T. An inexpensive portable inhalation chamber. Am. Ind. Ass. J. 31:645-646, 1970.

27. Folch, J., Lee, M., and Sloane-Stanley, G. H. A simple method for the isolation and purification of total lipids from animal tissue. J. Biol. Chem. 226:497-509, 1957.

CHAPTER 5

DETECTION AND QUANTITATION OF AUTOXIDATION IN TISSUE: A STUDY OF HEPATIC AUTOXIDATION INDUCED BY CARBON TETRACHLORIDE

Evaluation of autoxidation in biological systems has been based on the measurement of oxidation products of olefinic fatty acids (1-4). Damage is not limited to lipids, however. Generally not considered but equally important in the assessment of cellular dysfunction is oxidation of other cellular components, particularly oxidation of proteins. In this study, $^{18}O_2$ was used to determine incorporation of oxygen into residual organic material during autoxidation in the hepatocytes _in vivo_. Determination of isotopic enrichment provides a sensitive measurement of autoxidation of all cellular components. Conditions producing hepatic autoxidation were created by interperitoneal injection of carbon tetrachloride. Metabolism of carbon tetrachloride by the microsomal cytochrome P-450-mediated monooxygenase system in the liver produces CCl_3 and Cl radicals (5,6) which initiate autoxidation (5-7). Correlation between autoxidation and cytochrome P-450 activity is demonstrated by modulation of isotopic enrichment in liver tissue.

Lipid Peroxidation

Peroxidation of unsaturated fatty acids results in the formation of aldehydes, ketones, ethers, esters, epoxides, carboxylic acids, and hydrocarbons (8). The peroxidation of linolenic acid ($18{:}3\Delta^{9,12,15}$), for example, can result in the production of propane, 1,3-propiondialdehyde (malonaldehyde), and 9,11-dodecadienic acid during autoxidation of olefinic fatty acids (Figure 5-1).

Peroxidation of Linolenic Acid. Initiation of lipid peroxidation (reaction 1) occurs by abstraction of hydrogen from an allylic position by a free radical (8). Intramolecular rearrangement of the organic radical (reaction 2) yields a more stable conjugated system (9,10), which reacts with molecular oxygen (reaction 3) to form a peroxy radical

Figure 5-1. Peroxidation of linolenic acid. Peroxidation of linolenic acid leads to the formation of hydrocarbons, conjugated dienes, malonaldehyde, and fluorescent products during autoxidation.

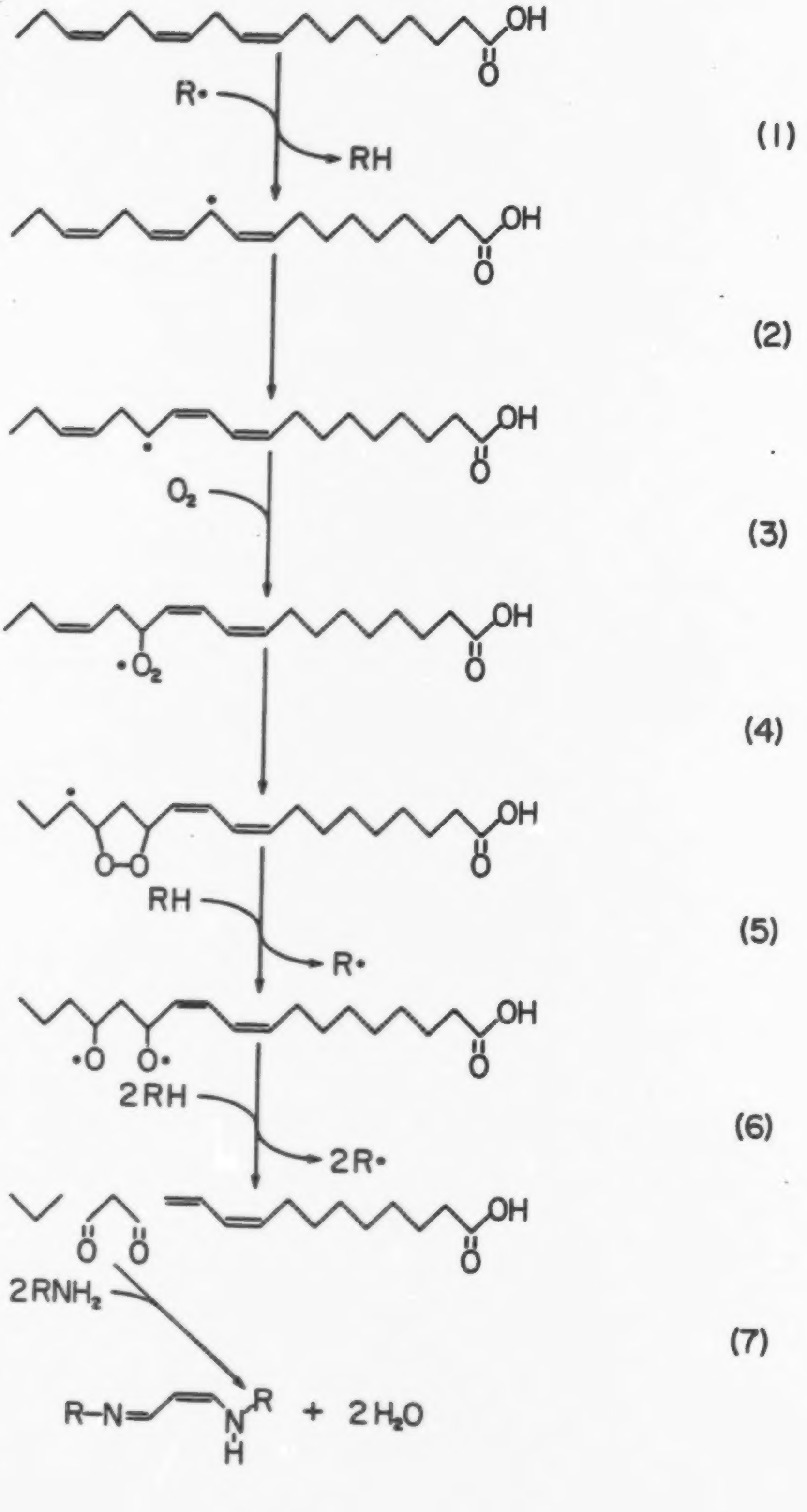
OH
O
R•
RH
(1)
(2)
O₂
(3)
•O₂
(4)
O–O
RH
R•
(5)
•O
O•
2RH
2R•
(6)
2RNH₂
(7)
R–N=
N
H
R
+ 2H₂O

(8,11,12). Only one of four possible isomeric peroxy radicals is shown in this example (1,8). Intramolecular cyclization of the peroxy radical (reaction 4) leads to the formation of a five-membered ring peroxide (1). Propagation of autoxidation proceeds by abstraction of hydrogen from other cellular components. Formation of an α,γ-diperoxy radical (reaction 5) is followed by formation and subsequent decomposition of a diperoxy radical (reaction 6), yielding propane, 1,3-propiondialdehyde (malonaldehyde), and 9,11-dodecadienic acid (1). Hydrocarbon production also results from decomposition of mono-hydroperoxides where ethane and pentane are the major products (4). Malonaldehyde readily reacts (reaction 7) with primary amines to form a di-Schiff base adduct (3). Less than 2% of the malonaldehyde produced during autoxidation of cellular material remains unbound (1).

Measurement of Lipid Peroxidation in vivo. The presence of malonaldehyde has been considered indicative of lipid peroxidation in biological matrices. Addition of 2-thiobarbituric acid to a solution containing malonaldehyde produces a water-soluble colored complex, which is a colorimetric indicator of the concentration of malonaldehyde. Analysis of lipid peroxidation in tissue requires liberation of bound malonldehyde, usually by heating in an acidic medium (1). Alternatively, production of conjugated dienes, inferred from an increased ultra violet absorption, in tissue has been used as evidence of lipid peroxidation. Absorption occurs between 220 and 250 nm, with an absorption maximum at 233 nm (2). The Schiff-base adducts formed by reaction of malonaldehyde with primary amines are similar to lipofuscene pigments found in aging (4). Macromolecular aggregates of malonaldehyde and phospholipids (13,14), proteins (14), and DNA (15) have been found to fluoresce with an excitation maximum at 360 nm and an emission maximum at 430-440 nm. Measurement of the fluorescent products in the chloroform-methanol extract of tissue also has been used as an indication of lipid peroxidation of biological material (16-18). Most recently, measurement of volatile hydrocarbons evolved in the breath has been used as an assay for lipid peroxidation (4).

Determination of the products of peroxidation of unsaturated lipids as a measure of autoxidation neglects oxidation of all other classes of compounds. The most general assay for autoxidation would be measurement of the incorporation of oxygen into organic material. Although the formation of Schiff-base adducts results in the loss of O_2-derived oxygen to water, other pathways, not shown on Figure 5-1, lead to the formation of stable products which retain O_2-derived oxygen (8,19). Retention of the O_2-derived oxygen in the organic residue is also expected with oxidation of other cellular constituents.

Carbon Tetrachloride Hepatotoxicity

Hepatotoxicity associated with carbon tetrachloride poisoning is characterized by the rapid intracellular accumulation of triglycerides. This dysfunction arises from inhibition of incorporation of lipids into very low density lipoprotein in plasma (5). Injury to hepatocytes proceeds from swelling of the rough endoplasmic reticulum, with decreases in microsomal enzyme activity and protein synthesis, to mitochondrial swelling and eventual necrosis (6).

Controversy arises, however, as to the nature of the histochemical lesion. Two distinct mechanisms have been proposed. One hypothesis holds that CCl_3 and Cl radicals, produced during metabolism of CCl_4 by the microsomal cytochrome P-450-mediated monooxygenase system, initiate autoxidative processes that lead to loss of structure and function of macromolecules, primarily membrane proteins (6). Initial damage is localized to the rough endoplasmic reticulum, the intracellular site of microsomal monooxygenases, but spreads throughout the cell as autoxidation progresses (6). An alternative hypothesis suggests that irreversible binding of carbon trichloride and chlorine radicals to cellular components, particularly microsomal and mitochondrial membrane proteins, is the cause of histological and biochemical dysfunction (20). In both views, hepatotoxicity is related to metabolism of carbon tetrachloride. The occurrence of lipid peroxidation, as indicated by the production of conjugated dienes (6,20) and ethane (21,22) during exposure to carbon tetrachloride, is undisputed. Autoxidation of other cellular components has only been inferred.

Microsomal Cytochrome P-450. The hepatic microsomal cytochrome P-450-mediated monooxygenase system contains at least six distinct isoenzymes with different, but somewhat overlapping, substrate specificties (23). Levels of specific isoenzymes can be increased by repeated administration *in vivo* of a variety of drugs and toxins which are normally substrates for these enzymes (24). Induction by phenobarbital affects four isoenzymatic forms and increases the rate of carbon tetra- chloride metabolism (25). Phenobarbital induction increases polysomal P-450 monooxygenase mRNA by 30-fold (26); however, it is not associated with the Ah (aromatic hydrocarbon) locus (27). Thus, activities of NADPH-dependent cytochrome c reductase, NADPH-dependent cytochrome P-450 reductase, epoxide hydroxylase, and glutathione S-transferase are generally unaffected (28).

A wide variety of compounds has been found to inhibit cytochrome

P-450 activity (29). Complete inhibition of carbon tetrachloride metabolism in vivo can be obtained by administration of piperonal butoxide. Inhibition occurs by metabolic activation of piperonal butoxide to generate an intermediate which has a high affinity for Fe^{3+} contained in the heme group of cytochrome P-450 (29-33). Metabolic activation requires NADPH and O_2, and a carbanion-cytochrome P-450 complex, which exists in a pH-dependent equilibrium, is formed (29,32). The carbanion-cytochrome P-450 complex is stable in vivo (30), but, as indicated by the Type I difference spectrum, it does not involve covalent binding or destruction of cytochrome P-450 (32,33).

Carbon-Tetrachloride-Induced Autoxidation. In this study, oxygen-18 labeled O_2 has been used as a tracer for molecular oxygen incorporated into biomolecules in the liver during autoxidation. Autoxidation was induced by metabolism of carbon tetrachloride by microsomal cytochrome P-450-mediated monooxygenases.

Male Fisher 344 rats were used in this study. Animals were divided into five groups. A summary of treatment of each group appears in Table 5-1. Animals in Group I were untreated and used to establish the natural abundance of oxygen-18. Animals in Groups II through V were ventilated by a mechanical respirator containing a mixture of N_2 and $^{18}O_2$ (80:20) for 60 minutes. Animals in Group II represented an experimental control, and received $^{18}O_2$ as well as I.P. injections of corn oil, but did not receive CCl_4. Animals in Groups III through V received I.P. injections of a solution of CCl_4 in corn oil. Hepatic microsomal mixed-function oxidase activity was normal in the animals in Group III, induced in the animals in Group IV, and inhibited in the animals in Group V. A portion of the liver from each animal was retained. Another

Table 5-1. Summary of Treatments of Groups

Group	$^{18}O_2$	corn oil[a]	CCl_4[b]	pheno-barbital[c]	piperonal butoxide[d]
I	-	-	-	-	-
II	+	+	-	-	-
III	+	+	+	-	-
IV	+	+	+	+	-
V	+	+	+	-	+

[a] dose = 5 mL/kg body weight.

[b] dose = 1 mL/kg body weight of carbon tetrachloride.

[c] dose = 20 mg/day of phenobarbital for 3 days prior to the exposure.

[d] dose = 25 mg/kg body weight of piperonal butoxide 60 minutes prior to receiving carbon tetrachloride.

portion of the liver was fractionated into an acid precipitate, a chloroform extract, and a methanol-water extract. Oxygen elemental and isotopic analyses were performed on all samples.

Results of isotopic analysis are shown in Table 5-2, and relative enrichments are shown in Table 5-3. Relative enrichments were calculated using equation 4-1, where $^{18}F_{TI,NA}$ was the average isotopic composition of Group I, $^{18}F_{TI,E}$ was the average isotopic composition of the experimental group, and $^{18}F_{TR} = 0.99$. Estimates of the sizes of the oxygen pools were derived from the weights of the sample and oxygen elemental analyses (Table 5-4). The amount of O_2-derived oxygen in whole tissue and in each fraction was calculated using equation 4-2 from the relative enrichment and the size of the oxygen pool in the sample. Results of these calculations are shown in Figure 5-2. Oxygen derived from O_2 is expressed as nanomoles per gram of liver.

Incorporation of O_2-derived oxygen in animals not receiving carbon tetrachloride (Group II) arises, in part, from basal activity of hepatic monooxygenases and mixed-function oxidases normally involved in metabolism, detoxification (34), and phagocytic processes (35). Isotopic enrichment in control animals may also reflect indirect incorporation of O_2-derived oxygen into organic molecules by exchange of oxygen (36) with $H_2{}^{18}O$ produced by oxidative respiration. The background enrichment in the livers from animals in Group II corresponds to an average incorporation of 650 nanomoles of O_2-derived oxygen per gram of tissue. The acid precipitate retained 18% of the label, the chloroform extract retained 11% of the label, the methanol-water extract retained 32% of the label, and 39% of the label was lost in the chemical work-up.

Table 5-2. Abundance of Oxygen-18 in Liver

Group	N	$^{18}F \times 10^3$			
		liver homogenate[a]	acid precipitate[a]	chloroform extract[a]	methanol-water extract[a]
I	5	2.0497 ± 0.0010	2.0416 ± 0.0005	2.0456 ± 0.0009	2.0432 ± 0.0015
II	5	2.235 ± 0.031	2.092 ± 0.002	2.291 ± 0.027	2.81 ± 0.16
III	6	2.404 ± 0.049	2.176 ± 0.040	3.07 ± 0.15	3.34 ± 0.12
IV	3	2.618 ± 0.098	2.261 ± 0.035	4.10 ± 0.29	3.80 ± 0.12
V	2	2.24 ± 0.04	2.093 ± 0.017	2.40 ± 0.13	2.780 ± 0.075

[a] x ± SE for N animals.

Table 5-3. Relative Enrichment in Liver[a]

Group	Relative Enrichment x 10^6			
	liver homogenate	acid precipitate	chloroform extract	water:methanol extract
I	0	0	0	0
II	190 ± 30	50 ± 2	250 ± 30	780 ± 160
III	360 ± 50	140 ± 40	1040 ± 150	1310 ± 120
IV	580 ± 100	220 ± 40	2080 ± 300	1780 ± 370
V	200 ± 40	50 ± 20	360 ± 130	750 ± 80

[a] Relative enrichments were calculated from average isotopic compositions of the samples from each group, where the isotopic composition of samples from Group I was used as natural abundance. The uncertainties are propagated standard errors of the means.

Table 5-4. Oxygen Pools in Liver

sample	weight mg	% oxygen	oxygen pool micromoles
liver	238 ± 18	23 ± 1	3400 ± 300
acid precipitate	168 ± 23	23 ± 1	2400 ± 350
$CHCl_3$ extract[a]	2.2 ± 0.2	14 ± 1	19 ± 2
CH_3OH-H_2O extract[b]	2.2 ± 0.3	28 ± 1	38 ± 5

[a] analysis of 0.07 aliquot of total chloroform extract.

[b] analysis of 0.15 aliquot of total methanol-water extract.

Figure 5-2. Incorporation of O_2-derived oxygen into liver. The incorporation of O_2-derived oxygen during free-radical-initiated autoxidation is shown. The amount of O_2-derived oxygen in whole liver, and the distribution in the acid precipitate, the chloroform extract, and the methanol-water extract of liver are shown. These values are expressed as nanomoles O_2-derived oxygen/gram liver.

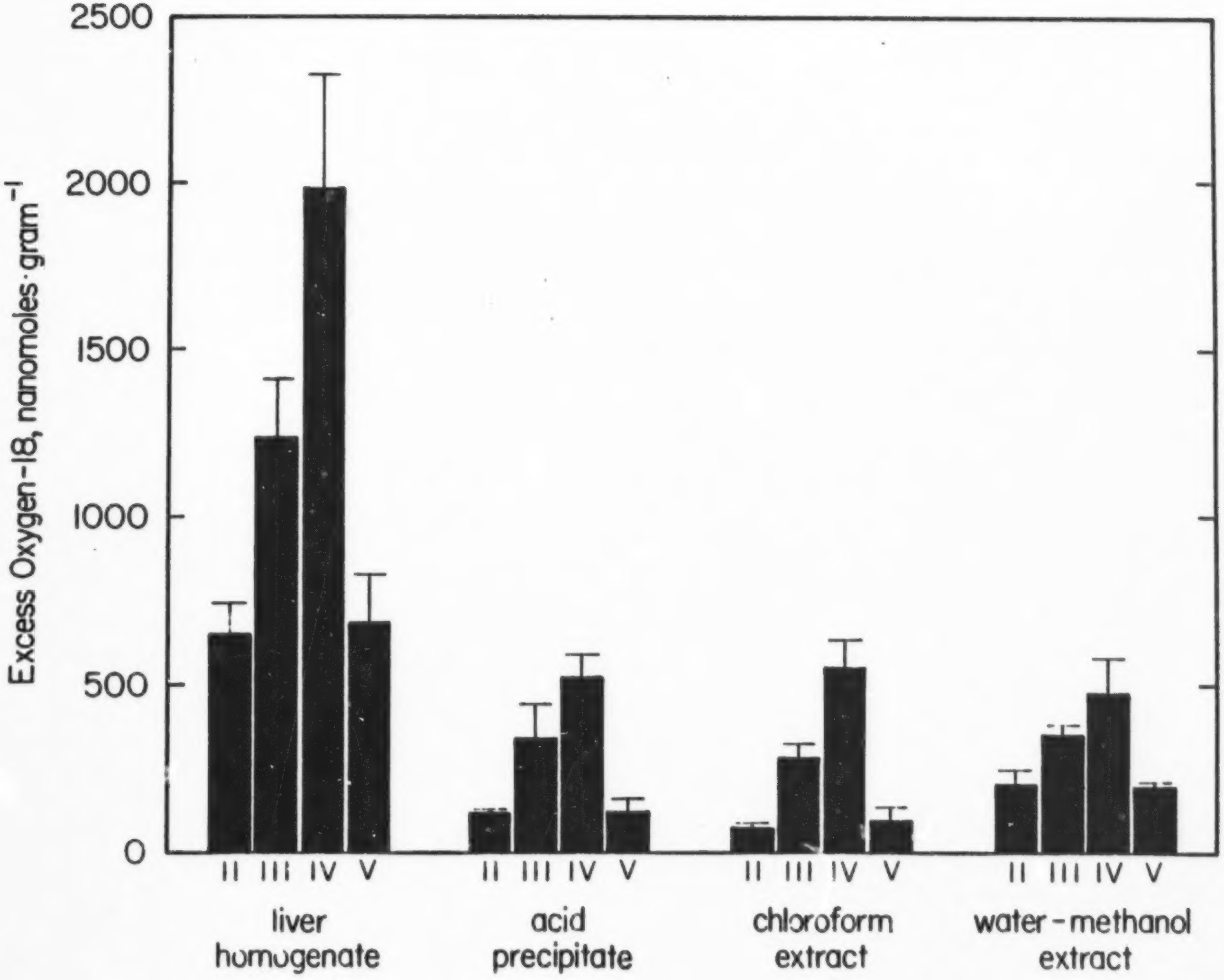
Excess Oxygen-18, nanomoles · gram^{-1}
2500
2000
1500
1000
500
0
II III IV V
liver homogenate
II III IV V
acid precipitate
II III IV V
chloroform extract
II III IV V
water - methanol extract

A direct correlation between P-450 activity and incorporation of O_2-derived oxygen in the liver by autoxidation was observed in Groups III through V. Autoxidation resulted in an average incorporation of 580 nanomoles O_2-derived oxygen/gram liver in Group III in excess of background levels (Group II). The molecular distribution of label within liver was different from that in the control group, in that the acid precipitate and chloroform extract retained 38% and 36% of the label, whereas the methanol-water extract retained only 26% of the label. A two-fold increase in the amount of O_2-derived oxygen was observed in the livers of animals in which cytochrome P-450 had been induced with phenobarbital. Autoxidation resulted in an average incorporation of 1330 nanomoles O_2-derived oxygen/gram liver in Group IV in excess of background levels (Group II). The distribution of the label among these fractions was identical to that found in Group III. A decrease in isotopic enrichment to levels found in Group II occurred in the livers of animals in which cytochrome P-450 activity had been inhibited with piperonal butoxide (Group V). All O_2-derived oxygen incorporated into liver by autoxidation (identified by enrichment above control levels) was recovered in the chemical fractions. Insignificant amounts of label were lost during the chemical work-up.

Isotopic enrichments in the chloroform and methanol-water extracts represent peroxidation products of unsaturated lipids. Upon decomposition of lipid peroxides, O_2-derived oxygen can be retained in the major portion of the lipid, thus appearing in the chloroform extract, or can be retained in a small organic fragment (8) which, because of the polar oxygen-containing functional group, would appear in the methanol-water extract.

The extent of incorporation of label in the acid precipitate is surprising. This suggests that macromolecules, proteins in particular, are also a major target for autoxidation, an observation missed in previous studies in which only peroxidation products of olefinic lipids were considered. Incorporation of the isotopic label in the acid precipitate could result from binding of carbon trichloro-alkoxy radicals directly to macromolecules (20). In fact, species differences in hepatotoxicity correlate most closely with the incorporation in macromolecules of radioactivity from $^{14}CCl_4$ as opposed to lipid peroxidation measured by absorbance at 243 nm (20). Distinction between these two mechanisms is of minor importance, in that incorporation of O_2-derived oxygen in macromolecules by either process most likely results in loss of structure and function. Isotopic enrichment of the tissue-oxygen pool is then a good indication of damage resulting from autoxidation.

CONCLUSIONS

This is the first study in which the incorporation of oxygen into tissue during autoxidation has been measured directly. This development is significant for the following reasons: i) this method provides a sensitive, quantitative assay for autoxidation, ii) these techniques are applicable to studies of autoxidation both in vitro and in vivo, and iii) determination of autoxidation is not limited to measurement of the products of lipid peroxidation, for any class of compounds which retains oxygen from $^{18}O_2$ can be identified by determination of isotopic enrichment. Thus, the procedures discussed in this chapter outline a general approach to the determination of autoxidation and provide a unifying approach to understanding the relationship between the environmental concentration of a compound and the physicochemical processes controlling transport, adsorption, and reactivity of the toxic agent in vivo.

EXPERIMENTAL SECTION

Protocol. Five groups of male Fisher 344 rats (Charles River) were used in this study; see Table 5-1 for a summary of the experimental protocol. Group I was untreated and used to determine natural abundance. Group II was injected I.P. with corn oil at a dose of 5 mL/kg body weight. Groups III, IV, and V were injected with 5 mL/kg body weight of a corn oil solution of carbon tetrachloride (20%). Group IV received I.P. injections of phenobarbitol at a dose of 20 mg/day for 3 days prior to the exposure. Group V received an I.P. injection of piperonal butoxide at a dose of 25 mg/kg body weight 60 minutes prior to receiving carbon tetrachloride.

Groups II through V were anesthetized with Nembutal at a dose of 50 mg/kg body weight. The trachea was surgically exposed and cannularized, and the animal was connected to an artificial respirator (Harvard Apparatus) containing a mixture of N_2 and $^{18}O_2$ (80:20). The animal was then injected I.P. with Anectine at a dose of 0.06 mL. Once the respiratory rate and heart rate had stabilized, the animal received an I.P. injection of corn oil or the corn oil solution of carbon tetrachloride. While on the respirator, some animals received additional Anectine (0.03 mL) as needed to maintain even and unstressed breathing. All animals were removed from the respirator 60 minutes after receiving carbon tetrachloride and allowed to expire.

Tissue Sampling and Preparation. Two one-gram liver samples were taken. One sample of liver was homogenized in 3 mL of distilled water using a Polytron homogenizer (Brinkmann Instruments). The homogenate was immediately frozen in liquid nitrogen and lyophilized to dryness. The sample remained frozen during lyophilization. Residual water was removed by placing the tissue homogenates under high vacuum overnight.

The other sample of liver was used for chemical separation. One gram of liver was homogenized in 7 mL of chloroform-methanol-water (2:4:1), with the addition of 2 drops of concentrated HCl. The homogenate was centrifuged at 20,000 x g and 5°C for 20 minutes. Two clear layers separated by a pellicle were visible. The upper layer was methanol-water and the lower layer chloroform. The pellicle was removed with forceps and lyophilized to dryness, and the layers were separated.

Elemental and Isotopic Analysis. Samples of the chloroform extract were obtained by evaporation of the solvent in a stream of dry nitrogen. The residual material was redissolved in 1.00 mL chloroform, 70 μL of this solution (0.070 aliquot) was added to a silver cup, and the solvent was removed by evaporation in a stream of dry nitrogen. A similar procedure was used to obtain samples of the methanol-water extract. Solvent was removed by evaporation in a stream of dry nitrogen. The residual material was redissolved in 200 μL of water, 30 μL of this solution (0.150 aliquot) was added to a silver cup, and the solvent was removed by evaporation in a stream of dry nitrogen. The pellicle was weighed, powdered using a mortar and pestle, and approximately 2 mg of the powder was placed in a silver cup.

Both oxygen-elemental and isotopic analyses of each sample were were obtained. Procedures for isotopic analysis were described in Chapters 2 and 3. Working standards (tissue identical to the samples) were calibrated as described in Chapter 2.

REFERENCES

1. Dahle, L. K.; Hill, E. G.; Holman, R. T. The thiobarbituric acid reaction and the autoxidation of polyunsaturated fatty acid methyl esters. Arch. Biochem. Biophys. 98:253-261, 1962.

2. Farmer, E. H.; Koch, H. P.; Sutton, D. A. The course of autoxidation in polyisoprenes and allied compounds. Part V. Observations on fish-oil acids. J. Chem. Soc. 1943, 122-125.

3. Malshet, V. G.; Tappel, A. L. Fluorescent products of lipid peroxidation: I. Structural requirement for fluorescence in conjugated Schiff bases. Lipids 8:194-198, 1973.

4. Dumelin, E. E.; Tappel, A. L. Hydrocarbon gases produced during in vitro peroxidation of polyunsaturated fatty acids and decomposition of preformed hydroperoxides. Lipids 12:894-900, 1977.

5. Recknagel, R. O. Carbon tetrachloride hepatotoxicity. Pharmacol. Rev. 19: 145-1 , 1967.

6. Recknagel, R. O.; Glende, E. A. Carbon tetrachloride hepatotoxicity: An example of lethal cleavage. Crit. Rev. Toxicol. 2:263-297, 1973.

7. Di Luzzio, N. R. Antioxidants, lipid peroxidation, and chemical-induced liver injury. Fed. Proc. 32:1875-1881, 1973.

8. Frankel, E. N. Hydroperoxides. Lipids and Their Oxidation. Schultz, H. W.; Day, E. A.; Sinnhuber, R. O. (eds), The Avi Publishing Company, Inc., Westport, Connecticut, 1962, pp. 51-78.

9. Farmer, E. H.; Koch, H. P.; Sutton, D. A. The course of autoxidation in polyisoprenes and allied compounds. Part VII. Rearrangement of double bonds during autoxidation. J. Chem. Soc. 1943, 541-547.

10. Farmer, E. H.; Sutton, D. A. The course of autoxidation in polyisoprenes and allied compounds. Part XI. Double bond movement during autoxidation of a monoolefin. J. Chem. Soc. 1946, 10-13.

11. Farmer, E. H.; Sutton, D. A. The course of autoxidation in polyisoprenes and allied compounds. Part IV. The isolation and constitution of photochemically formed methyl oleate peroxide. J. Chem. Soc. 1943, 119-122.

12. Bolland, J. L.; Koch, H. P. The course of autoxidation in polyisoprenes and allied compounds. Part IX. The primary thermal oxidation products of ethyl linoleate. J. Chem. Soc. 1945, 445-447.

13. Bidlack, W. R.; Tappel, A. L. Fluorescent products of phospholipids during peroxidation. Lipids 8:203-207, 1973.

14. Dillard, C. J.; Tappel, A. L. Fluorescent products from reaction of peroxidizing polyunsaturated fatty acids with phosphatidyl ethanolamine and phenylalanine. Lipids 8:183-189, 1973.

15. Reiss, U.; Tappel, A. L. Fluorescent product formation and changes in structure of DNA reacted with peroxidizing arachidonic acid. Lipids 8:199-202, 1973.

16. Fletcher, B. L.; Tappel, A. L. Fluorescent modification of serum albumin by lipid peroxidation. Lipids 6:172-175, 1971.

17. Dillard, C. J.; Tappel, A. L. Fluorescent products of lipid peroxidation of mitochondria and microsomes. Lipids 6:715-721, 1971.

18. Trombly, R.; Tappel, A. L.; Coniglio, J. G.; Grogan,Jr., W. M.; Rhamy, R. K. Fluorescent products and polyunsaturated fatty acids of human testes. Lipids 10:591-596, 1975.

19. Keenen, M. Secondary degeneration products. Lipids and Their Oxidation. Schultz, H. W.; Day, E. A.; Sinnhuber, R. O. (eds), The Avi Publishing Company, Inc., Westport, Connecticut, 1962, pp. 51-78.

20. Diaz Gomez, M. I.; de Castro, C. R.; D'Acosta, de Fenos, de Ferreyra, E. C.; Castro, J. A. Species differences in carbon tetrachloride-induced hepatotoxicity: The role of CCl_4 activation and of lipid peroxidation. Toxicol. Appl. Pharm. 34:102-114, 1975.

21. Koster, V.; Albrecht, D.; Kappos, H. Evidence for carbon tetrachloride- and ethanol-induced lipid peroxidation in vivo demonstrated by ethane production in mice and rats. Toxicol. Appl. Pharmacol. 41:639-648, 1977.

22. Burk, R. F.; Lane, J. M. Ethane production and liver necrosis in rats after administration of drugs and other chemicals. Toxicol. Appl. Pharmacol. 50:467-478, 1979.

23. Lu, A. Y. H.; West, S. B. Multiplicity of mammalian microsomal cytochromes P-450. Pharmicol. Rev. 31:277-295, 1980.

24. Nerbert, D. N. Multiple forms of inducible drug-metabolizing enzymes: A reasonable mechanism by which any organism can cope with adversity. Mol. Cell. Biochem. 27:27-46, 1979.

25. Walz, F. G.; Vlasuk, G. P.; Omiecinski, C. J.; Bresnick, E.; Thomas, P. E.; Ryan, D. E.; Levin, W. Multiple, immunoidentical forms of phenobarbitol-induced rat liver cytochrome P-450 are encoded by different mRNAs. J. Biol. Chem. 257:4023-4026, 1982.

26. Adesnik, M.; Bar-Nun, S.; Maschio, F.; Zunich, M.; Lippman, A.; Bard, E. Mechanism of induction of cytochrome P-450 by phenobarbitol. J. Biol. Chem. 256:10340-10345, 1981.

27. Pelkonen, O.; Nerbert, D. W. Metabolism of polycyclic aromatic hydrocarbons: Etiologic role in carcinogenesis. Pharmicol. Rev. 34:189-222, 1982.

28. Nerbert, D. W.; Jensen, N. M. The Ah locus: Genetic regulation of the metabolism of carcinogens, drugs, and other environmental chemicals by cytochrome P-450-mediated monooxygenases. Crit. Rev. Biochem. 6:401-437, 1979.

29. Testa, B.; Jenner, P. Inhibitors of cytochrome P-450s and their mechanisms of action. Drug Metab. Rev. 12:1-117,1981.

30. Ullrich, V.; Schnabel, K. H. Formation and binding of carbanions by cytochrome P-450 of liver microsomes. Drug Metab. Dispos. 1:176-183, 1973.

31. Hodgson, E.; Philpot, R. M. Interaction of methylenedioxy-phenyl (1,3-benzodioxole) compounds with enzymes and their effects on mammals. Drug Metab. Rev. 3:231-301, 1974.

32. Franklin, M. R. Inhibitors of mixed function oxidases by substrates forming reduced cytochrome P-450 metabolic-intermediate complexes. Pharmacol. Ther. A 2:227-245, 1977.

33. Ullrich, V. The mechanism of cytochrome P-450 action. Microsomes and Drug Oxidation . Ullrich, V.; Roots, I.; Hildebrandt, A.; Estabrook, R. W.; Coony, A. H., (eds.), Pergaman Press, Oxford, 1977, pp. 192-201.

34. Coon, M. J. Oxygen activation in the metabolism of lipids, drugs, and carcinogens. Nutrit. Rev. 36:319-328, 1978.

35. Johnson, R. B. Oxygen metabolism and the microbicidal activity of macrophages. Fed. Proc. 37:27-59-27-64, 1978.

36. Murphy, R. C.; Clay, K. L. Synthesis and back exchange of ^{18}O labeled amino acids for use as internal standards with mass spectrometry. Biomed. Mass Spectrom. 6:309-314, 1979.